RAPID ONLINE MEASUREMENT OF AMINO ACID FLUX OF CONTINUOUSLY PERIFUSED CELLS

By

Jason Greene

Dissertation

Submitted to the Faculty of the

Graduate School of Vanderbilt University

in partial fulfillment of the requirements

for the degree of

DOCTOR OF PHILOSOPHY

in

Interdisciplinary Studies: Biological and Applied Chemistry

December, 2009

Nashville, Tennessee

Approved:

Professor John P. Wikswo

Professor Darryl J. Bornhop

Professor Franz J. Baudenbacher

Professor David L. Hachey

Professor David E. Cliffel

Professor Owen P. McGuinness

ACKNOWLEDGMENTS

First and foremost, I would like to thank Rachel, my wonderful and supportive wife. She has provided essential academic, mental, and emotional support. Being in a related field, there have been countless times when I have been able to discuss my problems and bounced ideas off her. But, her biggest sacrifice has been the past ten months, where she has lived in east Tennessee with her mother and our daughter, allowing me to completely devote my time toward completing my degree.

Next, I would like to thank Dr. Robert Kennedy and Minshan Shou at the University of Michigan. Dr. Kennedy allowed me to visit his lab and showed me every detail of the capillary electrophoresis instrument that Minshan was using, upon which the AAFA was based. Since that visit, there have been a few other times when he has provided phone support when all other avenues of troubleshooting had been exhausted.

I would also like to thank members of the Wikswo group. David Schaffer helped numerous times with Autocad drawings. Dmitry Markov and Phil Samson have been a valuable resource for brainstorming ideas. Allison Price has helped proofread nearly everything I have written. The biggest help has come from Ron Reiserer. From his machine shop training, to his willingness to almost always drop what he was doing and help, and his strive for near perfection in the way things are done he has provided essential training during my years at Vanderbilt.

Lastly, I would like to thank my advisor, Dr. John Wikswo. His ability to think outside the box coupled with his strong mentoring skill has provided me with a strong interdisciplinary background that will provide extremely valuable in my future career.

TABLE OF CONTENTS

LIST OF FIGURES

LIST OF TABLES

CHAPTER I

INTRODUCTION

Overview

Cellular metabolism is a highly complex system of coupled reactions that take place at a variety of different time scales. Due to its complexity, studying only one reaction or species gives limited information about metabolism as a whole. In addition, by acquiring measurements at low frequency, much of the dynamics of the system will not be observable. This is especially true if the biological system is perturbed in some manner. By acquiring metabolic information on multiple species simultaneously and at high frequency, more information about the system can be ascertained. To this end, a multianalyte microphysiometer (MMP) was developed by Dr. Cliffel's group which measures extracellular concentrations of glucose, lactate, oxygen, and pH every two minutes from ~10^5 cells contained in ~3 μL. This gives a snapshot of general metabolism and the degree of aerobic versus anaerobic metabolism. This device has been used to observe the metabolic effects of a variety of pharmacological and real-world metabolic toxins. As useful as the MMP is, it has its limitations. Measuring only four analytes at once limits the metabolic information able to be derived. Metabolism of amino acids is intricately linked to a variety of glycolytic and TCA cycle intermediates. By measuring amino acid metabolism, a much more detailed view of cellular metabolism ought to be obtained.

Commercial instrumentation used to detect and quantitate amino acids such as high-pressure liquid chromatography (HPLC), capillary electrophoresis (CE), and ion exchange chromatography are offline batch techniques in which the user or autosampler injects samples from contained vial. These techniques are frequently labor intensive and time consuming. Since the goal of this research is to obtain dynamic time response of amino acid flux, online instrumentation is required. Therefore, construction of a home-built online instrument was required.

The goal of this research was to be able to observe amino acid flux from groups of cells with high temporal resolution. To accomplish this goal, a combination of the microbioreactor (MBR) and online amino acid flux analyzer (AAFA) was constructed as shown in Figure 1. Cell media continuously perifuses the MBR, which is designed to evenly perifuse cells at a high cell-to-media volume ratio and with minimal flow-through volume. Background and introductory material are presented in Chapter 1. The design, construction, and use of the MBR is shown in Chapter 3. As described in Chapter 2, the effluent is preliminarily evaluated to observe amino acid uptake and release offline, using HPLC. With our online AAFA, the effluent from the MBR is mixed with derivatization reagents which fluorescently label amino acids. The derivatized effluent is injected in batches onto the separation capillary where the amino acids are separated by micellar electrokinetic chromatography. The labeled amino acids are detected by a laser induced fluorescence detector. The design, construction, and preliminary evaluation of the AAFA are shown in Chapter 4. A proof-of-concept experiment, in which basal amino acid flux from cells as well as changes in metabolism upon exposure to pharmacological inhibitors are measured using the MBR and online AAFA, is shown in Chapter 5.

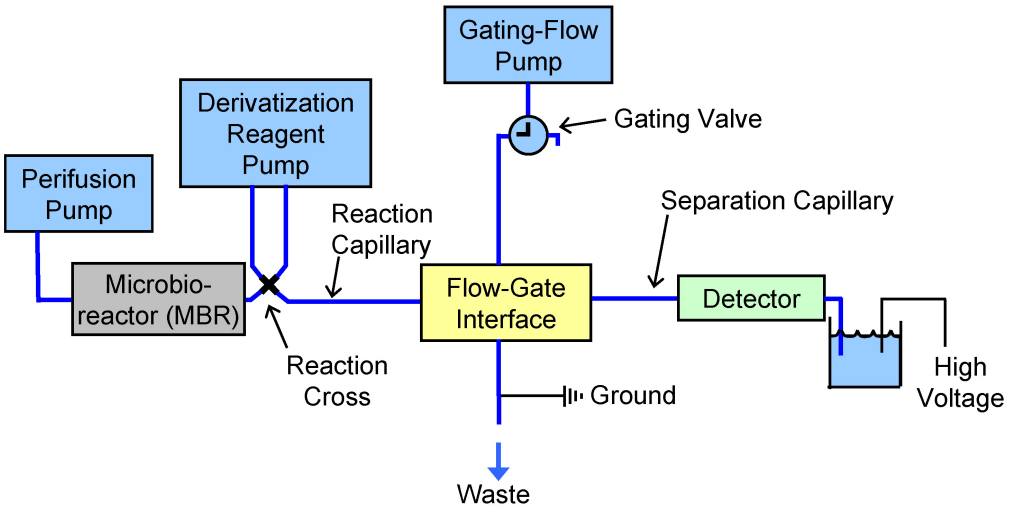

Figure 1. Diagram of MBR and AAFA created for this research. Media is pumped continuously through the MBR. The output is derivatized, labeling primary amines. The reaction mixture flows to the flow-gate where it is injected onto the separation capillary. Amino acids are separated by capillary electrophoresis and quantified by the detector.

There are a number of design criteria the MBR and AAFA must meet in order to fully reach the goals of the experiment as shown in Table 1. Many of these specifications are based upon the MMP, discussed later in this chapter, such as the chamber volume, cell number, inject-to-inject time, and response time. The media transit time and delay time were based on literature flux rates and calculating the amount of time necessary to change the concentration of amino acids in the media by a relatively large percentage.[1] The precision was based upon the Guidance for Industry published by the FDA.[2]

Table 1. MBR and AAFA specification goals.

Characteristic	Value
MBR Cell Number	$\sim 1 \times 10^5$
MBR Volume	< 5 μL
MBR Media Transit Time	< 5 min
Delay Time From MBR to AAFA	< 5 min
Response Time	< 2 min
AAFA Inject-to-Inject Time	< 2 min
Electropherogram Reproducibility (RSD)	< 15%

Chapter 1 presents background and introductory material which supports the need for the construction of the MBR and AAFA as well fundamental scientific information relevant to the work presented. First, glucose metabolism and the MMP is presented, upon which the fundamental purpose of building this instrument is based. Next, amino acid metabolism is presented follow by amino acid flux rates of a model system. This forms the basis of the sensitivity needed by the instrument in order to observe changes in amino acid flux. This is followed by background information on soft lithography, a technique which was used to fabricate the MBR, and information on other published examples of MBRs. Lastly, background on capillary electrophoresis and application to amino acid separation is presented along with derivatization chemistry necessary to detect amino acids.

Metabolism and the Multianalyte Microphysiometer

Glucose metabolism is one of the primary ways of obtaining cellular energy. A diagram showing the main elements of glucose metabolism is shown in Figure 2. Glucose enters the cell through transporters and then is converted to pyruvate through glycolysis. Pyruvate then has two fates: anaerobic metabolism by conversion to lactate and exportation from the cell, or aerobic metabolism by conversion to acetyl-CoA followed by oxidative physphorylation. The tricarboxylic acid (TCA) cycle converts acetyl-CoA to carbon dioxide and generates the electrons carried by NADH that are ultimately used in the production of ATP, a key energy source for the cell. Two key elements decide the fate of pyruvate. One, the electron transport chain requires oxygen, while the conversion to lactate does not. Two, aerobic metabolism produces over 10-fold more ATP than anaerobic metabolism.[3] Therefore, by measuring the extent to which metabolism is aerobic or anaerobic, one can get an estimation of energy production.

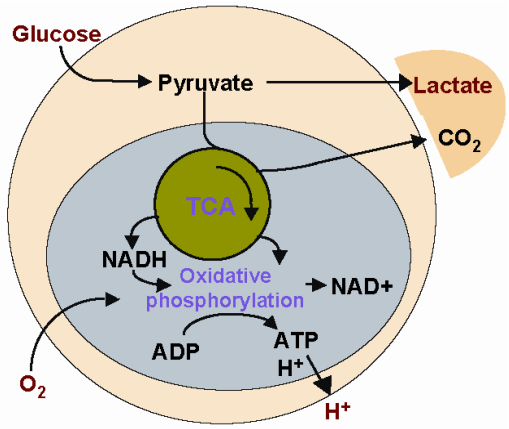

Figure 2. Simplified representation of glucose metabolism.

The Cytosensor Microphysiometer has been used by many researchers to obtain metabolic and signaling information.[4-14] The microphysiometer operates by stop-flow perifusion of cells in the presence of a low-buffered cell media in a 3 µL chamber. The perifusion is then stopped for 30 s during which the pH of the cell media in the

chamber decreases due to a buildup of excreted acid from a variety of sources. This change in the pH of the media is measured using a light-addressable potentiometric sensor. After 30 s, perifusion is resumed for 90 s and the process is repeated. Thus, the rate of acidification can be determined every two minutes, allowing rapid changes in extracellular acidification to be elucidated.[15]

Extracellular acidification is directly influenced by many factors, including lactate and carbon dioxide production, as well as the activity of hydrogen ion channels. However, the source of the change in extracellular acidification cannot be determined using the Cytosensor Microphysiometer as supplied. Therefore, the measurement of multiple elements allows for a better understanding of cellular metabolism. The Cytosensor has been recently modified to detect many important elements in cellular metabolism such as glucose, lactate, oxygen, and pH, resulting in the multianalyte microphysiometer (MMP), see Figure 3.[16-18] This device has been used to easily distinguish between fluoride, 2,4-dinitrophenol, and antimycin A which are common metabolic inhibitors of glycoloysis or the electron transport chain.[16]

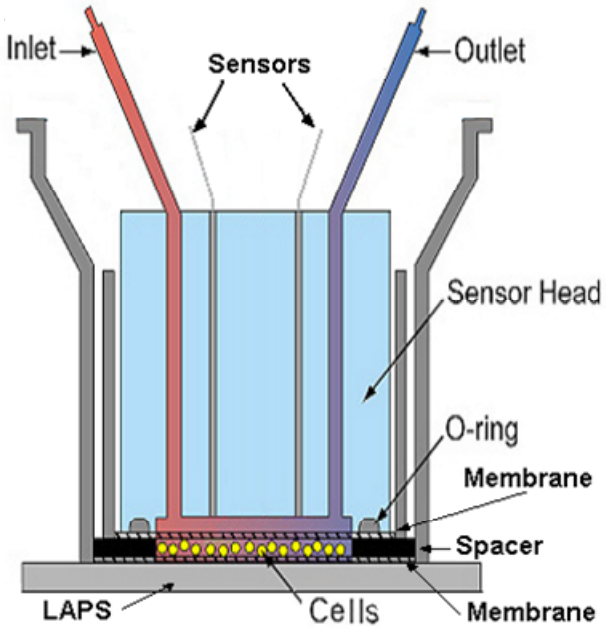

Figure 3. The multianalyte microphysiometer cell chamber and sensor head

Furthermore it has been able to differentiate between select list toxins such as botulinum neurotoxin A and ricin toxin with neuroblastoma cells, alamethicin and anthrax protective antigen with RAW macrophages, and cholera toxin and muscarine with CHO cells.[19]

Amino Acid Metabolism and Transport

Measuring extracellular concentrations of the compounds listed in Figure 2 gives a limited amount of metabolic information regarding the degree of aerobic or anaerobic metabolism. To obtain a more complete view of metabolism, a more detailed representation is required. In order to accomplish this, more compounds need to be considered. Due to the large role amino acids play in cellular metabolism, the measurement of amino acid flux would allow a more detailed view of cellular metabolism to be obtained.

There are two fates of amino acids metabolism in hepatocytes that result in the majority of amino acid flux as shown in Figure 4. One fate is gluconeogenesis, wherein amino acids are converted to TCA cycle intermediates or pyruvate where they can be used to make glucose. The other fate is ketogenesis, during which amino acids are converted to acetyl-CoA and converted to ketone bodies where other organs use them as fuel.[3] Protein synthesis, another fate of amino acid flux, can be ignored because the amino acid flux resulting from protein synthesis is an extremely small percentage of the total amino acid flux.[1]

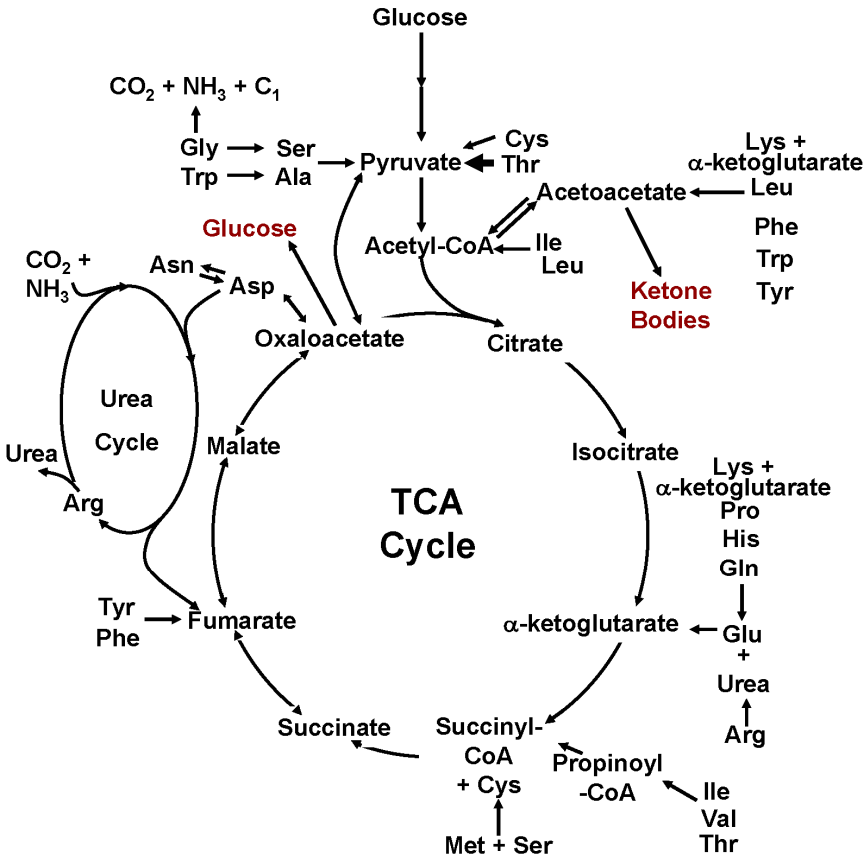

Figure 4. Amino acid catabolism and the urea cycle

Basal Amino Acid Flux and Hormonal Perturbations

In order to obtain an accurate perception of the change in amino acid concentration expected in our experiments, calculations with literature flux rates were performed. The literature flux values obtained were from primary hepatocytes cultured in 8 hour or 24 hour cultures. First, the change in the concentration in media caused by the basal metabolism of the cells was estimated. This was done by taking the flux rate from the literature[1] and converting it to the number of moles expected using the conditions in the MBR, that is, 2.0×10^5 cells being perifused at 0.5 µL/min with 2.0 µL media outside the cells. The percent change in the concentration of the media was

calculated from the number of moles in the 2.0 μL of media. Next, the percent change in flux rate caused by application of insulin or glucagon[20], two hormones that drastically change the metabolism of hepatocytes, was calculated by determining the percent change in the amino acid flux caused by the hormones. Finally, the percent change in the media caused by the change in flux was calculated by multiplying the change caused by the media by the change caused by the hormones. These results in the percent change in the concentration of the amino acids needed to observe the effects of insulin or glucagon. The results are shown in Table 2. Amino acids which have a large percent concentration change such as glutamine and glutamate which should be detectible by the AAFA, whereas those with a very small concentration change such as isoleucine and asparagine should not be detectable. Amino acids with intermediate percent concentration changes might be detectible depending on the reproducibility of the AAFA.

Table 2. Change in concentration of amino acids in DMEM:F-12 media caused by basal metabolism[1] of primary hepatocytes and the effect of insulin or glucagon[20] upon the metabolism using conditions found in the microbioreactor. Positive numbers indicate the concentration increases, while negative numbers indicate the concentration decreases.

Amino Acid	% Change Due to Basal Metab.	% Change Caused by Insulin	% Change Caused by Glucagon
alanine	-17	-4.6	-6.2
aginine	-11	-0.75	-3.5
asparagine	-1.0	-0.27	-0.45
aspartate	6.1	-6.4	-3.2
cysteine	-22	-8.9	-4.5
glutamate	67	17	0.0
glutamine	-34	-100	-100
glycine	-39	-6.5	-19
histidine	-11	-11	5.5
isoleucine	-5.2	-2.3	1.0
leucine	-6.8	-3.4	1.7
lysine	-17	-15	1.2
methionine	-38	0.0	0.0
phenylalanine	-34	-5.6	-14
proline	7.2	0.0	0.9
serine	-21	10.6	0.0
threonine	-10	-9.9	-3.3
tyrosine	-10	-6.4	-2.7
valine	-3.4	-10	0.7

Soft Lithography

In order to perform dynamic *in vitro* cellular perifusion experimentation, a device of a specific geometry must be made to contain cells in order to minimize extracellular volume and provide a smooth flow path for media across the cells. Soft lithography, which refers to any technique that employs an elastomer with embedded structures, is ideally suited for such a task. Originally, this elastomer was used as a stamp to form

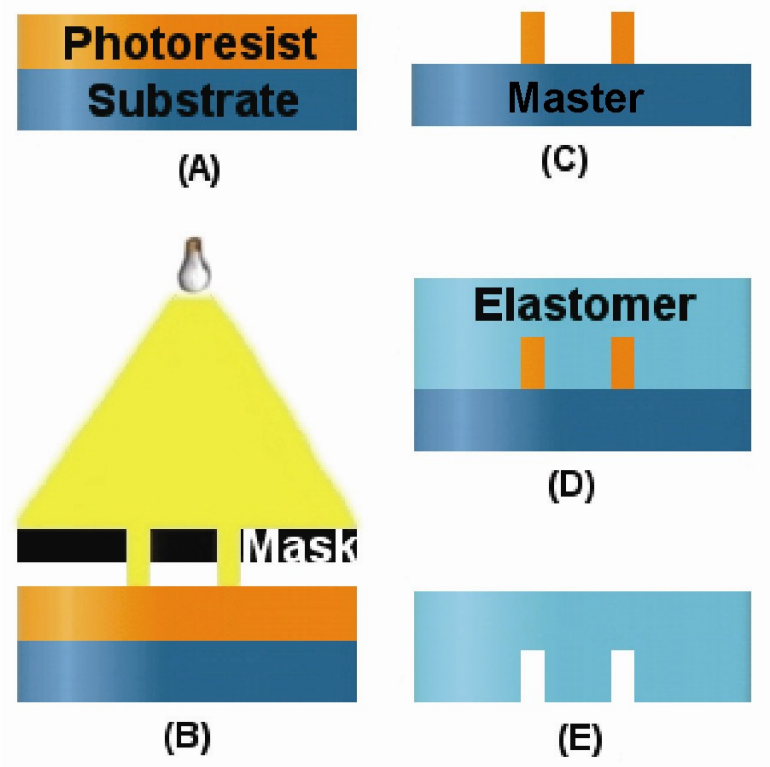

Figure 5. Process of fabrication of a soft lithographic device. A) Master construction begins by spinning a photoresist on a silicon substrate. B) A fabricated mask in the desired final shape is placed on the substrate and exposed to UV light, curing the photoresist in the form of the mask. C) The unexposed photoresist is developed away, completing master construction. D) Uncured elastomer is poured and molded over the master. E) After curing, the master is removed, producing the final elastomer.

other structures or patterned surfaces, but more recently, the elastomer itself is the desired product.[21-25] The process of generating the elastomer with microfabricated structures involves three steps: mask fabrication, master construction, and elastomer production. These three elements are shown in Figure 5.

A mask is used to define the relief in the desired structure via opaque and translucent regions. A mask can be fabricated by many different procedures depending on the resolution required. For low-resolution, a mask can be prepared using a simple

laser printer, while for high-resolution, a mask can be purchased from a variety of vendors.

A master is a mold used to make the desired structure. Construction of the master begins by coating a substrate, such as a silicone wafer, with a light sensitive resist. The resist can be any thickness up to ~100 μm. The mask is placed between a light source and the substrate during exposure of the master. The resist is only exposed to the light where the mask is translucent resulting in cross-linking of the polymer. Lastly, the resist is developed using a chemical developer that removes the unexposed portions of the polymer. While a negative resist is depicted in Figure 5, positive resists, where only the areas exposed to the light are removed during development, are also quite common.

An elastomer, often composed of Polydimethylsiloxane (PDMS), is the final product resulting from soft lithography. Production of the elastomer begins by pouring the elastomer prepolymer over the master where it conforms to the shape of the relief. The elastomer is then cured and removed from the master, producing the final structure. The elastomer can be used to form 3-D fluidic devices by bonding the elastomer to a substrate and providing fluidic access to the fluidic device. Using soft lithography, it is easy to create a cellular perifusion device of any shape desired. If one device becomes compromised, only the production of the elastomer must be repeated.

Microbioreactors

Microbioreactors (MBRs) are vessels which contain cells, either eukaryotic or prokaryotic, in a device which contains microliter quantities of cell media or broth. MBRs require some form of active nutrient exchange since cells are at a high enough

density to quickly deplete nutrients and build up waste products. Creating bioreactors on the microscale is advantageous for multiple reasons. They conserve valuable cell growth media and supplies, allow for easier access to parallel bioreactors to perform multiple simultaneous experiments, are less labor intensive to set up and run, and allow faster responses to be observed due to the decreased dimensions. MBRs can also be made inexpensively.[26,27] There is a great deal of variability within the design of MBRs. They may be designed to run for a time-period of a few hours to several weeks, there are several different ways to provide flow to the MBR, and there are a variety of materials in which MBRs are constructed.

There are many ways to feed media to a microbioreactor. The most common types of pumps used are the peristaltic pump[28-30] or syringe pump[27,31-36]. A peristaltic pump is useful for relatively high flow rates in the mL/min to high μL/min range. Syringe pumps are useful in the high to low microL/min range, but can only be used to dispense the volume contained within the syringe. When very low flow rates or long-term operation at low flow rates are desired, on-chip pumping mechanisms have been developed. Pneumatically operated, thin film PDMS is one mechanism whereby air pressure drives a thin PDMS film over a fluidic channel into the channel and occludes it. This creates a pneumatic valve. If a series of three or four of these valves are adjacent to each other in a channel, they can act like a pump when closed and opened in sequence.[37,38] Based on the same principle, Braille displays, in which pins are directly inserted over a fluidic channel can block the channel when activated.[39,40] Braille displays can be used as pumps in the same manner as pneumatic valves. Braille displays are simpler and occlude channels completely without special manufacturing techniques.

However, they are opaque and cannot be imaged through the way pneumatic PDMS pumps can.

A common manufacturing technique for MBRs is the use of photolithography. The power of this technique is that a 2-D design of nearly any complexity can easily be manufactured. The details of this technique were discussed in a previous section of this chapter. A few examples of how photolithography has been used to make microbioreactors follow. Tourovskaia created a series of round chambers based from a 1536 well plate in which each well was evenly perifused from one side of the chamber to the other.[31] Borenstein created several designs of an artificial capillary network of various capillary densities where endothelial cells were seeded in the network.[32] Wu created a parallel 30-well microfluidic device with on-chip pumping where one pneumatic input controlled the entire pumping action.[38]

Membrane bioreactors are another classification of bioreactor whereby cells are retained by means of a membrane and analytes are exchanged through the membrane. Saucer grew cells in a relatively large chamber which was perifused by thin hollow fibers progressing though the chamber.[41] Cells were introduced though a port into the chamber body and perifusion occurred through the fibers.[41] Villain created a hollow fiber membrane bioreactor for *E. coli*, with one set of fibers for media and one for gas exchange.[28] The presence of the gas exchange fibers greatly improved performance. Optical density (OD) and pO2 were measured, and cell growth and metabolism were comparable to shaker flasks.[28] As Villain showed, components in the media can be measured to acquire a basic picture of the metabolism of cells in a bioreactor.[28]

Oxygen, pH, and other parameters can be measured, and sometimes closed loop feedback control of these parameters is used to optimize cell growth rate and cell density. pH, oxygen, and OD have been measured in *E. coli* bioreactors.[28,36] Korin made linear microbioreactors and modeled oxygen and shear stress while measuring growth rate under various flow conditions as well as stop-flow.[34,35] pH and oxygen were measured from a stop-flow bioreactor in which instruments were calibrated during stop flow, and cellular metabolic rates taken during flow.[30] Oxygen concentration gradients were measured across a microfluidic channel.[29] Oxygen and pH were under closed-loop control in parallel *E. coli* bioreactors. pH was controlled by periodically injecting base from an on-chip reservoir and oxygen was introduced through pneumatic valves.[37]

The work presented uses a hepatocyte cell line. Primary hepatocyte culture systems frequently have unique applications and thus necessitate unique designs of MBRs. Some potential applications of primary hepatocyte MBRs include study of *in vitro* drug metabolism or use as a bioartificial liver.[42,43] Gebhardt describes a perifused hepatocyte system for the short or long-term (1 to 7 days) culture of hepatocytes by either recirculating media or sending effluent to waste.[42] Ostruvidov describes a system whereby hepatocytes are grown on a membrane where perifusion occurs both above and below the membrane simultaneously, which increases liver functions over bathing on only one side.[44] There have been several devices which have been designed to replace the functions of the liver while a patient awaits a donor liver or until the liver regenerates natural function, and two devices have been used in phase I clinical trials.[43]

This very brief overview of microbioreactors is not meant to be an all-encompassing review of different designs. There is a substantial literature on ways in

which cells have been successfully grown in a microfluidic environment. This presentation was only designed to show a few examples of the great variety of different designs that have been successfully applied to the growth of cells in a miniature environment.

Capillary Electrophoresis

Capillary electrophoresis (CE) is a high resolution, batch method for the separation of small samples. CE separates analytes based on differences in their charge to size ratio, termed the electrophoretic mobility, under the influence of an electric field. A sample is injected at one end of a capillary and a high voltage is applied between the two ends of the capillary, providing both the bulk flow though the capillary, termed electroosmosis, and the electrophoretic mobility. A detector positioned on the opposite end of the capillary measures analytes as they pass.

CE separates analytes based on differences in electrophoretic mobility, μ_{ep}, which follows

$$\mu_{ep} = \frac{q}{f} \tag{1}$$

where q is the net charge on the molecule and f is the friction coefficient, which is proportional to the size of the molecule and the viscosity of the solution. The total or apparent mobility (μ_{app}) of the analyte is the sum of the electrophoretic mobility (μ_{ep}) and the electroosmotic mobility (μ_{os}). Electroosmosis is bulk movement of solution toward one end of the capillary and results from the negatively charged silanol ($S\text{-}O^-$) groups on the inside wall of the fused silica capillary. An electric double layer forms between the negatively charged capillary and the positively charged solution at the capillary wall.

When an electric field is applied, the cations are attracted to the cathode while the anions are attracted to the anode. The positively charged solution at the walls of the capillary drives the solution toward the cathode. Frequently, the electroosmotic mobility is greater than the electrophoretic mobility; thus, all analytes move toward the cathode. In addition, electroosmosis is an advantageous method of fluid flow because the fluid velocity is the same at any point along the radius of the capillary, in comparison to pressure driven fluid flow, which creates a parabolic flow profile with higher velocity in the center and lower velocity near the walls. Additionally, CE is not subject to band broadening due to mass transfer and multiple paths, as is typical of chromatography. These result in decreased band broadening and increased resolution for CE in comparison to high-pressure liquid chromatography (HPLC).

The efficiency of the column to separate analytes is expressed as the number of theoretical plates (N), which follows:

$$N = \frac{\mu_{app} V}{2D} \tag{2}$$

where V is the applied voltage and D is the diffusion coefficient. Thus, the greater the voltage applied, the greater the number of theoretical plates, and the separation efficiency assuming longitudinal diffusion is the only source of band broadening. Thus, a longer capillary length does not necessarily equate to a more efficient separation. By having a high voltage and a short capillary length, very quick and high-resolution separations can be accomplished. Several sources cause variation from equation 2, including capillary heating, termed joule heating, injection plug length, detector length, and adsorption to the capillary walls.

Joule heating, resulting from the current due to the high voltage used in CE, results in the generation of heat and causes deviation from Equation 2. This creates a temperature gradient from the middle of the capillary to the outside edge, resulting in turbulence and band broadening. This heating is minimized by decreasing the electric field, decreasing the ionic strength of the separation buffer, cooling the capillary, and reducing the ID of the capillary.

Injection plug length is another potential source of band broadening. The sample is injected into the capillary through either hydrodynamic or electrokinetic injection. Hydrodynamic injection involves the use of a pressure difference between the ends of the capillary to drive the sample into the capillary. Electrokinetic injection involves the application of a voltage across the capillary, pulling sample in due to μ_{app}. With both of these methods, appropriate conditions need to be determined in order to provide enough sample for reliable detection, but not too much which leads to excessive band broadening.

Over extended replicate separations, molecules can adsorb to the wall of the fused silica capillary. This reduces the charge on the wall of the capillary and reduces the electroosmotic flow. This results in excessive band broadening and loss of resolution. Proteins and peptides are particularly prone to adsorption on fused silica capillaries. To reduce this effect, proteins can be removed from the solution or the walls can be coated with compounds which change the surface of the capillary. This change serves to prevent protein adsorption to the wall and prevent band broadening.

Most amino acids have not net charge and hence have no electrophoretic mobility and therefore cannot be separated by traditional capillary zone electrophoresis, which is

the type of CE that has been presented. In order to allow the separation of analytes with no charge, another driving force for separation is needed. Thus, micellar electrokinetic chromatography (MEKC) was created. In MEKC, a compound which forms micelles, such as sodium dodecylsulfate (SDS), is added to the electrophoresis buffer. The center of the resulting micelles is hydrophobic, allowing the micelles to act as a pseudostationary phase in which analytes can partition. Each derivatized amino acid has a different affinity for the micelles and is uniquely partitioned into them. Hence, when amino acds in solution encounter micelles, the fraction of time that molecule spends bound to any micelle depends upon the unique hydrophobicity of that amino acid. A free amino acid will migrate with the velocity of the solution while a bound amino acid will move with the velocity of the micelle. This partitioning is analogous to reverse-phase liquid chromatography where the more hydrophobic the analyte, the more it will be retained by the stationary phase. Therefore, in MEKC, analytes are separated by both their charge to size ratio and their hydrophobicity. The micelles have a particular μ_{ep} that which causes them to move at a different velocity than bulk solution. In the case of SDS, since they possess a negative charge, the velocity of micelles is significantly less than bulk solution. The more hydrophobic each individual analyte is, the larger the partition of that analyte into the SDS micelles, resulting in lower average velocity and hence longer retention time in the separation capillary.[45]

The last element of capillary electrophoresis is the detection of the separated analytes. While there are many CE detection methods, absorbance and fluorescence are the most common. Fluorescence detection is much more sensitive than absorbance, but the instrumentation is more complex and fewer analytes can be detected by fluorescence

than absorbance. Detection can be done on column, where the analytes are detected within the capillary, or end-column, where analytes are detected as they exit the capillary. Compounds which cannot readily be detected by these two modalities can be chemically modified by a number of derivatization reagents so that they can then be detected.

Unique challenges are put forth in CE based separations when speed of separation is of paramount concern. Several factors must be carefully controlled in order to produce efficient separation. In many cases, these are the same effects which cause band broadening and include joule heating, injection length, detection length, and detector sensitivity. In order to increase separation speed and increase resolution, higher electric fields and shorter capillaries are used. In order to prevent excess joule heating, smaller capillary IDs of 10 μm or smaller are frequently used. This reduction in size puts higher demands on detection and injection systems.[46]

For high-speed detection, laser induced fluorescence (LIF) has become commonplace. Lasers can be focused to a very small spot size and the high-intensity light increases the percentage of molecules in the excited state when compared to other light sources. Detection limits of yoctomoles (10^{-24} mol) and even single-molecule detection have been achieved using LIF detection.[47,48] The down side to LIF detection is that frequently analytes need to be derivatized in order to be detected.

Injection systems also require special attention as injection width is frequently the largest contributor to band broadening in fast separations.[49,50] One injection modality for fast separations is the optical gate. In this system, analyte is continuously introduced to the separation capillary. A high-intensity laser photobleaches the fluorophore near the inlet. To perform an injection, this laser is briefly stopped, resulting in a small plug of

non-bleached analyte which is separated. This method has been used to separate four FITC labeled amino acids in 140 ms.[51] A second injection modality is the flow-gate. In this method, a continuous stream of sample is divided from the separation capillary by a small gap (~100 μm) in which a strong gating flow that runs perpendicular to the sample and separation capillaries prevents the sample stream from contacting the separation capillary. During an injection, the gating flow is stopped, allowing the sample to make contact with the separation capillary and allowing an electrokinetic injection to be made. After the injection, the gating flow is resumed. Using this method, separations with over 480,000 plates in 35 s have been achieved with relative standard deviation of repeated injections of less than 4%.[52]

MEKC is particularly challenging to increases in separation time. Many factors that increase separation efficiency decrease with faster separation. In one study, three coumarine dyes were separated in a chip system. Only at low electric fields (<400 V/cm) were micellar-based band sources of broadening not contributing significantly.[49] In spite of these limitations, 10 amino acids have been separated by MEKC in less than 3 minutes with a 600 V/cm applied electric field.[53]

Application of Micellar Electrokinetic Chromatography to Rapid Separation of Amino Acids

Separation of amino acids by MEKC has received considerable attention due to the variety of fluorescent probes for amines, the continued miniaturization of CE instrumentation, as well as the importance of amino acids in a variety of biological processes. One area of biological importance is the use of amino acids and other amines as neurotransmitters. *In vivo* microdialysis of the rodent brain is an important

neuroscience tool. Traditionally, dialysate is collected and analyzed by HPLC offline. However online analysis of dialysate with CE separation is becoming popular. The first demonstration of online neurotransmitter detection with high recovery, multiple analyte detection, and good temporal resolution was published by Lada et.al.[54] The online coupling of microdialysis to capillary electrophoresis was accomplished by use of a flow-gate. The flow-gate was originally developed to couple capillary chromatography with capillary electrophoresis and was later adapted for use with coupling microdialysis to CE.[55,56] The initial success of online CE was further improved by reducing the capillary ID from 25 μm to 10 μm and implementing off-capillary detection using a sheath-flow cuvette.[57] This resulted in a reduction of separation from 300 s to 20 s while increasing the number of theoretical plates from 120,000 to over 500,000, and improving sensitivity by ~ 15-fold.[57] The derivatization reagent used for the two studies is OPA, which is excited in the UV but reacts very quickly (10-30 s). NDA is brighter than OPA, is excited at 440, but is slower to react at 120-240 s. The use of NDA allows the use of a less expensive laser and on-capillary detection. It was shown to provide comparable separation time and efficiency as OPA methods and still provide a very quick response time of 12-18 s, less than the time of a typical electropherogram.[58] More recently on-chip separation has been performed, although with reduced separation efficiencies, but results in a much simpler and smaller setup.[59,60]

On-chip capillary electrophoretic separation of amino acids is of great interest due to the small format and reduced complexity of chip based separations. To that end, there has been much development in on-chip amino acid separation using micellar electrokinetic chromatography. Heeren et al. separated six FITC amino acids

with a variable path length chip.[61] Minimal time to separation was less than 80 s with 101,000 plates. %RSD of peak area was 0.78 for arginine with a limit of detection of 3.3 nM. Xu et al. performed two-dimensional separations of 20 amino acids. [62] MEKC was used as one dimension with CZE as another. Separation took 20 minutes. Culbertson et al. created a 25 cm long spiral separation channel. [63] Over 1 million plates were possible with the chip. Nineteen TRITC labeled amino acids were separated in 165 s with an average number of theoretical plates of 280,000 with minimal resolution between peaks of 1.2. Chiral on-chip separation of amino acids has also been performed. Rodriguez et al. performed enantiomeric separations of 14 pairs of FITC-amino acids individually in less than 160 s using SDS and CD in the separation buffer resulting in 7000-28000 theoretical plates.[64] Ro et al. performed chiral separation of 5 amino acids with the derivatization reagents OPA/2,3,4,6-tetra-*O*-acetyl-1-thio-b-D-glucopyranose and no chiral selectors in the running buffer.[65] Resolutions were 2.5-6.1 for various diastereomers with separation times of less than 90 s.

One of the most interesting applications of on-chip separation of amino acids is the development of sensors to detect signs of life on Mars. The miniaturization provided by on-chip analysis is an absolute necessity. The first attempt resulted in baseline resolution for 4 FITC-labeled amino acid enantiomers plus glycine in 4 minutes.[66] These values closely matched that of HPLC upon analysis of the Murchison meteorite. Labelling with fluorescamine is also possible and results in limits of detection of ~50 nM.[67] The first complete Mars Organic Analyzer (MOA) with pumps, valves, and CE separation was completed in 2005.[68] Sensitivities of μM to 0.1 nM were demonstrated, and field tests of soil extracts from the Atacama Desert, Chile, were

performed with the MOA, including sample preparation, labeling, separation, and detection. More recently, the fluorescent probe Pacific Blue succinimidyl ester (PB) was used on the MOA.[69] This provides a 200-fold increase in sensitivity and increased resolution. 75 pM detection sensitivities were realized with resolution of 25 amino acids. There are a variety of applications and multiple instrumental configurations for separation and detection of amino acids with MEKC. Some of those techniques provide exceptional separation time, resolution, and sensitivity.

Fluorescent Derivatization of Amino Acids for Detection in Analytical Systems

Underivatized amino acids are difficult to detect and distinguish from other small molecules in a complex solution such as cell media. Fortunately, the fluorescent labeling of amines has developed as an industry standard so that it is now easy to label the amino acids in order to make them easier to detect. A common labeling method is a covalent reaction to the α-amine forming a fluorescent product. An extensive number of reagents have been formulated which label amines.[70] The properties of the derivatization reagent used for this project are: the reactants are non-fluorescent, the reaction occurs fairly rapidly at room temperature, the reaction occurs in an aqueous solution, the procedure does not require extraction steps, the reaction is quantitative, and the final

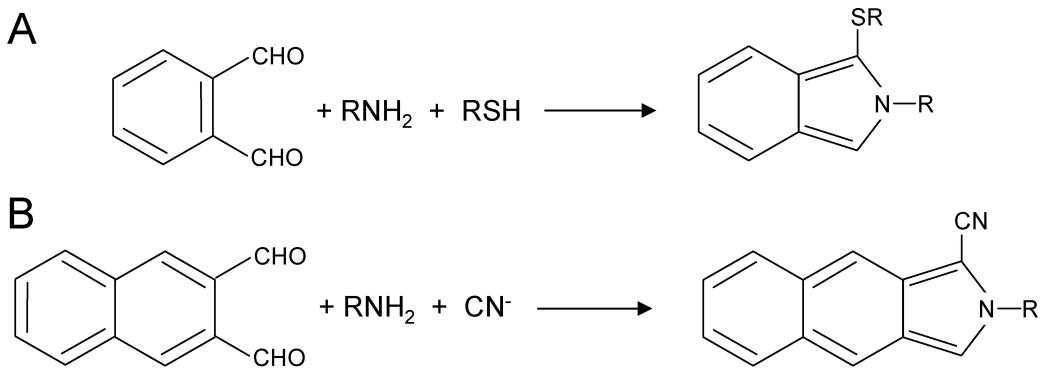

Figure 6. Reactions of primary amines with A) OPA/RSH and B) NDA/CN^-

product is very brightly fluorescent. There are two common reagents which meet these criteria, o-phthaldialdehyde (OPA)/organic thiol (R-SH) and naphthalene-2,3-dicarboxyaldehyde (NDA)/cyanide (CN^-). The reactions of OPA/R-SH or NDA/CN^- with a primary amine are shown in Figure 6.

Some properties of OPA and NDA derivatives are shown in Table 3. OPA is excited in the UV while NDA is visible. OPA has a considerably shorter reaction and degradation time in comparison to NDA.

Table 3. Properties of OPA/RSH and NDA/CN^- reaction with amino acids. Reaction times from Shou et al.[58], all other data from de Montigny et al.[71]

	Typical excitation max, nm	Typical emission max, nm	Typical reaction time, s	Degradation time
OPA derivative	340	450	10 – 30	$t_{1/2}$ = 1.5 hr
NDA derivative	420	490	120 – 240	< 10% in 10 hr

Fluorescent properties of selected NDA amino acid derivatives are shown in Table 3. The absorption and emission max are very similar for all three amino acids. However, the intrinsic fluorescence sensitivity, a measure of the brightness of each fluorophore varies considerably from amino acid to amino acid.

Table 4. Fluorescent properties of specific NDA-amino acid fluorophores.[72]

	Absorption max, nm	Molar absorptivity	Emission max, nm	Quantum efficiency	Intrinsic fluorescence sensitivity
Glycine	442	8900	493	0.75	2.3
Alanine	443	6500	496	0.73	1.5
Lysine	440	6500	486	0.55	0.7

CHAPTER II

RAPID AND PRECISE DETERMINATION OF CELLULAR AMINO ACID FLUX RATES USING HPLC WITH AUTOMATED DERIVATIZATION WITH ABSORBANCE DETECTION

Abstract

A method is presented for analyzing primary amino acids in complete cell media using an Agilent 1100 HPLC with a Zorbax Eclipse Plus C18 column with absorbance detection. Amino acids are derivatized with OPA using an online method, which decreases preparation time while increasing reproducibility over traditional offline methods. The method is rapid, with an injection-to-injection time of 26 min, and highly reproducible, with a %RSD of peak area of 0.9 to 4.1 for all amino acids, and most between 1 and 2%. Furthermore, this technique is applied to analysis of amino acid flux in the hepatocyte cell line AML12. The flux rate is quantifiable for 18 of 19 amino acids.

Introduction

Determination of amino acid flux in cultured cells is an important indicator of the metabolic rate and health of those cells. It can also be used as an indicator of the remaining carbon and nitrogenous fuel available. This is especially true in hepatocyte and hepatoma cells lines where extensive gluconeogenesis, urea production, and protein synthesis may consume larger quantities of amino acids than other cell types.

HPLC with pre-column derivatization is a standard technique in the analysis of amino acids. Pre-column derivatization of free amino acids in solution for HPLC

separations with UV or fluorescence detection is at times done offline, manually. Some immediate drawbacks to offline derivatization are sources of error due to operator skill, experience and laboratory technique, extra sample manipulation, additional time required, and increased risk of contamination. Automated online derivatization minimizes these error sources, immediately improves precision, and saves time. A rugged high-resolution HPLC method including online derivatization therefore can increase productivity compared to offline methods.

The small sample volume (1 μL), consistent automated OPA-derivatization using injector programming of the HPLC's autosampler, and short, highly efficient columns generate a rapid, reproducible amino acid method ideal for cell culture media. This method is convenient because the cell media samples are simply transferred to autosampler vials and analyzed. The selectivity of the Eclipse Plus C18 and the gradient mobile phase provide high resolution of 19 primary amino acids.

Experimental

HPLC

The Eclipse Plus AAA (amino acid analysis) method was performed using an Agilent 1100 HPLC system and is an adaptation of previously used methods:[73,74]

- G1312A binary pump, flow rate: 1.5 mL/min.

Gradient Timetable:

Time (min)	%B
0.0	2.0
0.5	2.0
16.0	47
16.1	100.0
19.5	100.0
19.6	2.0
Stop time 21.0	

- G1329A thermostated autosampler, with injection program:

1. Draw 2.5 µl from Borate vial (0.4 M, pH = 10.2)
2. Draw 1.0 µl from Sample vial
3. Mix 3.5 µl "in air," max speed, 5x
4. Draw 0.0 µl from water vial (needle wash)
5. Draw 0.5 µl from OPA vial (10mg/mL ortho-phthaldildehyde, 10mg/mL 3-mercaptopropionic acid)
6. Mix 4.0 µl "in air," max speed, 10x
7. Draw 0.0 µl from water vial (needle wash)
8. Draw 32 µl from Injection Diluent vial (Mobile phase A with 1.5% v/v conc. H_3PO_4)
9. Mix 20 µl "in air," max speed, 8x
10. Inject
11. Wait 0.1 min
12. Valve bypass

- Thermo Scientific Hot Pocket column heater, set to 40°C

- G1314AC Variable Wavelength Detector (VWD) 338nm wavelength 13.74Hz

Column

ZORBAX Eclipse Plus C18, 4.6 x 150 mm, 3.5 μm, PN 959963-902 with Eclipse Plus C18 4.6 x 12.5 mm, 5 μm Guard Cartridge PN 820950-936 in Guard Column Hardware Kit PN 820888-901

Mobile Phase and Injection Dilutent

Mobile Phase A: 2.8 g anhydrous Na_2HPO_4 + 7.6 g $Na_2B_4O_7.10\ H_2O$ + 16 mg NaN_3 in 2 L H_20. This makes a solution 10 mM in phosphate and 10 mM in borate. Adjust pH with 2.7 mL concentrated HCl, then add 100 μL aliquots until pH 8.15 (approx. 300 μL). Optional 8 ppm sodium azide prevents microbial growth.

Mobile Phase B: methanol: acetonitrile: water (9:9:2, v:v:v)

Instrument Control and Peak Integration

The Agilent 1100 HPLC was controlled by the Handheld Control Module with the exception of the VWD. The VWD, data collection, and peak integration were performed on a PC using Xcalibur software (ThermoFinnigan).

Cell Media and Amino Acid Standards

Complete Cell Media: 1:1 mixture of Dulbecco's modified Eagle's medium (DMEM) and Ham's F-12 media with 10% fetal bovine serum, 5 μg/mL insulin, 5 μg/mL transferrin, and 5 ng/mL dexamethasone.

Amino Acid Standard: Amino acid standard from Thermo Scientific PN 20088 with additions of l-glutamine, l-asparagine, and l-tryptophan. Standard was diluted to make the concentration of each amino acid 800 μM, except cystine, which was 400 μM.

Internal Standards: Internal standards were made using 80% cell media with 20% internal amino acid standard. Dilutions of this standard were used to prepare a calibration curve with five equally spaced points. The most concentrated internal standard increased the concentration of the standard relative to the cell media by 160 μM for most amino acids; exceptions were 320μM each of l-threonine, l-leucine, l-isoleucine, l-valine, and l-lysine, 1600 μM of l-glutamine, and 32 μM of tryptophan.

Cell Culture

The non-transformed hepatocyte cell line AML12 [75] was cultured in 5 wells of a 12-well plate at a density of 1×10^5 cells per well in 1 mL cell media described above. After 3 hours, the media was aspirated and cells were rinsed with Hank's buffered salt solution (HBSS) to remove any dead or unattached cells and 1 mL fresh media was applied. In addition, 5 wells of the sample plate were filled with 1 mL cell media without any cells. Each day for 3 days 50 μL media was collected from each well and 50 μL fresh media replaced. Collected media was stored at -20°C until analysis. After the final collection, the media was aspirated from all wells and cells were rinsed 3x with HBSS. Plates were stored dry at -20 °C for DNA assay.

DNA Quantification

DNA quantification was performed using a picogreen assay (Invitrogen) according to the supplied directions. Cells were lysed with Cell Culture Lysis Buffer (Promega) using 4 freeze-thaw cycles. The calibration was performed using a linear range of DNA standard from 0-4 μg/mL DNA. All calibration standards were run in duplicate, and all samples were run in triplicate. Fluorescence was measured on a CytoFluor II plate reader at 485/530 nm. DNA concentrations from all samples were averaged and subtracted from the averaged media controls to obtain the final concentration of DNA.

Results and Discussion

Complete cell culture media was analyzed on an Agilent 1100 HPLC using the conditions described in the experimental section. The chromatogram was compared to an amino acid standard solution containing 800 μM of each of the 20 standard protein amino acids (shown in Figure 7). The retention time of each amino acid in the culture media closely matches that of the amino acid standard. The concentration of each amino acid in the media is also labeled on the figure. Peak 19, lysine, contains two primary amine groups, thus doubling the concentration of fluorophores and doubling the relative peak intensity.

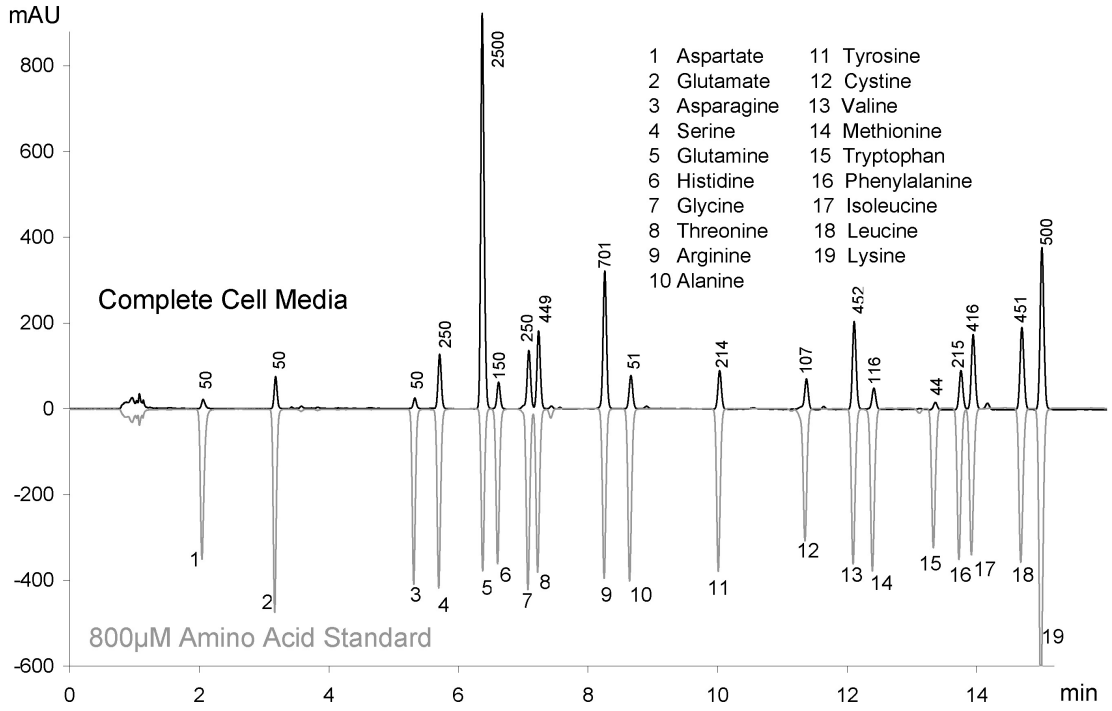

Figure 7. Separation of complete DMEM:F12 cell media (positive axis), 800µM amino acid standard (negative axis) on Agilent Eclipse plus C18 column on Agilent 1100 HPLC. Concentration of amino acids in media (µM) shown above each peak and the number of the amino acid in the key is shown below.

The reproducibility of this HPLC technique was measured by calculating the percent relative standard deviation in peak area and retention time for 5 complete cell media samples as shown in Table 5. The chromatograms were collected in one continuous sequence which included 39 samples. The individual replicates were spaced evenly throughout the sequence. Therefore, the standard deviations represent both random error and instrumental drift over almost 17 hours of continual instrument use. All but two amino acids demonstrated a relative percent standard deviation of less than 2% in peak area, and all amino acids demonstrated a less than 0.5% deviation in retention time with 12 of the 19 being less than 0.1%.

Table 5. Relative percent standard deviations of peak areas and retention time of 5 samples of online OPA derivatized amino acids in complete DMEM:F12 cell culture media. Peak numbers correspond to the numbers in **Figure 7**.

Amino Acid	Peak #	Peak Area %RSD	Retention Time %RSD
Aspartate	1	1.9	0.44
Glutamate	2	1.0	0.22
Asparagine	3	1.3	0.21
Serine	4	1.2	0.19
Glutamine	5	1.1	0.14
Histidine	6	1.2	0.13
Glycine	7	0.87	0.077
Threonine	8	4.1	0.062
Arginine	9	1.0	0.11
Alanine	10	1.1	0.052
Tyrosine	11	1.0	0.070
Cystine	12	2.7	0.048
Valine	13	1.4	0.045
Methionine	14	0.64	0.036
Tryptophan	15	1.9	0.041
Phenylalanine	16	1.3	0.040
Isoleucine	17	1.3	0.039
Leucine	18	1.0	0.061
Lysine	19	0.90	0.037

AML12 hepatocytes were cultured for 3 days in a 12-well plate. In addition, media without cells was also placed in the same plate as a control. Five replicates were cultured and aliquots were taken from each well for each of 3 days. Shown in Figure 8 is an example series of partial chromatograms from each of the 3 days, including a media control. As can be seen, glutamine decreased in concentration while glutamate increased in concentration due to flux from the cells. Other amino acids shown did not change appreciably. Since the cultured cells were replicating, the magnitude of the change increased for each successive day as the number of cells increased.

Quantitative flux rates of amino acids could be obtained for the AML12 hepatocytes as shown in. This was done by subtracting the media over cells from the control media without cells. To obtain accurate concentration changes, a five-point calibration curve, using internal standards as described in the experimental section, was constructed. The slope of this calibration was used to determine the change in

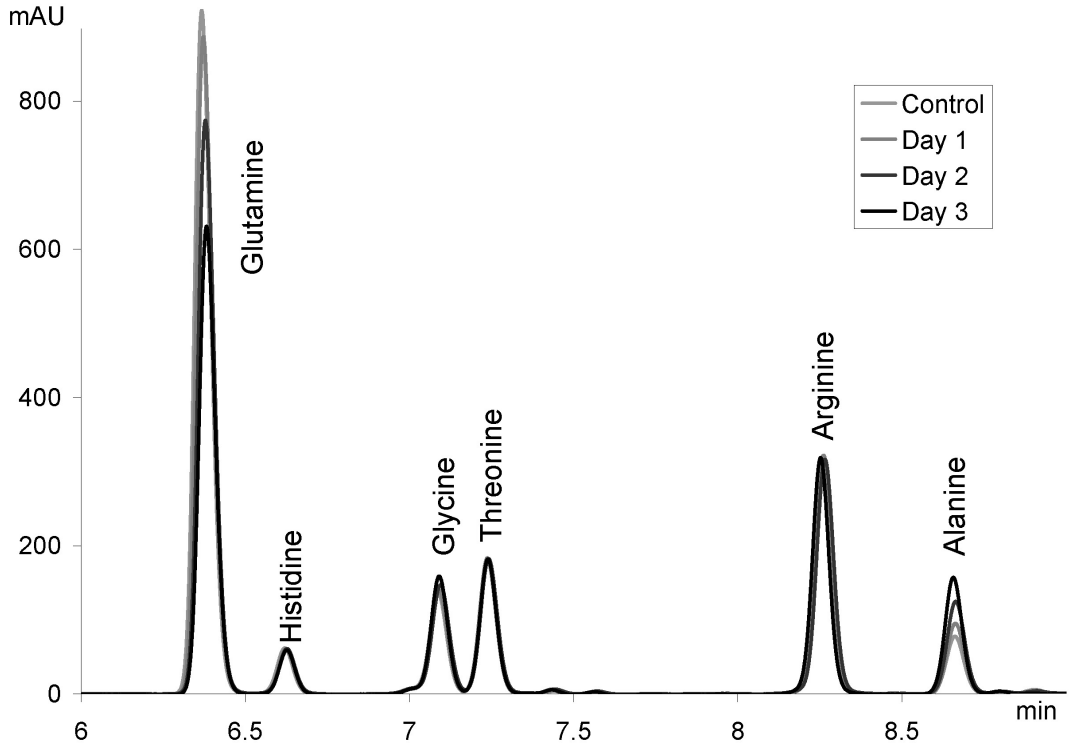

Figure 8. Time series of amino acids in cell media in contact with AML12 hepatocytes.

concentration. Data were normalized to DNA. The error represents the 95% confidence interval and was calculated by propagating the error from the media control, media over cells, and the calibration. A change in the amino acid concentration, demonstrated by having the confidence interval less than the calculated flux rate, was demonstrated for all but one amino acid. The high reproducibility is demonstrated given that the flux rate could be observed even though the percent change in amino acid concentration caused by the cells was as low as 5%.

Conclusion

Cell culture media was easily analyzed for primary amino acids with the Agilent 1100 HPLC equipped with a Rapid Resolution Eclipse Plus C18 column. Samples were

Table 6. Flux rates for cultured AML12 hepatocytes in complete cell media. Data is ± 95% confidence interval.

Amino Acid	Flux Rate (μmol day^{-1} mgDNA^{-1})
aspartate	-6.9 ± 0.8
glutamate	13 ± 2
serine	-38 ± 4
glutamine	-310 ± 20
histidine	-8 ± 2
glycine	18 ± 7
threonine	-8 ± 10
arginine	-21 ± 11
alanine	87 ± 5
tyrosine	-10 ± 3
cystine	-8 ± 2
valine	-25 ± 7
methionine	-14 ± 3
tryptophan	-3 ± 2
phenylalanine	-14 ± 3
isoleucine	-19 ± 6
leucine	-30 ± 6
lysine	-31 ± 7

measured using an automated online OPA-derivatization method. Reproducibility was exceptional (0.90-4.1%RSD), and likely better than offline precolumn derivatization methods due to minimizing several sources of error. The method is also rapid for standard pressure HPLC, with an injection-to-injection time of 26 min.

The method was used to measure quantitative flux rates of amino acids from AML12 hepatocytes. Flux rates could be measured in 18 of 19 amino acids despite having changes in concentration of amino acids in the media as low as 5%.

Acknowledgements

We would like to thank Rachel Greene and the Jeff Davidson group for the donation of supplies and technical assistance for the DNA assay. This work was funded by the National Institute of Allergy and Infectious Diseases (NIAID) Grant 1 U01 AI061223.

CHAPTER III

A HIGH-DENSITY PERIFUSED MICROBIOREACTOR WITH SIMULTANEOUS EFFLUENT COLLECTION AND CELL VIEWING FOR DETERMINATION OF AMINO ACID UPTAKE AND RELEASE

Abstract

A great advantage offered by microfluidics is the ability to use flow in restricted channels to maintain cells at a much higher density than is possible with conventional adherent or suspension cell culture. We present a microbioreactor (MBR) perifusion device that is capable of perifusing cells at a very high cell-to-media volume ratio while simultaneously visualizing all of the cells contained in the chamber. Our MBR contains ~2×10^5 AML12 hepatocytes in a poly(dimethyl)siloxane microfluidic cell chamber that has a cell growth area of 1.7 cm^2 with a volume of 4.2 μL. We confirmed high viability of cells in the MBR. The pH of solutions entering and exiting the MBR was similar to that in traditional cell culture. The effluent was collected and amino acid flux was determined using two separate methods. Glutamine and glutamate concentration change was monitored using HPLC-MS, and the amino acid flux rates were determined for 19 primary amines using HPLC. Fluxes for 15 of the 19 amino acids were determined to be non-zero, and 9 correlated with previous literature values determined from static 24 hour well plate experiments on primary hepatocytes. In this system, less than 5 minutes of media contact time is equivalent to 24-hours of contact time using traditional cell culture techniques, while continuous perifusion ensures cell viability. The observation of

dynamic changes in cell metabolism will be possible due to the high cell-to-media volume ratio resulting in rapid changes in the composition of the media.

Introduction

In the post-genomic, post-proteomic era there is an ever-increasing need for experimental methods which can acquire highly dynamic, multi-scale physiological data from intact systems.[76] The data need to be collected with a high bandwidth in order to observe biological processes which have short time constants.[77,78] Traditional methods only measure one or two variables, at time constants on the order of hours.[79] But there is a push to collect more variables simultaneously with faster time constants to obtain a clearer picture of the dynamics of the cell as a whole.[76] To meet this demand, there is an increasing need for experimental methods which allow access to this information. Traditional methods which have high bandwidths include electrophysiological and fluorescence methods.[76] These methods can detect only a specific set of physiological variables, and hence techniques are being developed to obtain dynamic information about a wider array of biological processes. One method which is amenable to a wide array of detection schemes is perifusion devices.

Perifusion devices in which the perifusate is collected can be used in a wide array of instrumentation and bioassays. There commonly exist two main types of commercial *in vitro* perifusion devices. The first type consists of a transparent Petri dish or glass slide with adherent cells attached, from which measurements are taken optically or electrophysiologically, such as the perfusion chambers by AutoMate Scientific®. The perifusion device usually contains several hundred microliters of media over fewer than a

hundred thousand cells, providing for a very low cell-to-media volume ratio. Also, the flow of media is not directed across the cells but simply introduced near the edge of the dish and removed near the opposite edge. The purpose of the perifusion for this type of device is primarily to maintain a constant environment for the cells and a limitation is that it is not designed for effluent collection for later analysis. The second type takes measurements from the effluent.[42,80-83] The cells are contained in a small tube or vessel, which is optically opaque or of a geometry not conducive to optical measurements of the cells. The chamber has a large cell-to-media volume ratio and the flow of perfusate is designed to flow evenly past the cells. The perifusate is collected and analyzed by any instrumentation technique the researcher desires. These devices have been limited to tissue samples and large cell aggregates such as islets of Langerhans.[80,81] Another limitation of this type is that there is no way to visualize the cells in the chamber. Also, perifusion is usually performed at relatively high flow rates in comparison to the amount of biomaterial present, requiring increased sensitivity of assays which limits analysis to compounds not already present in the perifusate.

There are several examples of microbioreactors in the literature. Hung et al. demonstrated even perfusion across microbioreactor chambers and showed growth of cells for 7.5 days in the chambers.[31] Thompson et al. demonstrated optical measurements of cells in a bioreactor and observed dynamic changes in gene experession via changes in fluorescence.[84] Kane et al. seeded cells in a well, then assembled the microbioreactor.[85] Daily albumin and urea synthesis was measured on the effluent.[85] Additionally, the consumption of glucose, a compound already present in the culture media, has been measured in the effluent of microbioreactors.[86,87]

In this paper, we combine the many features of these microbioreactors into one device. The MBR presented allows for simultaneous viewing of cells during smooth, even perifusion of media across attached cells at a high cell-to-media volume ratio. This allows for dynamic measurements of collected effluent of compounds already present in the media. We have chosen to monitor the amino acid flux of AML12 hepatocytes. Using our design, we have been able to detect concentration changes in 18 amino acids from cultured hepatocytes in 5 minutes.

Materials and Methods

Microbioreactor Cell Chamber

The cell chamber was formed by a layer of PDMS in which microfluidics were molded. The PDMS microfluidic layer was applied to a glass slide, forming a chamber which held the cells being perifused (Figure 9A). To allow fluidic access to and from the microbioreactor, Nanoports™ (Upchurch Scientific) were adhered, according to the instructions of the manufacturer, to a glass slide over 1 mm diameter holes formed using a diamond tipped drill bit (UKAM Industrial Superhard Tools). Cell media was introduced to the MBR using a gastight Hamilton syringe in a syringe pump (PicoPlus, Harvard Apparatus) connected to 0.004" ID PEEK tubing via a leur lock and 10-32 coned fitting (Upchurch Scientific). The effluent from the chamber was collected for later analysis.

The fluidic design of the cell chamber (Figure 9B) consists of a series of binary flow splitters resulting in sixty-four 50 μm wide channels each with the same flow velocity. The central portion of the chamber consists of 50 μm × 50 μm square posts with 50 μm separations from each post. The fluid is collected through another identical series of flow splitters. The total volume of the empty microbioreactor is 4.2 μL with a surface area of 1.7 cm^2.

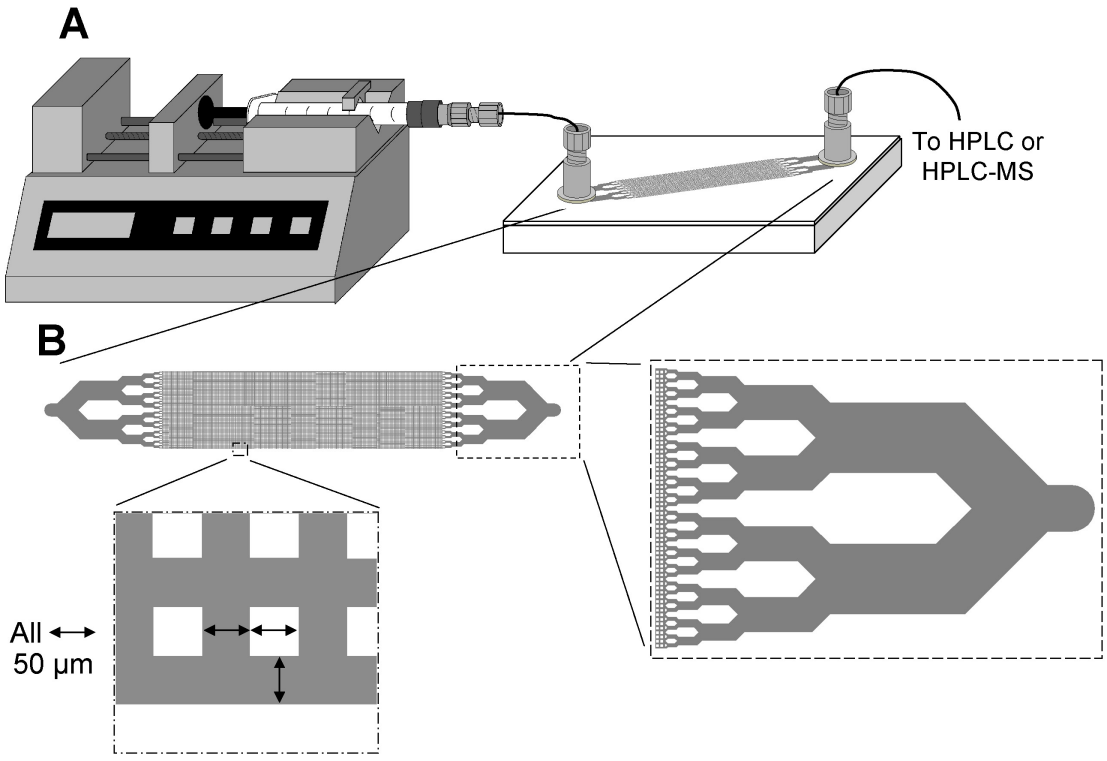

Figure 9. Overview of the operation of the microbioreactor (MBR). A) A syringe pump delivers cell media to the cell chamber via Nanoports™ adhered to a glass slide. The cell chamber consists of PDMS microfluidics clamped to the glass slide (clamp not shown for simplicity). The effluent leaves the cell chamber for analysis by HPLC or HPLC-MS. B) Design of the cell chamber where gray area the is cell chamber. A binary splitter delivers constant velocity of media across the width of the chamber body. The body contains 50 μm wide fluidic channels with 50 μm × 50 μm posts.

The PDMS microfluidics were created using standard rapid prototyping.[88] In brief, a master was formed on a silicon wafer from the negative photoresist SU8 by spinning SU8-2035 (MicroChem) at 3100 rpm for 30 s on a silicon wafer followed by a soft bake. A chrome mask was designed in AutoCad (Autodesk, San Rafael, CA) and created by Advance Reproductions. The mask was placed on the SU8 coated wafer and exposed to UV light at 300 mJ/cm^2 using an Exfo Novacure 2100 followed by a post expose bake. The master was developed resulting in a 25 μm thick SU-8 master in the design of the fluidics. To increase the visibility of SU8 on the wafer in order to aid in alignment at a later step, it was hard baked at 250 °C for 30 minutes.

To form the PDMS layer, Dow Corning Sylgard 184 was mixed in a 1:10 w/w ratio, vacuum degassed, poured over the silicon wafer master to a thickness of ~4 mm, and cured at 70 °C for 1-2 hours. To form the exact shape of the PDMS fluidic layer a guide consisting of the fluidic pattern printed on transparency paper was placed on the cured PDMS with the pattern on the transparency paper directly over the pattern on the mask. A scalpel was used to cut the PDMS around the edges of the transparency paper resulting in a 2" × 2" × 4 mm thick PDMS block with the molded fluidics positioned precisely in the center in order to allow for proper alignment of the inlet and outlet on the slide to be positioned over the inlet and outlet of the PDMS fluidics.

Cell Culture

All cell culture reagents were purchased from BioWhittaker, except dexamethasone, which was purchased from MP Biomedicals, LLC. AML12 cells were cultured as previously described.[75,89] Briefly, cells were cultured in 25 cm^2 flasks in

complete media. Complete media is 10% fetal bovine serum (BioWhittaker), 90% DMEM:F-12 1:1 mix with 5 μg/ml insulin, 5 μg/ml transferrin, 5 ng/ml selenium and 40 ng/ml dexamethasone. Cells were grown to 70-90% confluence and were suspended at 2.85×10^5 cells/ml for seeding in the MBR at 2×10^5 cells/0.7 ml.

Collagen Coating and Cell Seeding

Introduction of cells into the MBR was accomplished by seeding on an open-faced slide, followed by assembly of the PDMS fluidics on the slide and perifusion of the assembled MBR. In order to seed the cells on the slide, the slide was first cleaned, then collagen coated, sterilized, and seeded as depicted in Figure 10. In preparation for collagen coating the glass slide with fluidic ports (Figure 9C) was thoroughly cleaned by using the following procedure: dip the non-port side in piranha solution (3:1 conc. H_2SO_4:30% H_2O_2) for ~1 min, rinse with DI water, dip non-port side in a base bath (KOH saturated ethanol) for ~1 min, thoroughly rinse with DI water, dry by vigorous nitrogen blowing, and cover non-port side with Scotch® Magic Tape to remove any particulates. The tape was then removed and the glass slide was placed in a Petri dish in a sterile cell culture hood.

In order to form a well into which solutions could be dispensed and hence be contained on the glass slide, we utilized a small, custom-fabricated glass wall, as shown

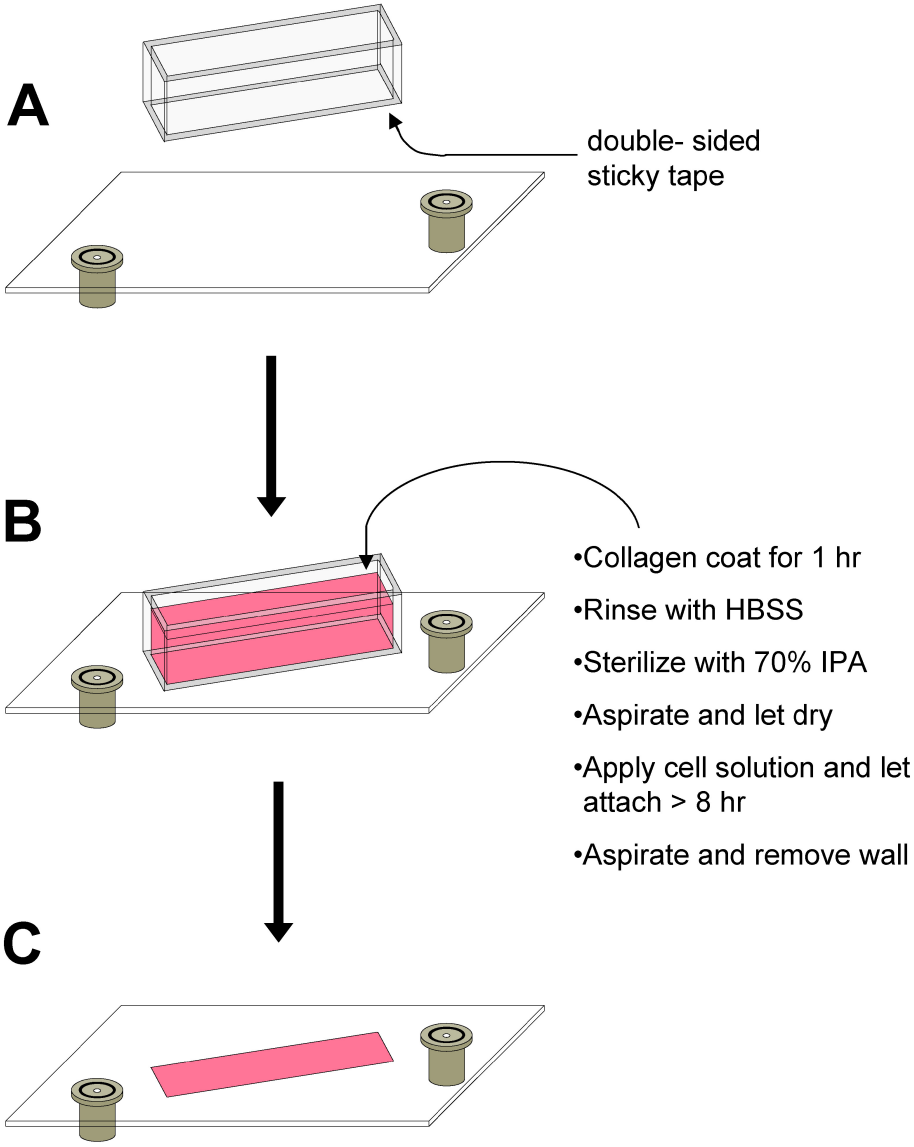

Figure 10. Procedure for seeding cells on glass slide. A) A silanized glass wall is applied to the glass slide with double sided 3M biocompatible tape cut to the size of the wall, taken care that the glass wall is centered between the nanoports B) The surface of the slide is collagen coated, alcohol sterilized, and the cell suspension is added. C) The cells are attached to the surface overnight, after which the cell media can be aspirated and the glass wall removed. The fluidics are now ready for immediate assembly in the clamp shown in Figure 11

in Figure 10. The glass wall was formed from a piece of square tubing which was cut and joined to form a rectangle with dimensions of 23 mm x 13 mm x 9.5 mm high. The glass wall was then silanized with 5% dimethyldichlorosilane (DMDCS) in toluene (Sigma-Aldrich) according to the manufacturer's instructions. The silanization reduces the meniscus formed when introducing aqueous solutions to the well, resulting in more even dispersion of attached cells.

In order to prevent bubbles from forming in the MBR microfluidics during assembly, the open-faced fludics must be filled with solution prior to assembly. Due to the hydrophobic nature of PDMS, aqueous solutions do not wet the surface; however, 2-propanol does. A few microliters of 2-propanol were used to wet the fluidic surface of the PDMS. Several hundered microliters of complete media were then put on the fluidics which will now wet the surface. Two cycles of aspiration of media and introduction of fresh media were performed in order to eliminate residual 2-propanol. The PDMS with complete media was put in a CO_2 incubator overnight.

The procedure to collagen coat and seed cells is shown in Figure 10. The glass wall was temporarily affixed to the glass slide by means of bio-compatible double-sided sticky tape (3M, 9965) (Figure 10A) forming a well. 50 μM collagen (Type I, rat tail, BD Biosciences) solution in 20 mM acetic acid was added to the well made by the glass wall. After 1 hr, the solution was aspirated and rinsed with HBSS (BioWhittaker). The well was sterilized by filling with 70% 2-propanol and sitting for 30 min. The 70% 2-propanol was aspirated and the slide was allowed to completely dry. A cell suspension of 2×10^5 cells in 700 μL was applied and the Petri dish was covered and placed in a 37 °C, 5% CO_2 incubator overnight to allow for cell attachment. The next day the media was

aspirated and rinsed with cell media to remove any unattached cells, followed by removal of the glass wall (Figure 10C). The PDMS fluidics were then immediately placed in the MBR clamp and perifusion was begun.

Microbioreactor Clamp

A clamp was designed to apply pressure between the fluidic layer and the 2" × 2" slide to prevent leaks and to align the inlet and outlet of the slide to the fluidics. The general construction of the MBR clamp assembly is shown in Figure 11. The brass clamp applies pressure between the PDMS fluidics, D, and top glass slide, C. It consists of the top, A, which screws to the base, F, with 6-32 socket-head cap screws and contains additional socket-head cap screws, with the ends sanded flat, which apply pressure to the spacer, B, against the slide, C. The top is designed to apply even pressure to the fluidics even if the thickness of the PDMS fluidics varies slightly. The bottom glass slide, E, provides a rigid and transparent support to complete the glass sandwich around the fluidic layer, further preventing leaks. The size of the fluidics is based upon the size of the two 2" × 2" glass slides, C and E.

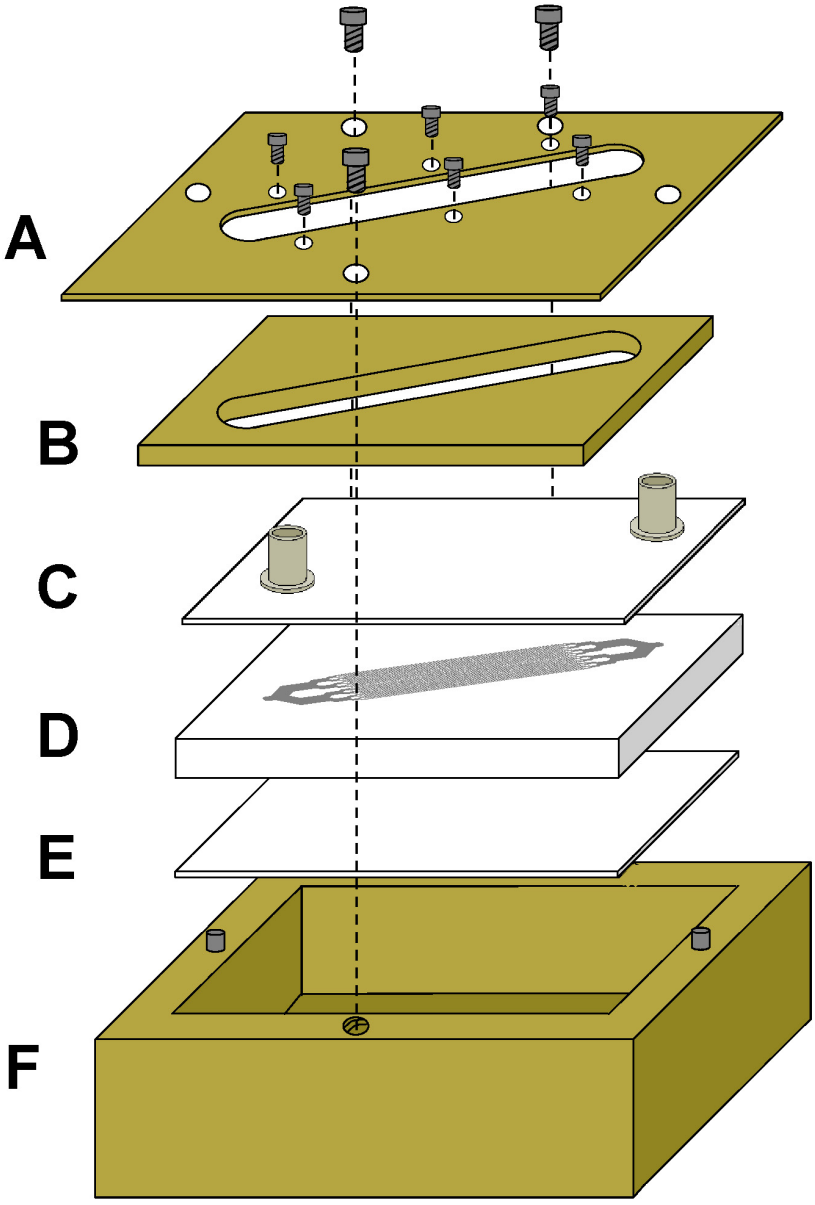

Figure 11. Design of microbioreactor (MBR) clamp for containing and perifusing cells. A) Top of clamp screwed to clamp base, with screws to provide a compressive force to seal fluidics. B) Spacer for distributing the force between top and fluidics. C) Glass slide with Upchurch Nanoports for fluidic connection. D) PDMS fluidic layer. E) Bottom glass slide. F) Clamp base with guide pins and screw holes.

Cellular Perifusion and Effluent Collection Using MBR

The MBR was assembled according to Figure 11. Care was taken to avoid introduction of air bubbles into the MBR during assembly by slowly placing the slide on the fluidics and filling the nanoports with media prior to assembly of the perifusion tubing. Cell media was perifused at 1.0 μL/min using a 500 μL gastight Hamilton syringe in a syringe pump (PicoPlus, Harvard Apparatus) connected to 0.004" ID PEEK tubing and checked for leaks using a microscope. Another length of PEEK tubing was connected to the outlet. Once fluid was exiting the outlet, the MBR was placed in a 37°C incubator and the flow was reduced to the starting flow rate for that experiment. After a 1 hr equilibration, collection of the effluent was begun.

Cell Imaging and Counting

Cells perifused in the MBR were imaged on a Zeiss Axiovert 25CFL using an Achromat 10x objective. Images were acquired using a CCD camera (QImaging Micropublisher 5.0). For cell counting and determining viability, the MBR was perifused with DMEM/F-12 base media containing 4 μM ethidium homodimer-1, which stains dead cells red, and 0.5 μM SYTO 11, which stains all cells green, from Molecular Probes for 30 minutes. Light from an HBO 100 lamp was filtered using a Chroma 11001 filter set. Images were taken from several locations and cell counts were determined from those images.

HPLC and HPLC-MS Analysis Amino Acids

HPLC-MS of glutamine and glutamate was performed using the following procedure. Dansyl derivatives of amino acids were formed by mixing 5 μL of MBR effluent sample, 5 μL isotopic standard with 5 μL 25mM Dansyl Chloride in acetonitrile and diluted with 100 μL 100 mM borate buffer, pH = 9. The isotopic standard consisted of 50 μM U-13C5; 15N l-glutamic acid and 500 μM U-13C5; U-15N2 l-glutamine (Cambridge Isotope Laboratories, Inc., Andover, MA) in 100 mM borate buffer pH=9. HPLC-MS analysis of glutamine and glutamate was performed on a Surveyor HPLC (Thermo Finnigan) with a Zorbax SB-C18, 2.1 x 50mm column on a TSQ Quantum (Thermo Finnigan) mass spectrometer in positive ion electrospray ionization mode. Masses were monitored as follows: glutamine (m/z 380), glutamate (m/z 381), glutamine and glutamate internal standard (m/z 387). HPLC mobile phase A was 95:5:0.5 water:acetonitrile:formic acid, and B was 5:95:0.5 water:acetonitrile:formic acid. The gradient ran from 0% B to 30% B after 4 min, then to 100% B after 5 min, and was held until 9 min; the column was reset to 0% B and flushed for 3 min prior to the next injection for an inject-to-inject time of 12 min. Peak integration was performed with Xcalibur.

After demonstrating amino acid flux, a second HPLC method for analysis of 19 amino acids was used as described previously.[90] Briefly, 5 μL of cell media was diluted to 25 μL in DI water. Separation was performed on an Agilent 1100 HPLC with an Agilent 4.6 x 150 mm Zorbax Eclipse Plus C18 column. Derivatization of amino acids by o-phthadialdehyde was automated using injection programming on an Agilent G1329A autosampler. Separation time was 16 minutes and injection-to-injection time

was 25 minutes. For each experiment, five replicates of 5 μL samples were collected in PCR tubes which contained 20 μL DI water at a flow rate of 0.5 μL/min for 10 minutes. This resulted in 25 μL total volume, the minimum required to ensure proper handling by the autosampler. After the experiment, 5 samples of media that were not introduced into the MBR were collected in the same manner to provide a control.

pH Measurments

Measurements of pH were recorded on a fiber-optic based WPI pH Optica micro. For measurements on media leaving or entering the MBR, the tip of the sensing fiber was placed into the pool of media exiting the tubing for 1-2 minutes until the pH stabilized. Measurments of the pH of the inflow to the MBR were performed after the conclusion of an experiment by disconnecting the inflow from the MBR and measuring the flow exiting the tubing. For measurements media from cells cultured in T-flasks, samples were aliquoted into microcentrifuge tubes, capped and then subsequently left at room temperature for 30 minutes. Measurements were made by uncapping the tubes and submerging the fiber into the liquid and allowing the measurements to stabilize.

Results and discussion

Microbioreactor Assembly

The design of the cell chamber is shown in Figure 9B. The binary splitter divides the flow into two identical streams with identical flow rates. Repeating this process several times in series ensures that the flow rate is the same across the width of the

reactor. The reactor consists of 50 μm square posts with 50 μm spacing. An early design consisted of 50 μm wide channels the entire width of the cell chamber; however, it was discovered that cell debris or a group of cells would frequently occlude the channel and prevent any fluid from traversing that channel.

PDMS replica molding was chosen due to the ease of creating new masters with differing heights. This allows the MBR to be tailored to the researchers needs. For example, a change in cell line might require an adjustment of chamber height or a different cell-to-media volume ratio. This is easily accomplished by creating a new master with different feature heights from the same mask.

The seeding of hepatocytes was accomplished with aid of a temporary glass wall, whereby various solutions could be introduced and contained within a specific area of the glass slide with ports. This method proved very successful. One problem initially encountered was the much higher density of cells near the edges of the wall than in the middle of the well. This was due to the tall meniscus which significantly increased the height of the cell suspension near the wall. The solution was to silanlize the glass wall with DMDCS making the surface of the glass hydrophobic and thereby producing essentially no meniscus at the wall. This resulted in an even density of cells across the entire MBR.

Since the cells are introduced into the chamber by first attaching them to one surface, a choice had to be made between the PDMS or the glass. Both techniques were demonstrated successfully; however, there were several reasons for choosing to adhere the cells to the glass slide. Seeding the cells to the PDMS inevitably requires cells to be seeded on the binary splitter portion of the cell chamber. This is not desirable as the flow

rates are not as uniform in the binary splitter as they are in the main chamber. After several trials, it was discovered that the morphology of the cells was closer to traditional cell culture techniques as well as more reproducible when cells were seeded on the glass slide. Seeding the cells on glass took fewer steps and was easier to accomplish, in part due to the difficulty in adhering the temporary glass wall to the hydrophobic PDMS surface.

One potential drawback of using pressure to clamp a glass slide to PDMS is the difficulty in preventing leaks at the perimeter of the chamber. The MBR presented in this paper provides several techniques to prevent leaks. The clamp top (Figure 11A) contains six screws positioned around the edge of the chamber providing very even clamping pressure. This also provides constant pressure even if the PDMS was not cast completely level. The clamp spacer (Figure 11B) distributes the forces of the screw to a larger area and it prevents the screw torque from acting directly on the glass slide, reducing the likelihood of breaking the slide. The bottom glass slide (Figure 11E) provides a rigid, yet transparent bottom surface to allow the PDMS layer to be completely sandwiched on both the top and bottom and helps prevent leaks.

The macro-to-micro fluidic connections were completed using Upchurch Nanoports on the glass slide instead of the more common technique of punching holes through the PDMS and inserting tubing through the holes. This was done for several reasons, which included reducing leaks and flow-through volume. Leaks tend to form around PEEK tubing when inserted through punched holes in PDMS. PEEK tubing was chosen due to its very low compliance and availability in very small IDs. Nanoports remain leak free when properly adhered and are very quick and easy to connect to and

disconnect from the tubing. Nanoports also provides a reduction in flow-through volume. When inserting tubing into punched holes in PDMS it is difficult for the tubing to reach all the way to the end of the hole due to the elastic nature of PDMS, this results in a small gap between the end of the tubing and the beginning of the fluidic device. This gap can lead to a few microliter flow-through volume. In the design presented here, a very small 1 mm hole is drilled through the glass slide that is only 1 mm thick, resulting in less than one-microliter flow volume. This reduction is critical since the flow rate through the MBR is less than 1 μL/min. A flow-through volume of a few microliters would lead to significant delays in transport of the effluent from the MBR to the collection vial.

Cell Images in MBR

Figure 12 shows photomicrographs of identical fields of AML12 hepatocytes perifused in the MBR. Figure 12A shows a phase contrast image in which cells are approximately 50-70% confluent. This demonstrates that a proper confluency can be reached in which the cells are dense enough to cause a large modulation of the content of the effluent from the MBR, but not so dense that the cells are contact inhibited or piled on top of each other. Figure 12B is the same field under fluorescent illumination. Cells have been stained with ethidium homodimer-2, which stains dead cells red, and SYTO 11, which stains all cells green. Approximately 80% of the cells are alive, which indicates minimal damage during cell seeding and MBR assembly. Most of the dead cells are adjacent to the posts; therefore, future designs incorporating fewer posts could possibly lead to a smaller percentage of dead cells.

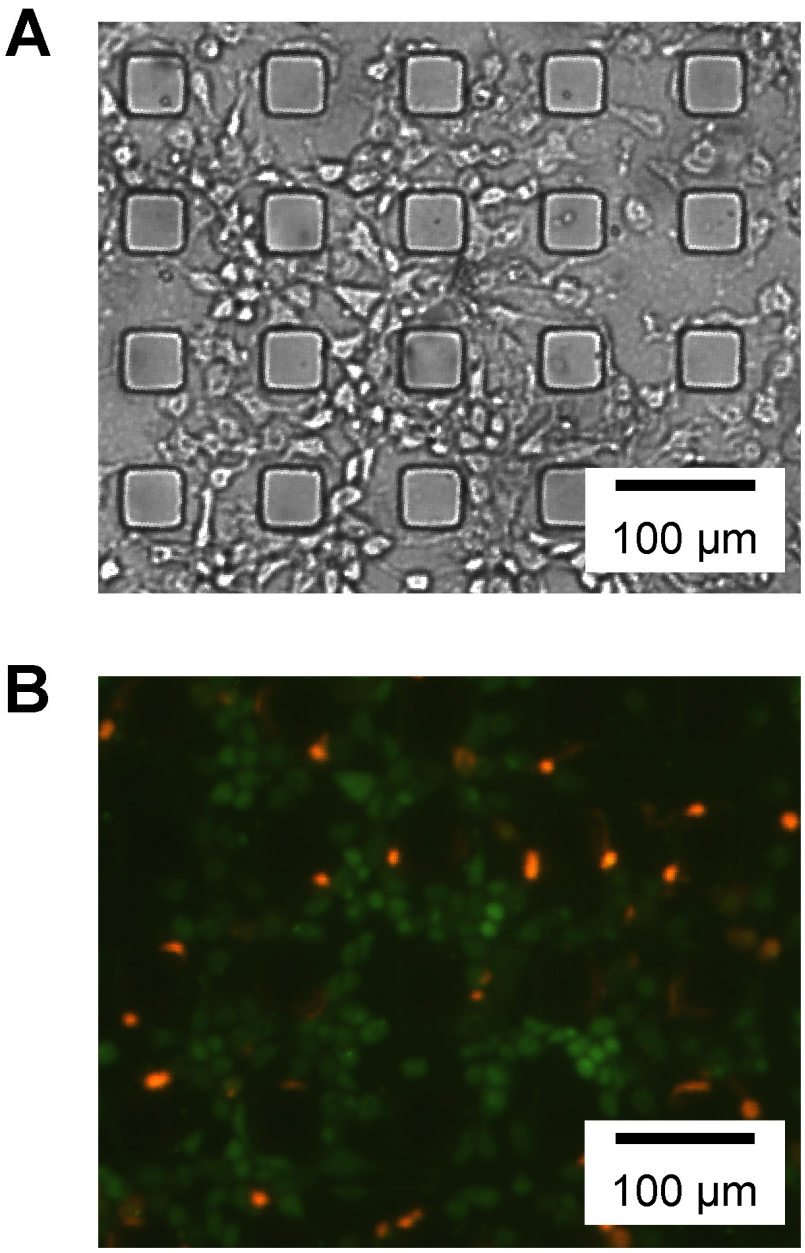

Figure 12. Photomicrograph of adherent AML-12 hepatocytes perifused in the MBR. A) Phase contrast image. B) Fluorescent image of lived cells stained with SYTO 11 (green) and dead cells stained with ethidium homodimer-2. Both A and B are of the same field.

pH Measurements

We measured the pH of MBR perifusate inflow and outflow and compared the results to traditional cell culture. Since there is no gas exchange mechanism employed in our design, pH was measured as an indicator of proper CO_2 concentration in the inflow and of general metabolism in the outflow. Table 7 shows the results of the pH measurements. Media was initially equilibrated to a 5% CO_2 environment before loading into syringes for MBR perifusion. The low CO_2 permeability of the glass syringe and PEEK tubing was verified, as the pH was similar to the pH of media taken directly from a 5% CO_2 environment. This was considerably lower than media from a 100% air environment, despite inflow measuring taking place after the conclusion of an experiment which allowed the maximal length of time for any potential gas exchange through the syringe or tubing. The pH of the effluent from the MBR was also very similar to media taken from 24 hrs of contact with 70% confluent cells in a T-flask, indicating that the metabolic rate is similar. In addition, the pH of the media is close to the normal physiological pH range of 7.35-7.45. This indicates that the cellular environment within the perifusion device is similar to the cellular environment within traditional cell culture techniques and normal physiology.

Table 7. pH of cell media from traditional *in vitro* cell culture as well as MBR perifusate**.**

Cell Media Condition	pH
In 100% air	7.75
In 5% CO_2 95% air	7.43
Over cells for 24 hours	7.36
Perifusate into MBR	7.5
Perifusate out of MBR	7.3

Calibration Curves

Calibration curves of glutamine and glutamate obtained from HPLC-MS are shown in Figure 13. The concentration of amino acids used in the calibration curves were chosen based upon the concentration in cell media. The concentration of glutamine is higher than glutamate in the media and as such is more reproducible as is indicated by the smaller confidence intervals for the slope.

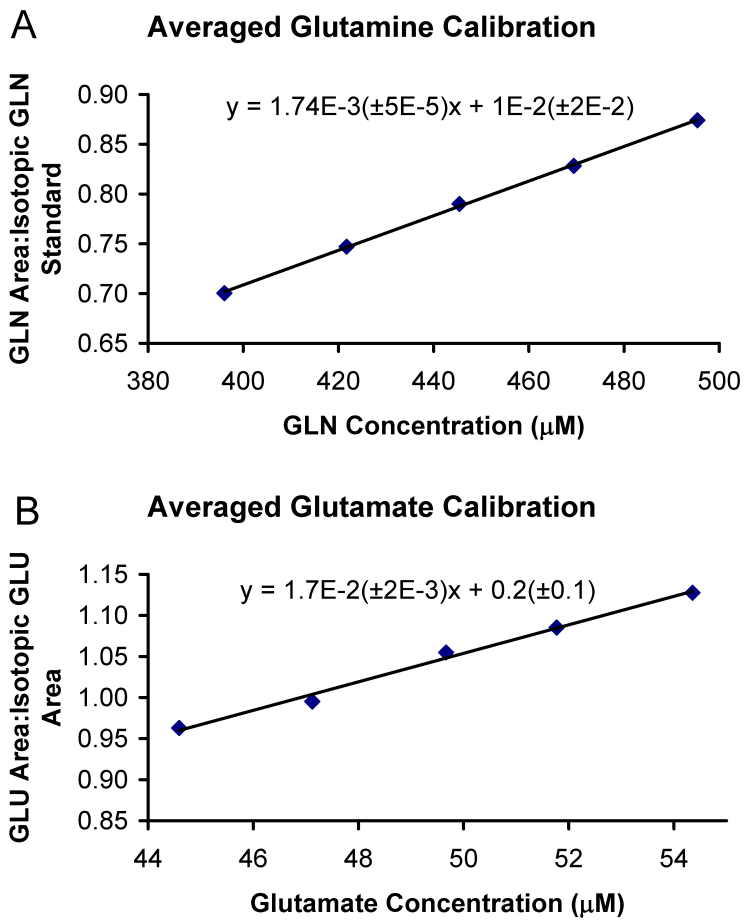

Figure 13. Calibration curve for glutamine and glutamine using HPLC-MS. Errors are the ± 95% confidence intervals.

A table of sensitivities, intercepts, and correlation coefficients for calibration curves of amino acids analyzed by HPLC are shown in Table 8. The sensitivities were very similar being between 8.3×10^3 and 1.0×10^3 for all amino acids accept lysine and cystine. Lysine contains two possible locations for reaction with the OPA/CN^- derivatization reagents as such the added sensitivity is expected. All amino acids accept histidine have larger errors in the intercept than the value therefore the calibration passes through zero as expected. The correlation coefficients (R^2) are all over 0.999, indicating a high degree of linearity between concentration and peak area.

Table 8. Calibration curve parameters for amino acids analyzed by HPLC. The slope indicates the sensitivity, and R^2 is the Pearson's correlation coefficient. Error is the ± 95% confidence interval.

Amino Acid	Slope (μAU·s/μM)	Intercept (μAU·s)	R^2
Aspartic Acid	8.31E+03 ± 9.E+01	-1.E+03 ± 6.E+03	0.99991
Glutamate	9.51E+03 ± 9.E+01	-2.E+03 ± 7.E+03	0.99992
Asparagine	8.7E+03 ± 1.E+02	-2.E+03 ± 9.E+03	0.99984
Serine	9.4E+03 ± 2.E+02	-5.E+03 ± 1.E+04	0.99964
Glutamine	9.27E+03 ± 9.E+01	-3.E+03 ± 2.E+04	0.99993
Histidine	7.9E+03 ± 1.E+02	2.E+03 ± 9.E+03	0.99979
Glycine	9.5E+03 ± 2.E+02	6.E+03 ± 1.E+04	0.99963
Threonine	8.55E+03 ± 9.E+01	-5.E+02 ± 6.E+03	0.99992
Arginine	9.1E+03 ± 1.E+02	-4.E+03 ± 8.E+03	0.99988
Alanine	9.6E+03 ± 1.E+02	-9.E+02 ± 9.E+03	0.99987
Tyrosine	9.2E+03 ± 1.E+02	-4.E+03 ± 7.E+03	0.99990
Cystine	1.7E+04 ± 2.E+02	-9.E+00 ± 7.E+03	0.99990
Valine	9.23E+03 ± 1.E+02	1.E+03 ± 7.E+03	0.99991
Methionine	1.0E+04 ± 1.E+02	-5.E+03 ± 9.E+03	0.99988
Tryptophan	8.4E+03 ± 2.E+02	-4.E+03 ± 1.E+04	0.99957
Phenylalanine	9.04E+03 ± 9.E+01	-3.E+03 ± 6.E+03	0.99993
Isoleucine	9.5E+03 ± 1.E+02	-3.E+02 ± 8.E+03	0.99987
Leucine	9.6E+03 ± 1.E+02	3.E+02 ± 9.E+03	0.99985
Lysine	1.7E+04 ± 5.E+02	-3.E+04 ± 3.E+04	0.99941

Measurement of Amino Acid Flux

In order to demonstrate the feasibility of the MBR as a perifusion device which is capable of measuring small cellular fluxes, we measured cellular amino acid flux. Amino acids are present in the media at a high concentration and have a low relative flux rate. In order to verify whether amino acid consumption and/or production could be observed, we used HPLC-MS to measure the flux of two amino acids, glutamine and glutamate. These amino acids were chosen for the test due to their high relative flux rates. Additionally, their flux is in opposite directions, which was important, as any changes observed would be due to cellular metabolism, and not systematic error such as evaporation or dilution. HPLC-MS data of glutamine and glutamate flux from AML12 cells are shown in Figure 14. Data calculated from literature values for flux rates of primary hepatocytes, are shown along with the experimentally determined values.[1] The calculated flux rate of glutamine and glutamate at 0.5 μL/min flow rate were, 7.68 and -0.11 $\mu mol \cdot day^{-1} \cdot 10^6$ $cells^{-1}$, respectively, which correlates well with the literature values of 3.1 and -0.12 $\mu mol \cdot day^{-1} \cdot 10^6$ $cells^{-1}$, indicating that this method closely approximates the conditions found in traditional well plate experiments.[1] The literature data correlated more closely with the experimental data at the lower media contact times. This is thought to be due the high cell-to-media volume ratio within the MBR which caused toxic waste products and lower nutrient concentration at longer contact times.

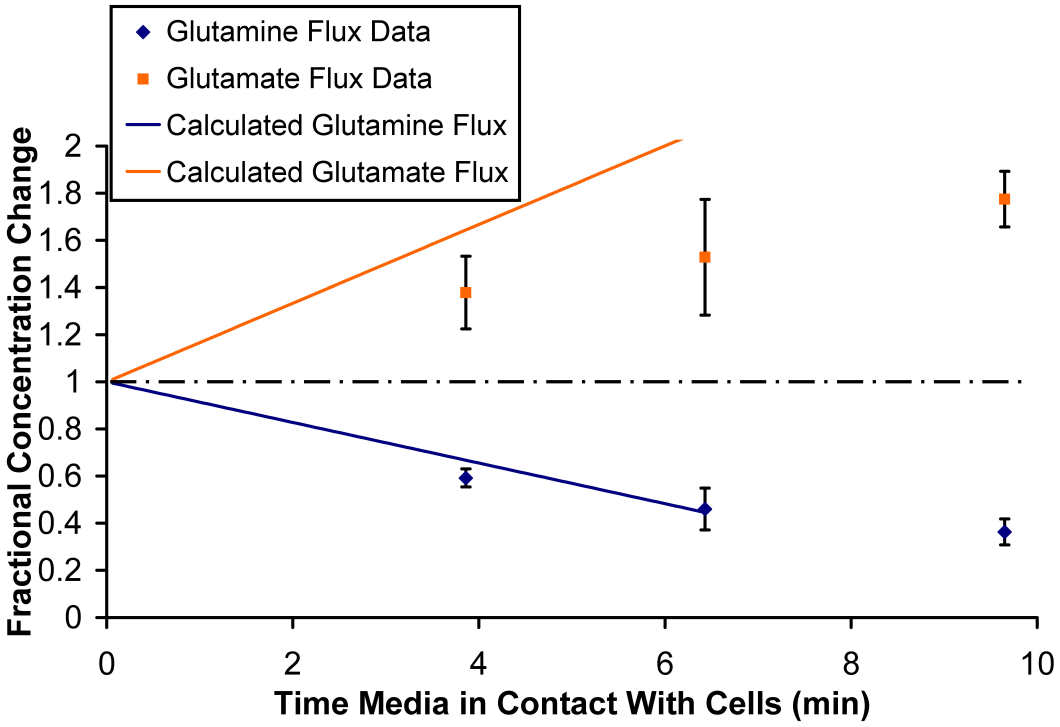

Figure 14. Graph of the change in concentration of glutamate and glutamine in cell media caused by cellular flux. Measured change by AML-12 hepatocytes in MBR is 1.38 ± 0.15, and 0.59 ± 0.04 for glutamate and glutamine, respectively, after 3.9 min. Calculated fractional change for glutamate and glutamine is 1.64 and 0.67 respectively after 3.9 minutes of contact determined by using literature flux rates.[1]

After amino acid metabolism had been observed for two amino acids, we utilized an improved HPLC technique which did not require using a mass spectrometer and expensive isotopic standards. This technique did not require any sample preparation, was highly reproducible, and had a low injection-to-injection time.[90] The MBR was used in the same way as before and basal metabolism of all 19 primary amino acids are shown for each of the three replicates in Figure 15A. The perifusion flow rate used, 0.5 µL/min, is the same as the highest flow rate, and thus lowest contact time, used with the HPLC-MS experiments shown in Figure 14. Each of the three replicates agreed closely with each other. However since the variation within each replicate was smaller than the

variation between the replicates testing the three replicates with an ANOVA demonstrated significant difference between replicates. To combine the data, only the average flux rates were used. In Figure 15B, the three replicates were combined and normalized to isoleucine, the amino acid with the median average flux rate. Fourteen of the nineteen amino acids showed a significant difference from the control. Only two amino acids, alanine and glycine, had literature values, shown in Figure 15B, that were outside the confidence intervals of the experimental data. The literature values were taken during assumed steady-state conditions in a 24-hour well plate experiment using primary hepatocytes which likely have significantly different amino acid metabolism than AML12 cells. Our results demonstrate that the effluent from the MBR is similar in composition to well plate methods. The advantage of the MBR is that the media is only in contact with cells for a few minutes in the MBR, thus enabling a more dynamic picture of cell metabolism to be observed. The differences in the flux of glycine and alanine from literature values are most likely due to differences in cell types, but differing growth environment or differences due to the short time scales with the method presented in this paper are also possibilities.

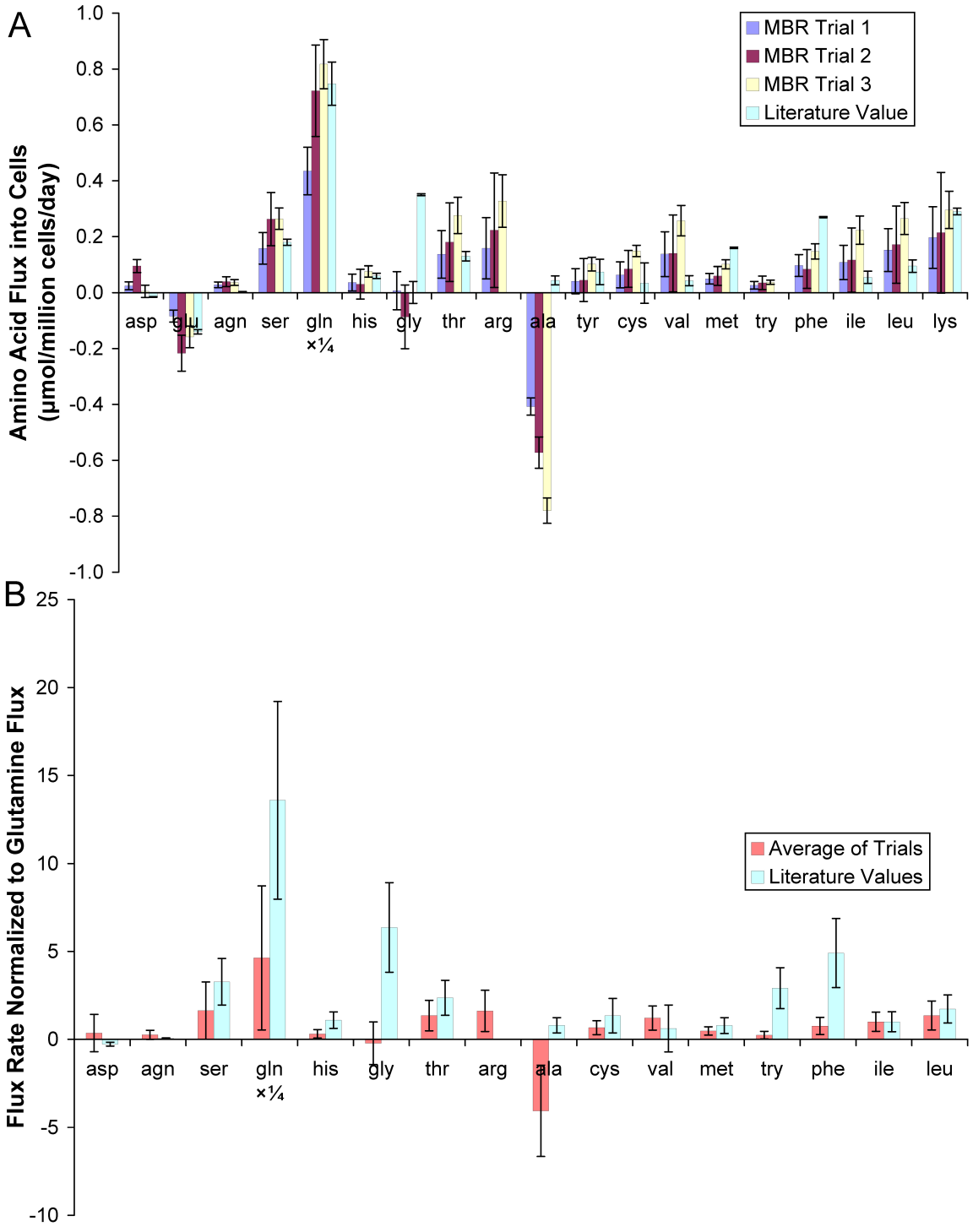

Figure 15. Graphs of 19 amino acid flux rates from MBR perifusate measured by offline HPLC. A) Three separate experiments and from literature values.[1] Error bars are ± the 95% confidence intervals of 5 replicates. B) Three experiments combined and fluxes normalized to isoleucine. Error bars are the propagated 95% confidence intervals.

The MBR we describe has capabilities beyond counting cells within the cell chamber and measuring amino acid flux rates. Optical measurements on the entire cell population within the operating MBR are possible. Additionally, any compound(s) of interest could be analyzed from the effluent and would be present at a higher concentration than in many other perifusion devices. Lastly, these two types of measurements could be collected simultaneously from the same cell population, allowing a much more detailed look at cellular physiology than is available from other cellular perifusion devices.

Conclusions

In this chapter, we present a microbioreactor perifusion device that is capable of perifusing ~10^5 attached cells. The design of the fluidics ensures even flow velocity across all cells, which reduces the heterogeneity of response from the cells. The MBR is designed to minimize flow-through volume for connecting inflow and outflow tubing. The MBR also has a very high cell-to-media volume ratio. All of these design characteristics result in inducing large changes in the composition of the perifused media due to cellular metabolism in a short time period. The MBR produces a change in media composition in 5 minutes that is equivalent to 24 hours using traditional cell culture. This enables measurement of more dynamic processes than would be possible with traditional cell culture and analytical techniques. In addition, the cells are adhered to a transparent 2-D surface, which enables microscopic examination of cells during perifusion. This

provides the important capability of optical measurements on the cells while being able to simultaneously collect the effluent for offline measurement.

CHAPTER IV

THE AMINO ACID FLUX ANALYZER

Introduction

A major goal of this research is to develop an instrument which can quantitate amino acids from a cellular perifusion device online and with high temporal resolution. The high temporal resolution is required in order to observe rapidly changing metabolic phenomena occurring in the cells. There have been several techniques developed for fast separation of amino acids, but only a few which have been shown to separate more than a small number of amino acids. The work shown here represents an extensive modification of work on neurotransmitter detection published by Dr. Robert Kennedy at the University of Michigan. Modifications include changes in valves and pumps, extensive addition of plumbing, and completely new capillary holder and detector optics.

Methods and Materials

Overview of AAFA

Our Amino Acid Flux Analyzer (AAFA) is an online instrument capable of measuring amino acid concentrations in cellular effluent from a microbioreactor (MBR) every 30-60 s. We chose amino acids because their metabolism involves a variety of glycolytic and TCA cycle intermediates, but the instrumentation could be modified to

measure several classes of analytes. A general diagram of the instrument is shown in Figure 16. The MBR, described in Chapter 3, is not part of the AAFA, but is shown here to demonstrate how the system operates. Media is pumped into the MBR and the output or effluent continuously flows into the reaction cross. In the reaction cross, media is continually mixed with the derivatization reagents to fluorescently label primary amines. This process is described in detail in the next section. The mixture leaves the reaction cross and enters the reaction capillary. The labeling reaction requires 200 s for completion and occurs as the mixture flows through the reaction capillary. The mixture then enters the flow-gate interface. The flow-gate injects small plugs of fluorescently labeled amino acids in the separation capillary. The details of the flow-gate will be described in a later section. The labeled amino acids are separated and quantified by micellar electrokinetic chromatography (MEKC). MEKC, as described in Chapter 1, is a batch technique, whereby a small plug of the amino acid mixture is injected onto one end of the capillary, then the plug is pulled toward the other end by electroosmotic flow. Amino acids are separated based on differences in electrophoretic mobility as well as interaction with sodium dodecylsulfate (SDS) micelles forming a pseudo-stationary phase. As the separated fluorescently labeled amino acids pass by the detector, the fluorescence is detected. The strength of the signal is directly proportional to the concentration of amino acids.

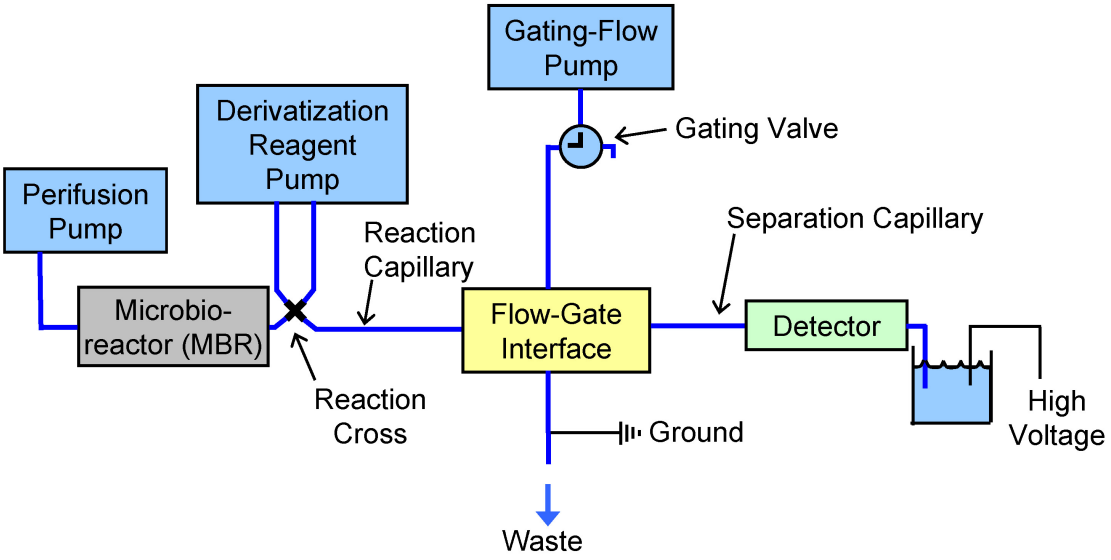

Figure 16. Diagram of the amino acid flux analyzer (AAFA). Media is pumped continuously through the MBR. The output is derivatized, labeling primary amines. The reaction mixture flows to the flow-gate where it is injected onto the separation capillary. Amino acids are separated by capillary electrophoresis and quantified by the detector.

Online Derivatization

NDA/CN- was chosen for this research. The two components of the derivatization reagent, NDA and CN^-, necessitate their being stored separately since they will form fluorescent products when stored together. The first reagent consists of 5 mM NDA in 1:1 (v:v) mix of acetonitrile:15 mM tetraborate buffer pH=9.2. The second reagent consists of 20 mM KCN in 15 mM tetraborate buffer pH=9.2 with 1 mM EDTA and 30 µM norleucine. EDTA was used to prevent formation of a brown precipitate during the reaction process.[58] The use of norleucine, a non-protein amino acid, was added as an internal standard which significantly increases the reproducibility of CE (and MEKC) as it allows the user to normalize for variability due to injection and detection.[91] The flow rate of both derivatization reagents was 7.0 µL/min and the cell media flow rate was 0.5 µL/min. The concentration of all amino acids in the cell media is 7.3 mM,

resulting in an almost 10-fold molar excess of NDA. In order to allow for 200 s of reaction time, the reaction capillary should contain 48 μL, which equates to a 99 cm length of 250 μm I.D. × 360 μm O.D. fused silica capillary used in this setup.

Flow-Gate

The flow-gate is used to inject samples from the reaction capillary onto the separation capillary. Flow-gates have used for several years and their general design has remained fairly constant.[46,55,58,92] A diagram of a flow-gate and injection timing is shown in Figure 17. The reaction capillary is separated from the separation capillary by a small, ~100 μm gap. During a separation, the strong, ~1 mL/min gating flow sweeps the solution from the reaction capillary to waste, preventing it from contacting the separation capillary. When an injection is to be performed, the gating flow is stopped by switching a computer-controlled 3-way rotary valve (Scivex) upstream of the flow-gate, and the separation voltage is turned off. The sample then crosses the small gap during the delay and encounters the separation capillary. An electrokinetic injection is performed by applying a small voltage to the separation capillary. The rotary valve is then switched, resuming the gating flow and sweeping the sample away from the separation capillary during the post-injection delay, leaving a small injected plug at the end of the separation capillary. The voltage is controllably ramped up to the separation voltage, starting the separation.

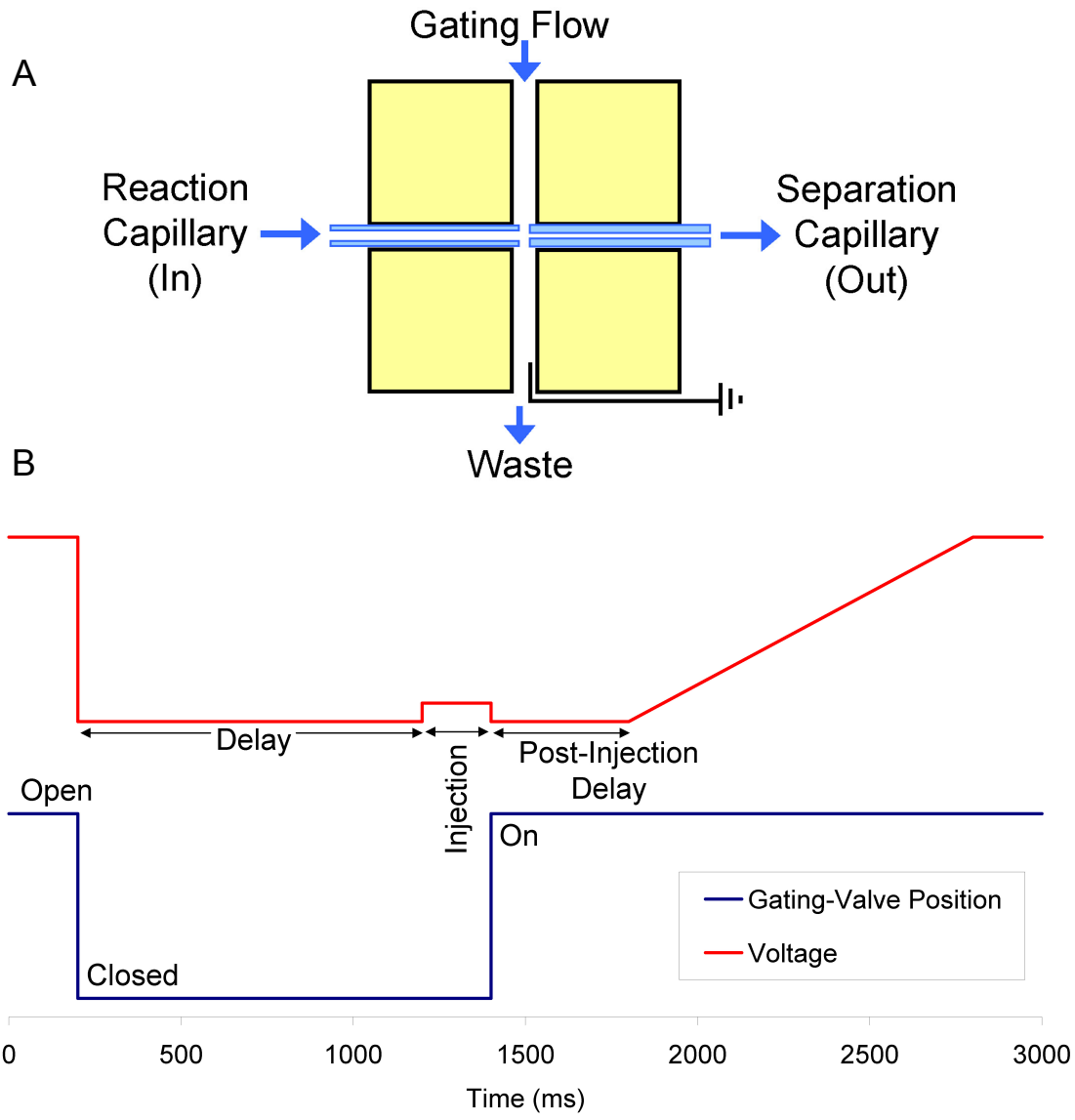

Figure 17. Diagram of flow-gate and injection timing. A) Diagram of the flow-gate. B) Graph of injection timing showing voltage applied to the capillary and gating valve position. The solution from the reaction capillary is swept away from the separation capillary by the gating flow during a separation. When an injection is to be performed, the gating flow is stopped and the voltage is removed. During the delay, the reaction capillary solution crosses the small gap and makes contact with the separation capillary where an electrokinetic injection is performed by applying a small voltage. The gating-flow is then resumed. Any remaining sample is swept out of the gap during the post-injection delay. The voltage is then ramped back to the voltage required for separation.

A machine drawing of the flow-gate is shown in Figure 18. The flow-gate was made of acrylic which is an easily machinable transparent material. It is important that it be transparent, as the reaction and separation capillaries need to be carefully aligned during assembly for proper operation. Of critical importance is the quality of the intersection of the cross. The two flow paths need to be as close to perfect alignment as possible for proper operation. The mounting holes fit 8-32 fillister machine screws for mounting the flow-gate. The ports are designed for 8-32 coned port fittings, and the cross accepts 360 μm OD fused silica capillary tubing. The flow-gate was machined at the University of Michigan machine shop, Mr. Albert Wilson supervisor.

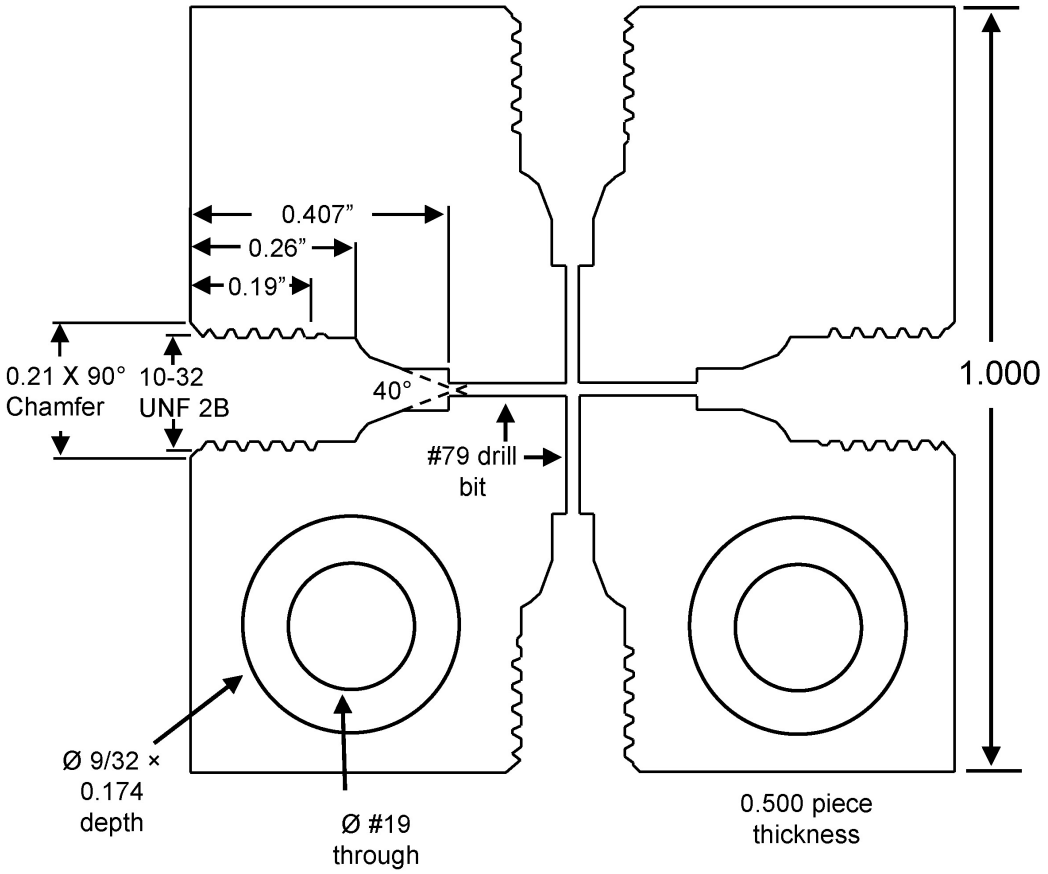

Figure 18. Machine drawing of flow-gate.

MEKC Separation of Amino Acids

The MEKC separation of amino acids in this work necessitates a very fast separation in comparison to commercial capillary electrophoresis (CE) instruments. In order to accomplish this goal, several modifications to traditional CE are required. The capillary length must be significantly shortened. For this research, a 12 cm long capillary with 9.5 cm injection-to-detector length was used. However, simply shortening the capillary will lead to large drop in resolution. To overcome this obstacle, the electric field is increased. 15-23 kV was applied to the capillary resulting in electric fields of 1.25-1.9 kV/cm in comparison to electric fields of 40-200 V/cm for traditional CE.[46] Since resolution is directly proportional to the applied electric field, increasing the electric field increases resolution. However, increasing the electric field also increases current, resulting in increased joule heating. To reduce joule heating, a small 10 μm ID capillary was used, which has a larger ratio of surface area to volume than the 25-75 μm ID capillaries used in traditional CE. A smaller diameter capillary equates to smaller sample volumes and fewer molecules to detect. This requires a highly sensitive laser-induced fluorescence (LIF) detector in order to give signals with high signal-to-noise ratios. In addition, the injection plug and detection length need to be kept as short as possible in order to observe any separation which may be occurring. The computer-controlled flow-gate allows for injection of carefully controlled plugs of sample. The detector is a single-pass on-capillary detector that only observes a length of capillary about equal to the ID of the capillary.

Capillary Conditioning

In order to perform the MEKC separation of amino acids, the capillary must be conditioned to provide the charged silanol groups which produce electroosmotic mobility. The separation capillary consists of a fused silica capillary with 360 μm OD and 10 μm ID with a length of 12 cm with a 9.5 cm injection-to-detector length. The injection tip was beveled to a cone by hand-grinding on a Dremel with a polishing. The polyamide coating was burned off using a small torch at the point in the separation capillary which will be used for detection. The capillary was conditioned by flushing with 0.1 N NaOH in DDI water for 15 minutes. This was followed by flushing with separation buffer for 20 minutes. The separation buffer was 15mM phosphate pH=8.0 with 30mM SDS. The capillary was then positioned in the flow-gate, ready for assembly in the detector.

The small ID of the capillary necessitated a pressure vessel for flushing the capillary with the NaOH and separation buffer. The pressure vessel delivers fluid at 80 psi to the separation capillary. This was done by attaching the separation capillary to a 100 μm ID capillary using a small piece of Teflon tubing with a slightly smaller ID than the 360 μm OD of the two capillaries. The other end of this transfer capillary was in a vial of the flushing solution that was inside a pressure vessel. The pressure vessel was attached to a 3-way valve that had at its other two ports an 80 psi N_2 supply line or venting to air. In this way the valve could be switched between supplying pressure to the vessel which would fill the capillary, or venting the chamber to air to change solutions when not in use.

Generation I Detector

The Generation I detector was closely based on published work of Dr. Kennedy's group.[58] Valuable information was obtained from this detector, and several components and design features were used in the Generation II detector. Therefore, a detailed description of both detectors will be presented.

The general diagram of the Generation I detector is shown in Figure 19. The optical path was from a Zeiss Axiovert 25CFL inverted microscope. A capillary holder was constructed and was mounted to the XY mechanical stage of the microscope. It consisted of mounting holes for the flow-gate, capillary-holding brackets near the objective, and a cover for blocking light during an experiment. The objective used was a CP-Achromat 100× 1.25 NA oil immersion lens. For excitation, a continuous wave, diode-pumped solid-state 440 nm laser (BCL-025-440, Crystal laser) was mounted in the lamp-housing socket. A custom-made lamp housing socket adapter was machined and attached to an XY-stage onto which the laser was mounted. The fluorescence filter set was Chroma Z442BP, which is a very narrow band 442nm laser excitation set with bandpass emission. A custom-made ultra-sensitive light detection module, discussed in detail below, was mounted to the camera-port for fluorescence detection. The module was mounted to a diagnostic instrument HRD100-CMT coupler with a ZV-Clamp adapter. To reduce stray light from going to the detector, an iris was mounted at the camera mount intermediate image plane. A custom-made holder attached to the end of the camera adapter held the iris at proper location. The iris constricted the field of view to a small opening, corresponding to the area of the capillary illuminated by the laser.

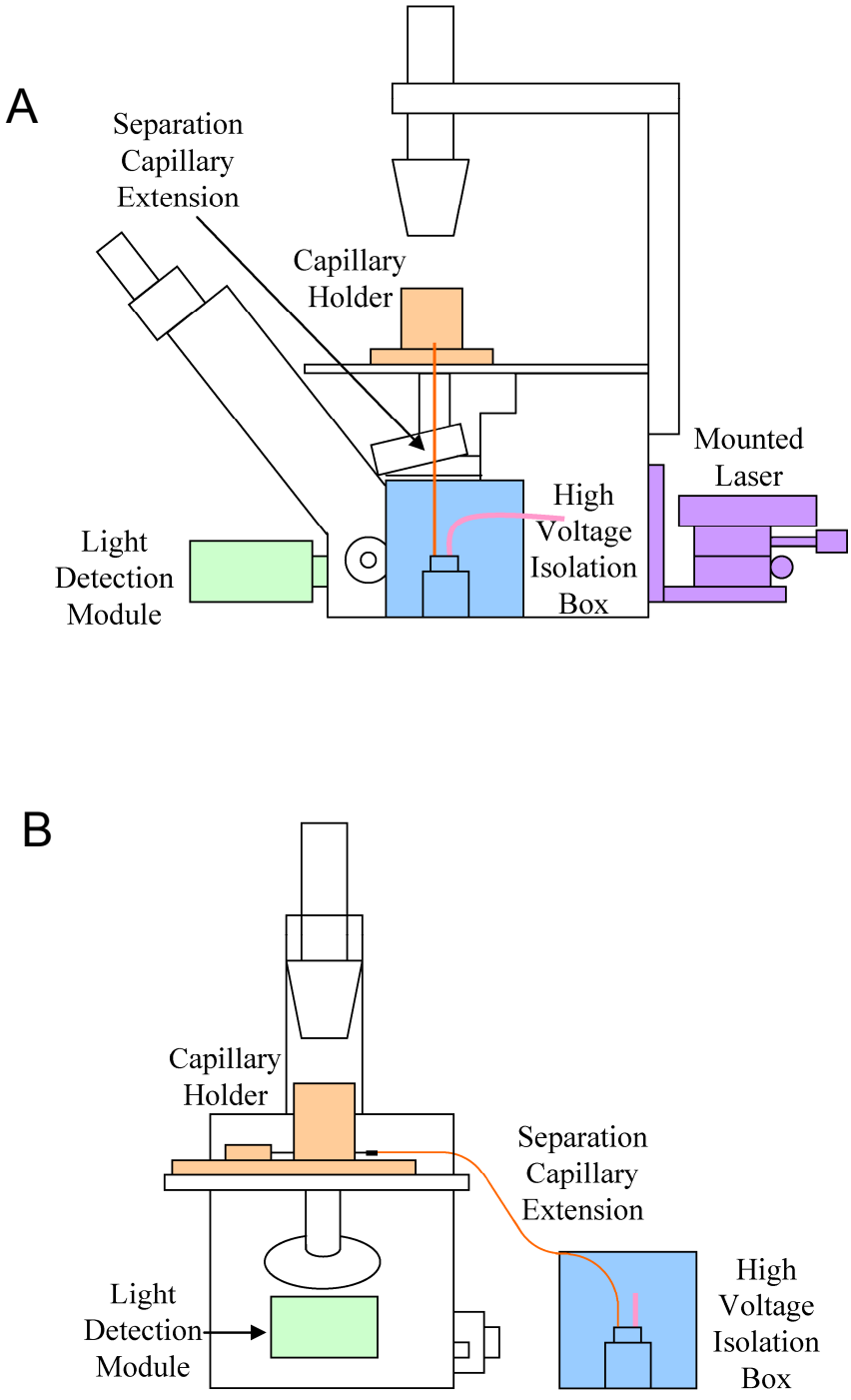

Figure 19. Overview of Generation I LIF detector. A) Side view B) Front view shown without body tube and eyepieces. The high sensitivity light detection module is shown in light green, high voltage isolation box in light blue, the capillary holder in light orange, and laser in purple mounted on a Zeiss Axiovert 25CFL microscope. The separation capillary extension, shown in orange, connects the separation capillary to the high voltage. The high voltage cable, shown in pink, goes to the high voltage power supply, which is not shown for clarity.

The separation capillary was connected to high voltage by a buffer reservoir held at high voltage in an isolation box. A 100 μm ID capillary extension was connected to the detector end of the separation capillary by a short, ~1 cm piece of Teflon tubing which fit tightly over the two ends of the capillary. The other end of the capillary extension was dipped into a vial of separation buffer located in an acrylic isolation box. The end of the high voltage line was also dipped in the buffer vial. The box lid was connected to an interlock which prevented the high voltage power supply (CZE1000R, Spellman High Voltage Electronics Corp.) from turning on unless the lid was closed.

The Generation I LIF detector required the custom machining of several parts, including an adapter for connecting the excitation laser to the lamp-housing socket on the microscope, a C-mount camera adapter for connecting the light detection module to the camera adapter, a holder for the attachment of the end of the camera adapter, which holds an iris at the intermediate image plane, and a capillary holder that aligns the separation capillary to the focal point of the objective and prevents outside light from entering the objective.

The laser-to-lamp house socket adapter is shown in Figure 20. The four taped holes hold an angle bracket connected to an XY stage on which the laser is mounted. The stage allows the laser to be aligned perfectly in the center of the field of view in the detector. The small 1/8" hole allows the laser beam to pass. The groove in the OD of the adapter allows a series of set screws on the microscope to hold the adapter in place. The adapter is machined out of aluminum and anodized black by Midwestern Anodizing in Milwaukee, WI.

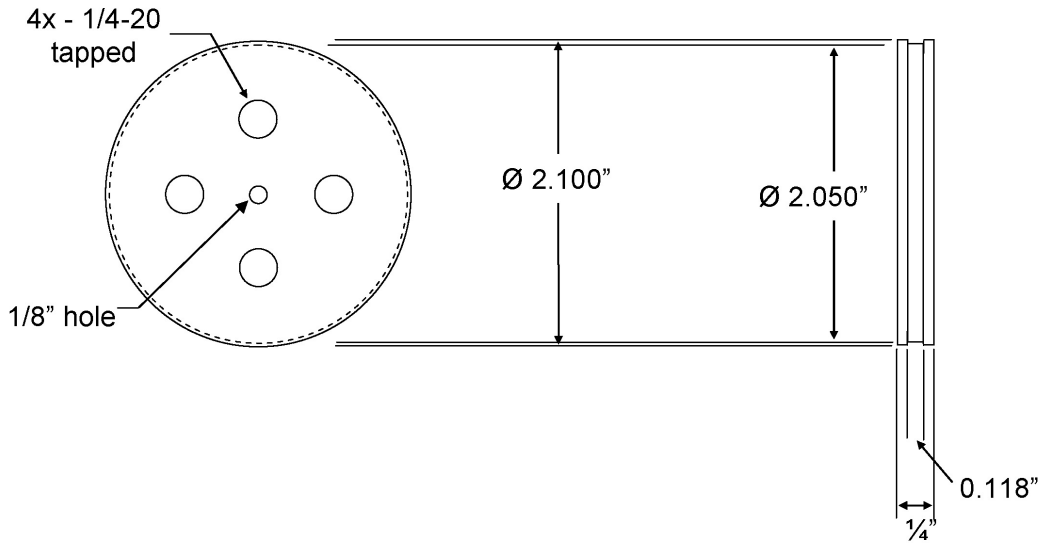

Figure 20. Adapter for mounting the laser on an XY stage to the lamp housing on an Axiovert 25CFL microscope.

The C-mount camera adapter is shown in Figure 21. The adapter connects the light detection module to the camera adapter mounted in the camera port of the microscope. The total thickness of the piece corresponds to placing the PMT in the focal plane according to C-mount standards, thus guaranteeing sharp focus on the PMT and assuring that as much light as possible enters the photomuliplier tube (PMT). The four

small holes allow four mounting screws to attach the PMT housing. The large hole allows light to pass to the PMT. The 1”-32 thread is the female C-mount thread. The C-mount adapter is machined out of aluminum and anodized black by Midwestern Anodizing in Milwaukee, WI.

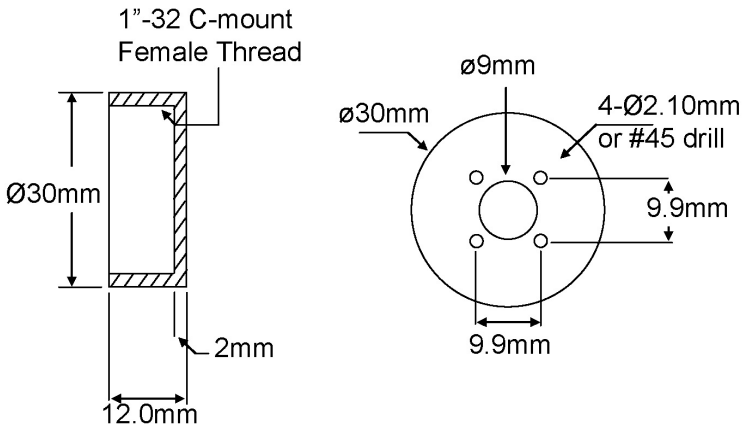

Figure 21. C-mount adapter for light detection module

The detector spatial filter is shown in Figure 22. The large diameter end slips over the end of the camera adapter and is secured by the set screw. The iris slips on the smaller diameter end and butts next to the shelf. The iris is held in by a retaining ring. The slot in the smaller diameter end allows the size of the hole in the iris to be adjusted by means of an arm on the iris. The part is machined out of aluminum and anodized black by Midwestern Anodizing in Milwaukee, WI.

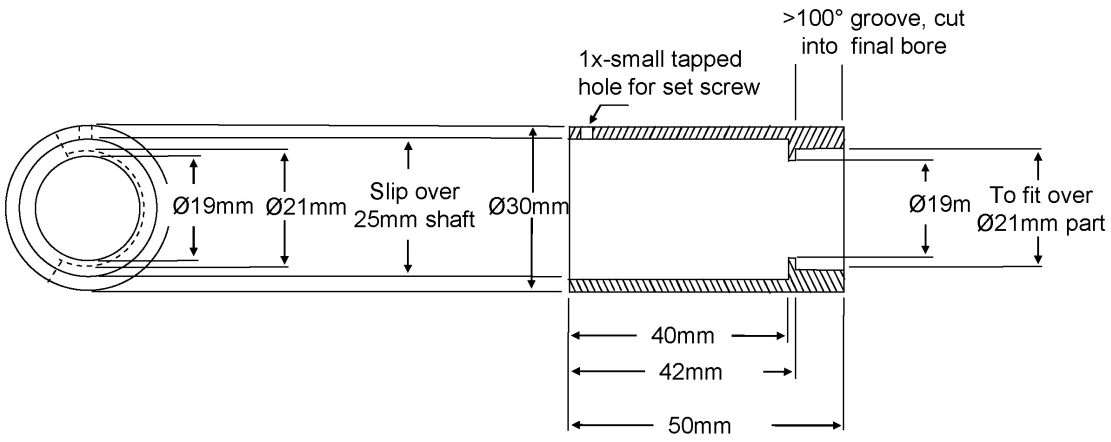

Figure 22. Detector spatial filter adapter

The capillary holder is shown in Figure 23. Part A shows the holder assembled as it is used during an experiment, with the exception of a top to the blackout box. The holder consists of a series of tapped holes on the left where the flow-gate is mounted. The large number enables the use of a variety of lengths of capillary. On the right are three walls of a blackout box and a groove for a lid. The lid consists of the front and the top of the box (not shown). The capillary is assembled and aligned by visualizing the capillary through the eyepiece and adjusting the focus and the XY-stage. Once aligned, the lid is added, visualization is switched to the camera port and an experiment can begin. The blackout box prevents light from entering and interfering with the fluorescence detection. The box lid was also wired to an interlock for the laser (not shown). This prevents the laser from turning on unless the box lid is on to prevent accidental exposure to intense laser light. Inside the box are capillary clamps. In the detail, the capillary fits in the groove, with a small portion of the capillary protruding above. The top is then clamped to the bottom by two nylon screws attached into the bottom of the clamp. The

top applies pressure directly to the capillary, securing it in place. This is crucial, since movement of even a micron or two will significantly affect the detection, and the high voltage imparts a force on the capillary. The large hole in the bottom of the box provides microscope objective access to the capillary. In the top of the holder are holes to mount the capillary holder to the XY stage of the microscope. The holder is machined out of black Kydex T thermoplastic.

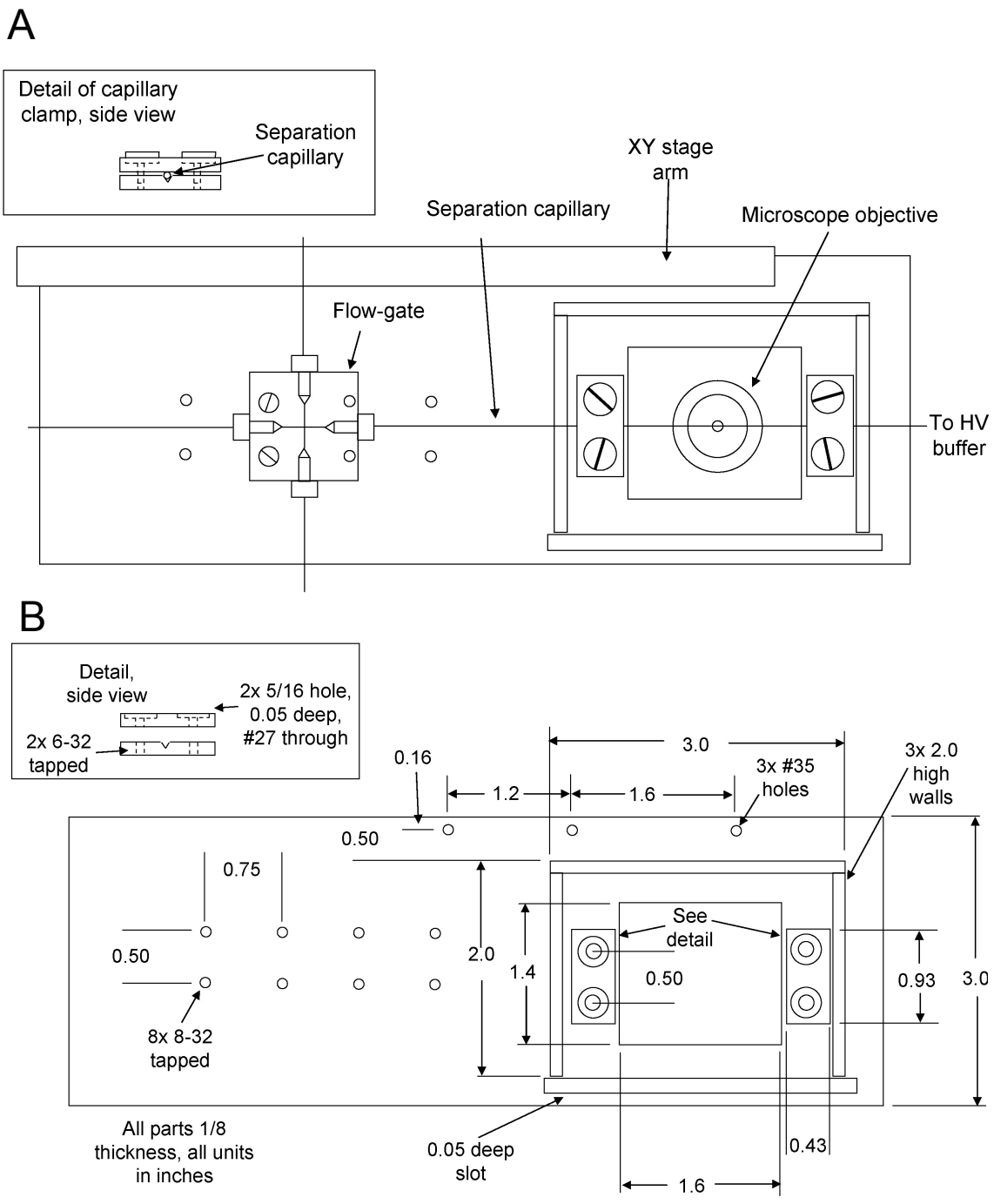

Figure 23. Capillary holder for the Generation I AAFA. A) Holder assembled showing flow-gate, separation capillary, microscope objective, and XY stage arm. B) Machine drawing. Detail shows side view of capillary clamp.

A high voltage isolation box was constructed as shown in Figure 24. The purpose of the isolation box is to protect operators and bystanders from the high voltage encountered during MEKC separation. The box holds a vial filled with separation buffer inside of a holder. The high voltage cable is brought through the box through a tight-fitting hole, and separation capillary extension is brought into the box between the box side and the lid. Both the cable and capillary are inserted in the buffer in the vial. The box contains a safety interlock such that the high voltage power supply can only be operated when the lid is closed. The box is made from ¼" thick acrylic.

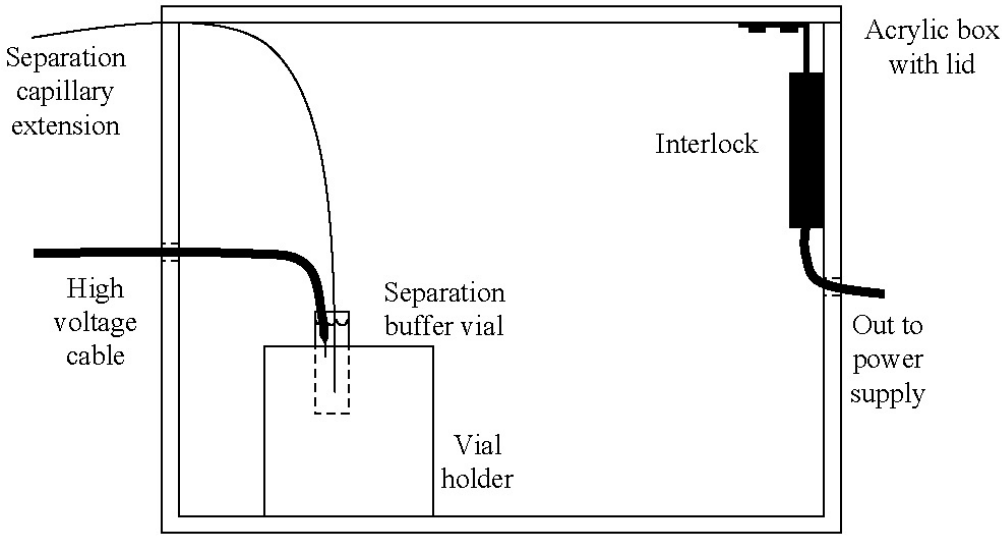

Figure 24. High voltage isolation box.

An ultra-sensitive light detection module was fabricated to use as a fluorescence detector. The heart of the module is a Hamamatsu H5784-40 PMT module mounted inside an aluminum box. The module connects to the camera mount via the C-mount camera adapter described earlier. On the side of the module are an on/off toggle switch, a poteniostat for gain adjustment, a DIN connector to power, and a BNC connector for

signal output. The module was powered by an Eplac external power supply providing the +15 V and –15 V power to the PMT module.

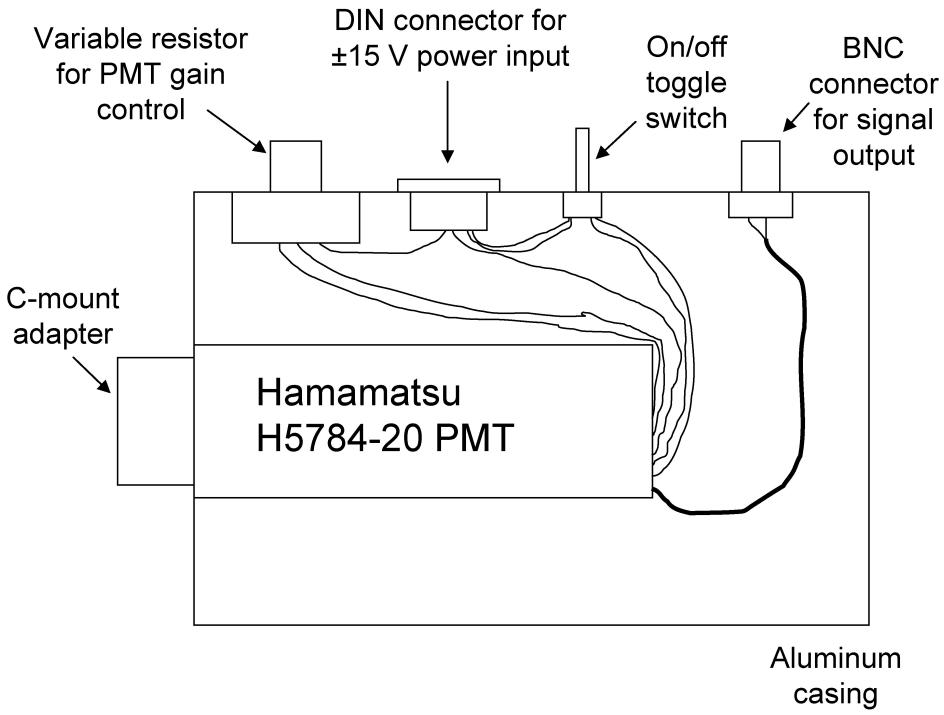

Figure 25. Light detection module.

Generation II Detector

The Generation I detector proved to be unreliable due to an intermittent problem with arching as is described in detail in the results and discussion section. Therefore, we designed and constructed a Generation II detector. The general layout of the Generation II LIF detector is shown in Figure 26. This layout allows the separation capillary to be mounted vertically, rather than horizontally. The separation capillary was

mounted in a holder attached to an XYZ stage that allowed the capillary to be properly focused to the objective. The injection end of the capillary was inserted in the flow-gate as in Generation I. The detection end of the separation capillary was inserted into a buffer reservoir in which a high voltage was applied. The optical path of the detector was assembled exclusively from individual optical components, rather than using a microscope as in Generation I. As in Generation I, the detector is designed with epi-illumination where the laser excitation light is reflected off the dichroic mirror and reflected 90° to the objective. The emitted fluorescence is collected by the objective, passes through the dichroic mirror and excitation filter, to the tube lens. The tube lens focuses the light on the same light detection module used in Generation I. To align the capillary, a flip-down mirror is flipped up, focusing the capillary on an eyepiece. The alignment illumination is turned on and the XYZ stage is adjusted to bring the objective to sharp focus on the capillary ID.

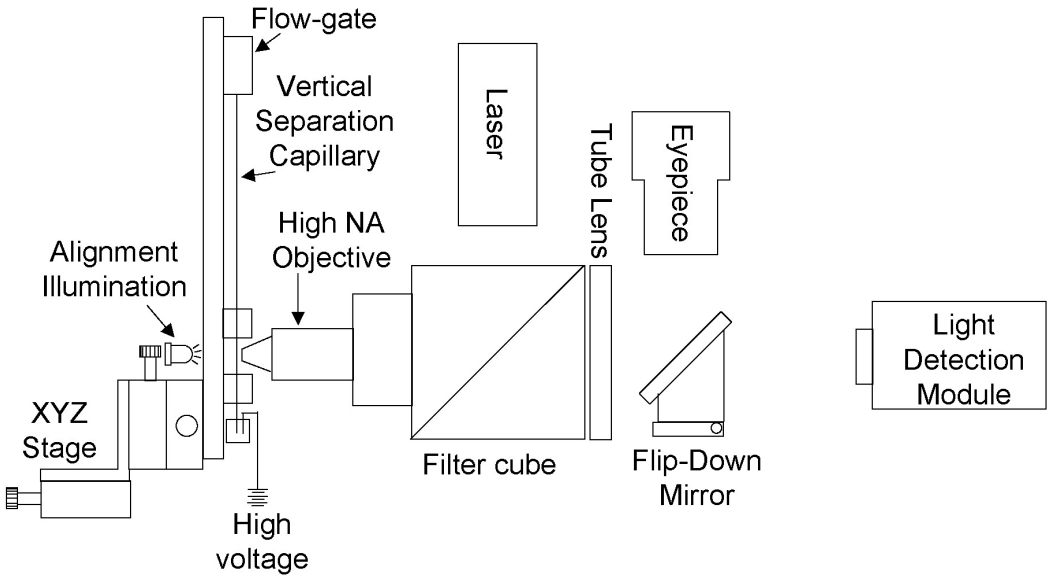

Figure 26. Overview of Generation II LIF detector.

The capillary holder is designed using the same principles as the first generation holder. A machine drawing is shown in Figure 27. The flow-gate mounts in one pair of the tapped holes on the left and the detection window is mounted in between the capillary clamps on the right.

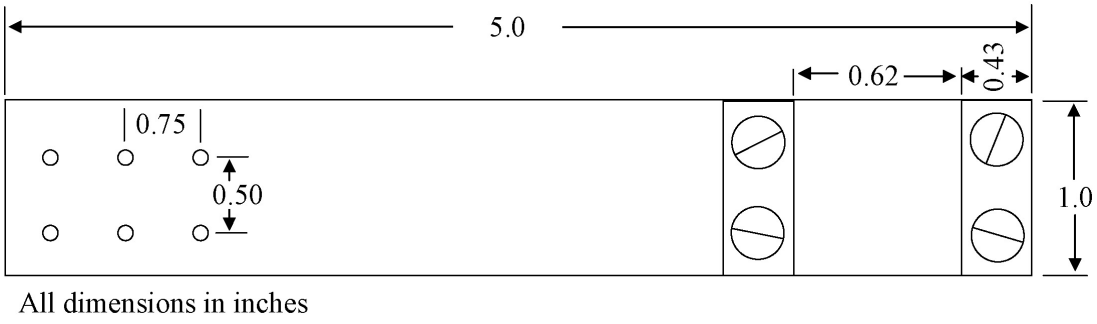

Figure 27. Capillary holder for Generation II. All parts thickness of 0.21. The capillary clamps are identical in design to those used in generation I. (see **Figure 23**).

The capillary holder is mounted inside a sealed box filled with SF_6 gas, which has a high dielectric strength of 8.5-9.8 kV/mm (several times that of air, which is 0.4- 3.0 kV/mm).[93] The box is shown in Figure 28. Part A shows the empty box and its aspects in detail. Part B shows the assembled unit, with capillary holder and detector objective in place. In the absence of SF_6, arching and corona discharge occur, making experimentation impossible. The box is mounted to an XYZ stage by three nylon flat-head mounting screws located at the bottom of the box. The capillary holder is inserted into the box by sliding the holder down from the top of the box, moving it forward to the stops, then screwing a long nylon screw from the back of the box to the holder, clamping the capillary holder firmly in place. The lid is then placed on the box. The objective for the detector is introduced through a hole where a sheet of soft rubber with a hole smaller than the objective is clamped in place. The microscope objective is inserted into the box through the hole in the soft rubber. A seal forms around the objective, yet XYZ movement is still possible. This allows the stationary objective to be focused on the capillary by moving the entire box. A small groove is machined on the back of the box, allowing an illumination source to be inserted. SF_6 gas is introduced at a low flow rate though a small port in the bottom of the box, allowing for uniform filling of the heavier-than-air gas. The end of the separation capillary protrudes though a hole in the bottom of the box. A removable high voltage buffer reservoir is attached through this hole. The box is made of acrylic and spray painted black on all but one side, allowing observation of the capillary holder.

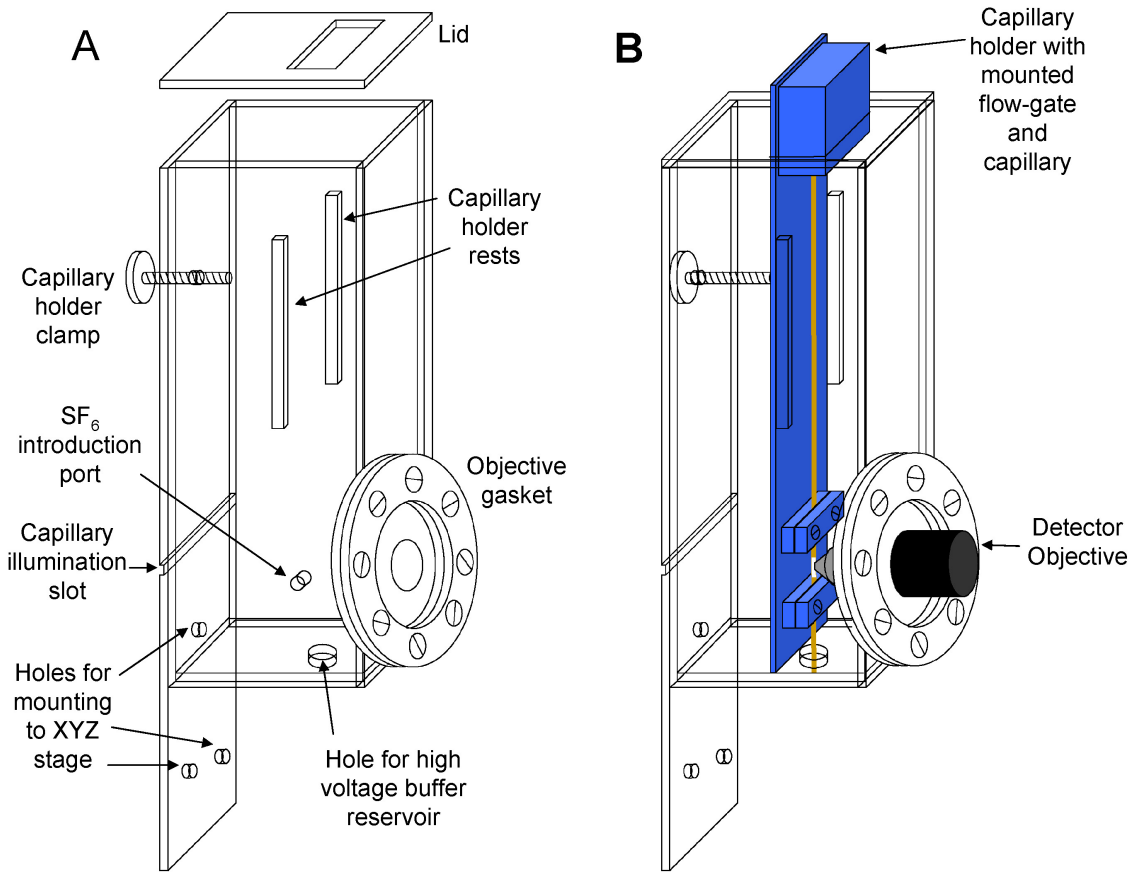

Figure 28. SF_6 box. The capillary holder is mounted in an SF6 box to prevent arching. A) Empty box. B) Box with capillary holder in place and detector objective focused on capillary.

The high voltage buffer reservoir is shown in Figure 29. At the top of the reservoir is an O-ring groove. The reservoir is inserted into the hole at the bottom of the SF_6 box until the body of the reservoir contacts the box. The O-ring allows for a leak-free attachment to the bottom of the SF_6 box. The pressure provided by the O-ring also holds the reservoir to the box. The separation capillary dips down into the cavity in the reservoir. Electrophoresis buffer fills the cavity and provides electrical contact between the high voltage from the platinum wire and the separation capillary. The high voltage cable from the power supply is inserted into the opening in the right of the reservoir. The

end of the cable contains a male connector which is mated to the female connector in the reservoir. The female connector and platinum wire are epoxied into the reservoir, holding them in place and preventing buffer from contacting the high voltage cable. The cable is inserted into the reservoir until it is stopped by the insulation at the change of diameters. The buffer reservoir is made from acrylic, and the outside is spray painted flat black.

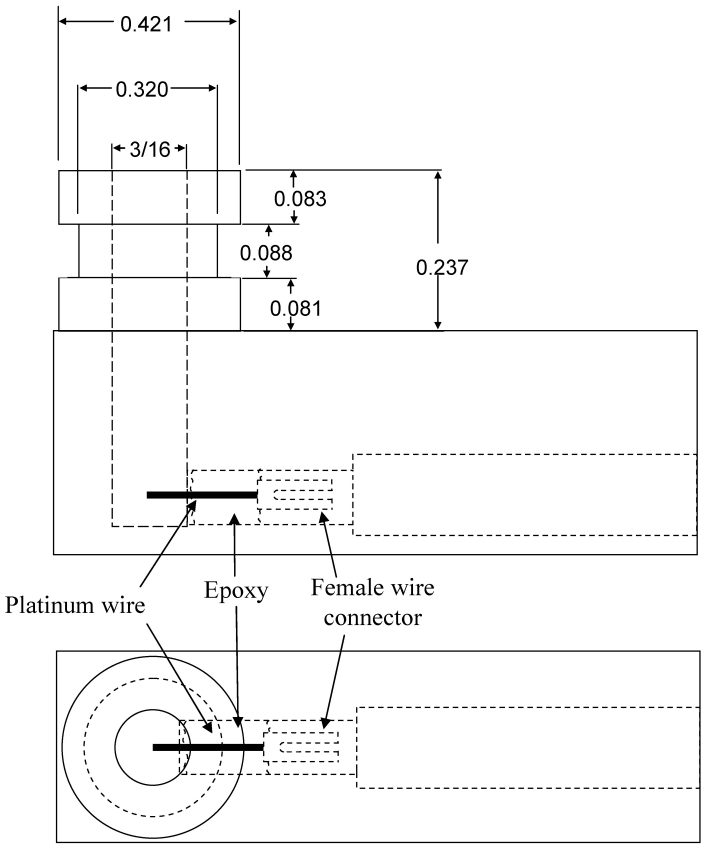

Figure 29. High voltage buffer reservoir.

Figure 30 shows the optics used for the Generation II detector. The main components and working principles are the same as Generation I, but the optical path was totally rebuilt. The microscope objective, laser, filter set, and detection module are

reused in Generation II. The laser, U, enters through a small hole in the lens tube, G, where the filter set is housed. The Zeiss filter cube is a near-perfect fit in the 2" diameter lens tube. The laser passes through the excitation filter and is reflected off the dichroic mirror and projected toward the objective, A. The objective is focused on the center of the separation capillary. Emitted fluorescence is collected by the objective and passes into the filter set, where it passes through the dichroic mirror and the emission filter to the tube lens. The distance between the objective and the filter cube, and the filter cube and the tube lens, was designed to be close to that of the microscope to prevent any optical effects that might occur as a result of changing distances. The tube lens brings the infinity space after the objective to a focal point. The tube lens used was an achromatic lens with a focal length of 150 mm. This is fairly close to the Zeiss tube lens focal length of 165 mm, ensuring that the magnification is similar to the microscope and reducing any imaging artifacts. The tube lens focuses directly on the sensor of the PMT so that as much of the emitted light as possible enters the PMT. During focusing of the capillary ID on the objective, the flip-down mirror is flipped up, directing light after the tube lens to the eyepiece. The distance from the tube lens to the eyepiece or the PMT was made the same by temporarily attaching a C-mount camera to the C-mount where the detection module attaches. The rear cage plate adapter, D, attached to the C-mount was slid along the cage assembly rods until both the eyepiece and camera were in focus. The cage plate adapter was then locked in place. During focusing of the capillary, an external illumination source is needed to properly observe the capillary.

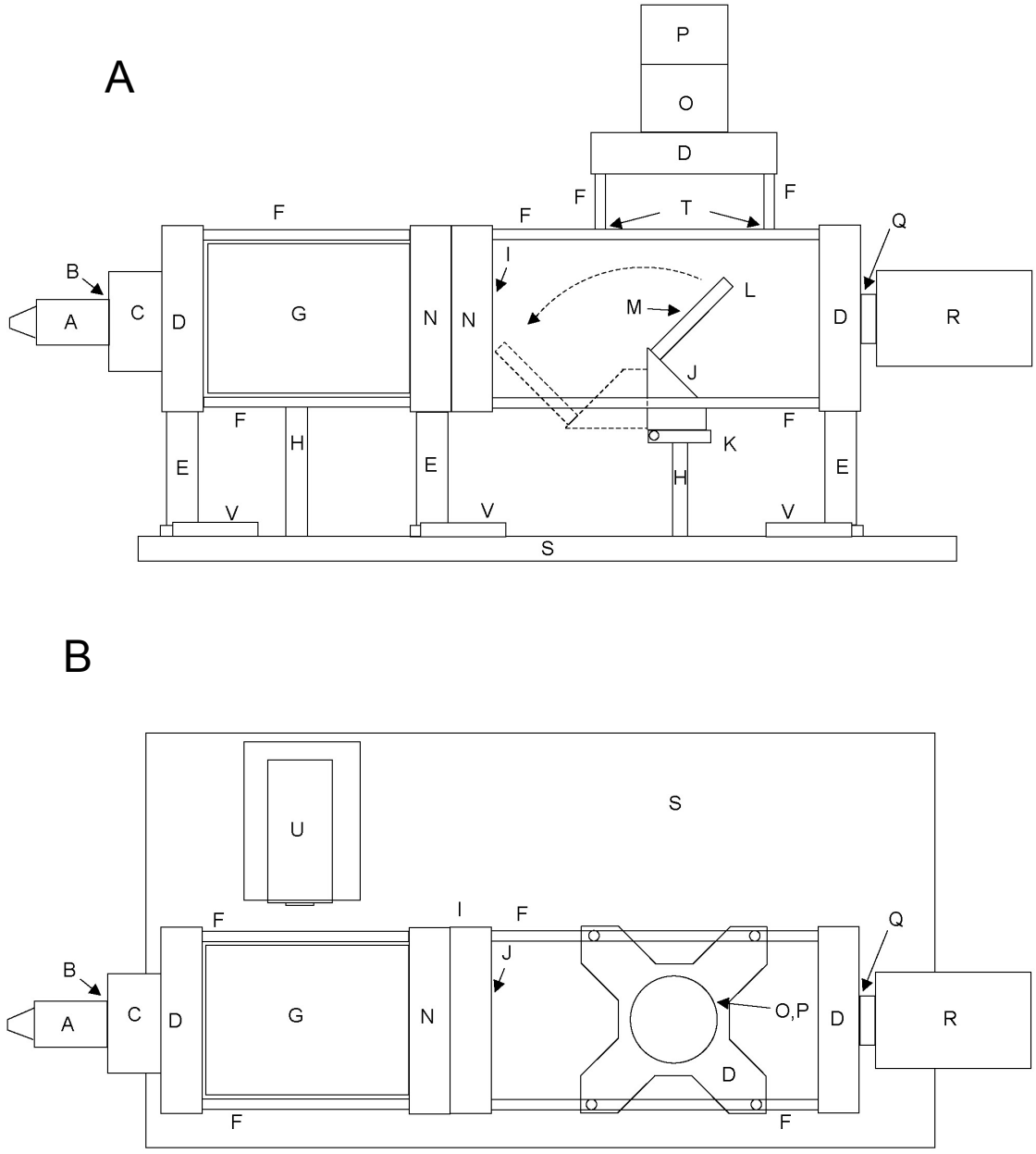

Figure 30. Diagram of Generation II LIF detector optics. A) Side view, B) Top view. Letters correspond to the parts list in **Table 9**.

Table 9. Parts list for LIF detector optics shown in Figure 30. All parts are from Thorlabs except where noted. Two letters assigned to the same part indicate that both parts are used at that location.

Letter	Model #	Description	Notes
A		Microscope Objective, Achromat 100X oil immersion, NA 1.25	From Zeiss
B	SM1A3	RMS to SM1 Thread Microscope Adapter	
C	SM1ZM	SM1 Series Zoom Housing	
D	LCP02	30mm to 60mm Cage Plate Adapter	
E	RS3P	1" Diameter Pillar Post, 2" Long	
F	ERX	Cage Assembly Rods - 0.5-6"	
G	SM2L20	SM2 Lens Tube, 2" Long, One SM2RR Included	
H	MS2R	Mounting Post, 2" Long	
I	C32-886	Achromatic Lens 50mm Dia. x 150mm FL, MgF2 Coating	From Edumund Optics
I	SM2L03	SM2 Lens Tube, 0.3" Long, One SM2RR Included	
J	FM90	Flip Mount - Imperial	
K	MA45-2	45° Mounting Adapter	
L	FMP1	Fixed 1" Holder	
M	PF10-03-P01	1" Protected Silver Mirror	
N	LCP01	60mm Cage Plate, ø2" Threaded Aperture, 1/2" Thick	
O	C03-628	Male C-Mount to Eyepiece	From Edumund Optics
O	SM1A9	Camera C-Mount Adapter, External C-Mount Threads	
P	C36-130	Eyepiece 10x	From Edumund Optics
Q	SM1A10	Camera C-Mount Adapter, Internal C-Mount Threads	
R		High Sensitivity Light Detector	
S	MB1224	Aluminum Breadboard 12" x 24" x 1/2", ¼-20 Thread	
T	ER90C	Right Angle Rod	
U		440nm Solid State, Diode Pumped, Continuous Wave 25W Laser	From CrystaLaser
V	CF125	Small Clamping Fork	

During capillary alignment, additional illumination is needed. Due to the tight physical constraints of the area, a custom-made illumination source was constructed. A diagram of the illumination source by itself and in use is shown in Figure 31. All parts were purchased from Digi-Key. The illumination source was constructed in a 3.15x1.57x0.67" black ABS box. It contains a 9 V battery for electrical power, an on/off toggle switch, a resister, and a white LED (PN: 365-1177-ND). The resister was chosen to provide the proper 20 mA of current at 3.2 V. The LED was chosen due to its high luminous intensity of 24 cd and small viewing angle of 15°, which provides a lot of light in the center of the LED where it is needed to illuminate the capillary.

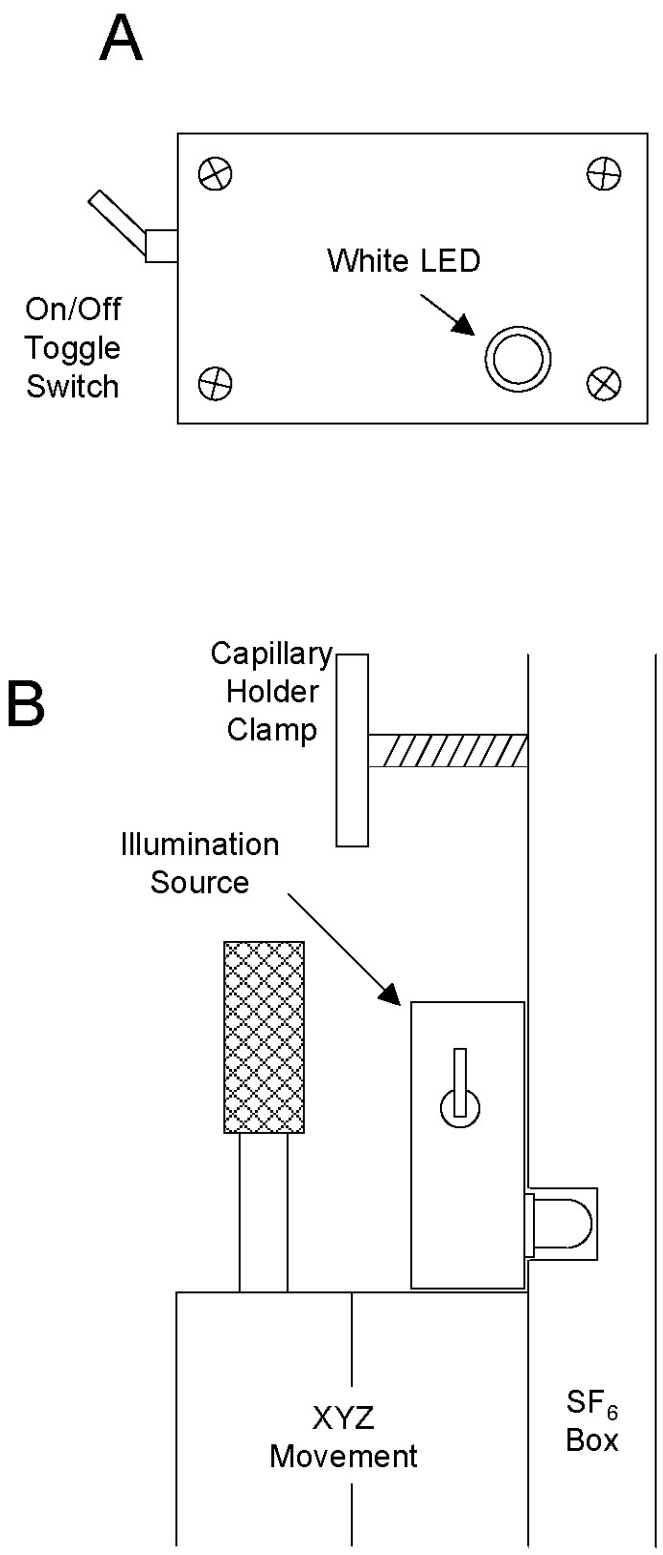

Figure 31. Illumination source used to illuminate capillary during detector alignment. A) Front view of illumination source. B) Side view of illumination source during use.

Data Acquisition

The AAFA is computer-controlled. A program written in LabVIEW controls a National Instruments PCI-6036E DAQ card. The card is connected to a connector block for connection of the input and outputs. The program controls the flow-gate valve and high-voltage power supply and collects voltage and current input signals from the power supply and collects the fluorescent data input. The fluorescent data are filtered with a low-pass RC filter circuit with a 20 Hz cutoff frequency attached to the connector block. The flow-gate valve is controlled by contact closure. To interface the DAQ card with the contact closure, a pair of optically isolated relays was employed. When a positive voltage is applied, one relay closes, causing the valve to divert the gating flow away from the flow-gate. When a negative voltage is applied, another relay closes, causing the valve to resume the gating flow to the flow-gate.

The LabVIEW program which controls the AAFA and collects and stores the data was written by Jonathan Shackman at the University of Michigan, a graduate student of Dr. Robert Kennedy.[94] I performed modifications to the program to make it suit the individual needs of my instrument. The user inputs the delay time, inject time, post-inject delay time, ramp time, injection voltage, separation voltage, collection frequency, and separation time. The settings used for the bulk of the work were delay time 1000 ms, inject time 200 ms, post-inject delay 150 ms, ramp time 1000 ms, injection voltage 2 kV, separation voltage 12-23 kV, collection frequency 60 Hz, separation time 40-80 s. Additional details are provided in Appendix A.

A second LabVIEW program was utilized during an experimental run. It includes all of the functionality of the first program, but allows running an automated

sequence of experimental runs. It includes user inputs of number of runs and time between runs, and displays the total experimental time required. The program automatically saves the current electropherogram with the time stamp and starts another run. The process is repeated for the specified number of runs. This allows a time course to be constructed of time versus peak area for each peak. To obtain peak area, the electropherogram must be integrated.

Data Processing

After the series of electropherograms are collected, they need to be processed in order to extract a time course of concentration as a function of time for each peak in the electropherogram. A stand-alone program, Cutter, written in LabVIEW by Jonathan Shackman, was used for the high-throughput peak picking required for these experiments.[94] Cutter was used as it is the only freeware high-throughput chromatographic data analysis software available. Cutter allows the user to load the entire series of electropherograms from an experiment at once. Electropherograms can be visualized as the entire series and individually in the same screen. Since the retention times of the peaks from sequential electropherograms are close but not exact, the program allows the user to perform a temporal normalization, so one peak is aligned for all electropherograms by adding or subtracting retention time to the electropherograms. The user is allowed to perform a baseline subtraction. This was done by setting the smallest signal value equal to 0. Finally, the area of that peak for all electropherograms is integrated. The process of normalization and integration is repeated for all peaks. If the retention time of several of the peaks is very close for all electropherograms, as is often

the case, more than one peak can be integrated without normalization. Typically, only three to five normalizations are required to integrate all amino acids.

Once the area of all peaks has been determined, further data processing is performed in Microsoft Excel. Sometimes the retention time of the peaks systematically increases during the course of an experiment. This needs to corrected for since longer retention time means the analytes are moving slower though the capillary and therefore spend a longer time in the detector window, equating to larger peak areas for the same concentration. To correct for this, a few electropherograms that were evenly spaced in the sequence were integrated without being temporally normalized. The time stamp of the electropherogram and retention time were noted for each peak in each electropherogram. A graph of retention time vs experimental time was constructed and the slope of the regression line obtained. The area of each peak was divided by this slope to correct for the changing retention time. If the retention time of the peaks did not change significantly during the course of the sequence, this correction factor was not necessary.

During each experiment an internal standard, usually norleucine or fluorescein, was added with the KCN solution since they do not interact with CN^-. They allow for correction due to injection or detector focus variability to be made since the concentration of standards should not change during the course of an experiment. The peak area of all the peaks was divided by the internal standard, producing a peak area normalized to the internal standard.

Results and Discussion

To test the ability of the Generation I AAFA to separate amino acids in cell media, no MBR was used initially. Instead, cell media was loaded in a syringe and pumped directly into the instrument. An example electropherogram demonstrating separation of amino acids from DMEM:F-12 cell media for the Generation I AAFA instrument is shown in Figure 32. Thirteen of 19 primary amines, including the norleucine internal standard, were separated to the baseline in less than 30 s. Serine, threonine, asparagine, and glutamine were partially separated and eluted first. Phenylalanine and leucine co-elute, and alanine were not seen. Separation conditions are given in the methods section. Peak identifications were made by spiking the cell media with one amino acid at approximately three times the nominal concentration of that amino acid, making the peak immediately identifiable. This process was repeated for all 19 primary amino acids.

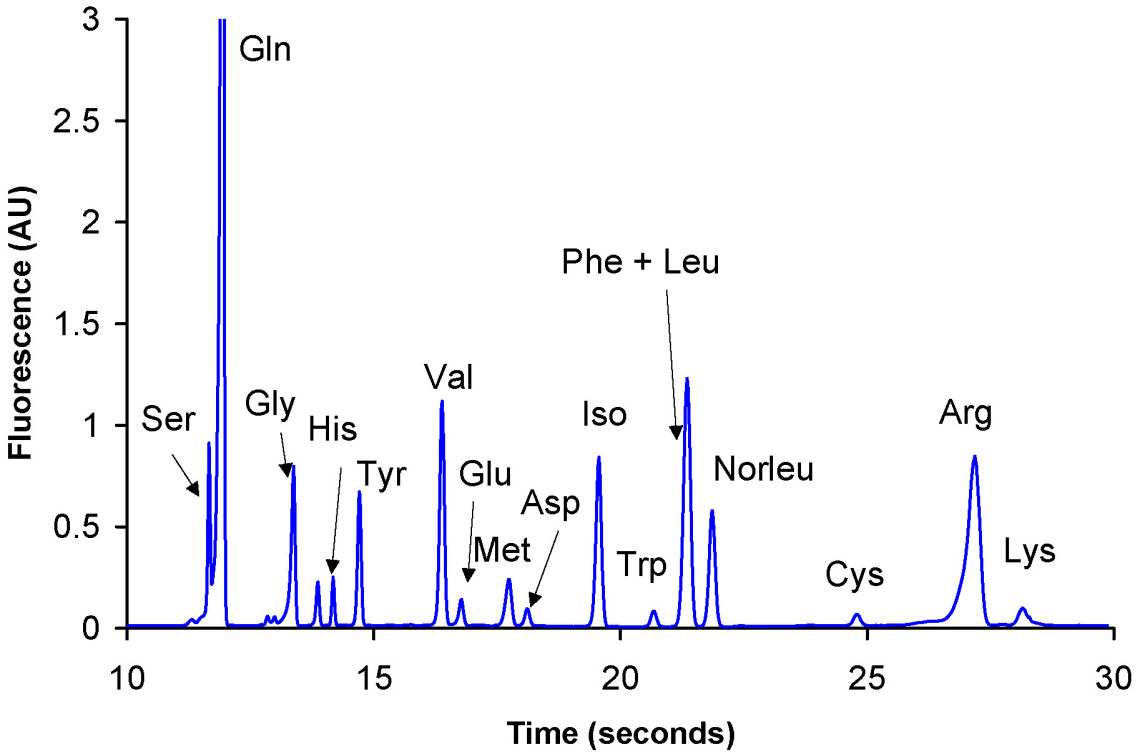

Figure 32. Example separation of primary amino acids in DMEM:F-12 base cell media using the Generation I AAFA.

The reproducibility of the technique was tested by running a 120 min long sequence with electropherograms collected every 45 seconds. The percent relative standard deviation (RSD) was calculated for the normalized peak area for each amino acid. The results are shown in Table 10. Seven out of 12 peaks have RSDs of less than 10%, which indicated that the AAFA is very stable. The retention time of the later eluting peaks varied considerably throughout the experiment in a non-systematic way, making accurate quantitation of cystine, arginine, and lysine impossible.

Table 10. Long-term reproducibility of normalized peak areas for amino acid in DMEM:F-12 base media analyzed on the AAFA Generation I. Data are collected approximately every 45 s continuously for 2 hours.

Amino Acid	Relative % Standard Deviation
Serine	8.1
Glutamine	7.3
Glycine	5.4
Histidine	13
Tyrosine	9.0
Isoleucine	8.3
Tryptophan	36
Leucine + Phenylalanine	5.6
Glutamic Acid	15
Valine	6.6
Aspartic Acid	23
Methionine	18

Several problems were encountered during the course of instrumental setup. The first major problem involved the flow-gate valve. The original setup used a 3-way solenoid valve. After a very short period of use, usually 1-10 days, no injections could be observed. This was verified using a microscope to visualize the injection of food coloring at the flow-gate. When the valve was working, the food coloring would cross the gap and a plug of the food coloring was seen traveling down the separation capillary after an injection. When the valve was not working, the food coloring still crossed the gap, but none was injected into the separation capillary. It was presumed that after a short use, the valves stopped most but not all of the gating flow during an injection. Several different brands were tested, but all failed. The solution was to use a rotary valve with an electronic actuator (Scivex V-2500). The rotary valve is a much more expensive and slower acting valve, but it worked flawlessly for all of this work. As a result of the slower action of this valve (~150 ms vs ~8 ms), a post-injection delay was added to the

voltage timing, allowing time for the valve to completely resume the gating flow before separation was started. If this were not done, a much longer injection band, or a double injection would result.

The coupling of the separation capillary to the capillary extension proved very difficult with the Generation I detector. In order to have the detector end of the separation capillary at a high voltage, a second capillary of much larger internal diameter, 100 μm versus 10 μm, was coupled to the end of the separation capillary. Since the larger diameter has a lower electrical resistance, almost all of the voltage drop, and therefore electric field, is isolated to the separation capillary. The coupling of these two capillaries is of utmost importance since high voltage easily leaks out of all but the tightest seals. In addition, the coupling needs to be easily removable and use as little capillary space as possible, since any additional length needed for coupling would result in a reduced electric field in the separation capillary. A short 1 cm piece of Teflon tubing, of slightly smaller ID than the OD of the capillaries, provides a very tight seal. Unfortunately, it was unreliable, frequently emitting corona discharge from around the edges of the coupler. The corona discharge produced large and erratic noise in the signal from the detector. Several different designs were attempted to solve this, but ultimately it was decided that elimination of the extension was necessary. The only way to do this is to orient the capillary vertically, inserting the end of the separation capillary directly into the high voltage buffer. To this end the Generation II instrument.

The detector optical train for the Generation II AAFA is horizontal, and composed of optical components rather than the microscope of Generation I. This configuration allows the capillary to be mounted vertically, which provides for direct

contact between the separation capillary and the high voltage buffer. This direct contact eliminates the need for any high voltage coupling of capillaries and any leaks from the coupling.

The original design for the capillary holder did not include the SF_6 box. The capillary holder was attached to the XYZ movement and the capillary was inserted into a vial in which the high voltage line was placed. This design resulted in severe arcing from the buffer to the objective along with extensive corona discharge. Several geometries of buffer vials were attempted and some were successful in eliminating arcing, but none were able to eliminate corona discharge. Due to these issues, it was decided to encase the high voltage buffer and separation capillary in a box which could be filled with SF_6, a gas with approximately three times the dielectric strength and with much higher resistance to corona discharge than air.[93] This design was used throughout the rest of this dissertation.

An example electropherogram for the Generation II AAFA instrument is shown in Figure 33. The order of elution, run time, and signal to noise ratio is comparable to the Generation I AAFA. The peak heights have changed slightly, but can be attributed to older cell media which has reduced levels of glutamine and increased levels of glutamic acid, and a sharper arginine peak, thus increasing the height while maintaining similar area. There are slight differences in resolution of peaks. Serine and glutamine were resolved from asparagines and threonine, however valine and aspartic acid were not resolved. Phenylalanine and leucine were partially resolved, but not quantitatively. Lastly, fluorescein was added as a second internal standard, which allows for normalization independent of derivatization. However, it was never used, as the RSD

was greater for the fluorescein peak than for other amino acids. The reason for this is not understood.

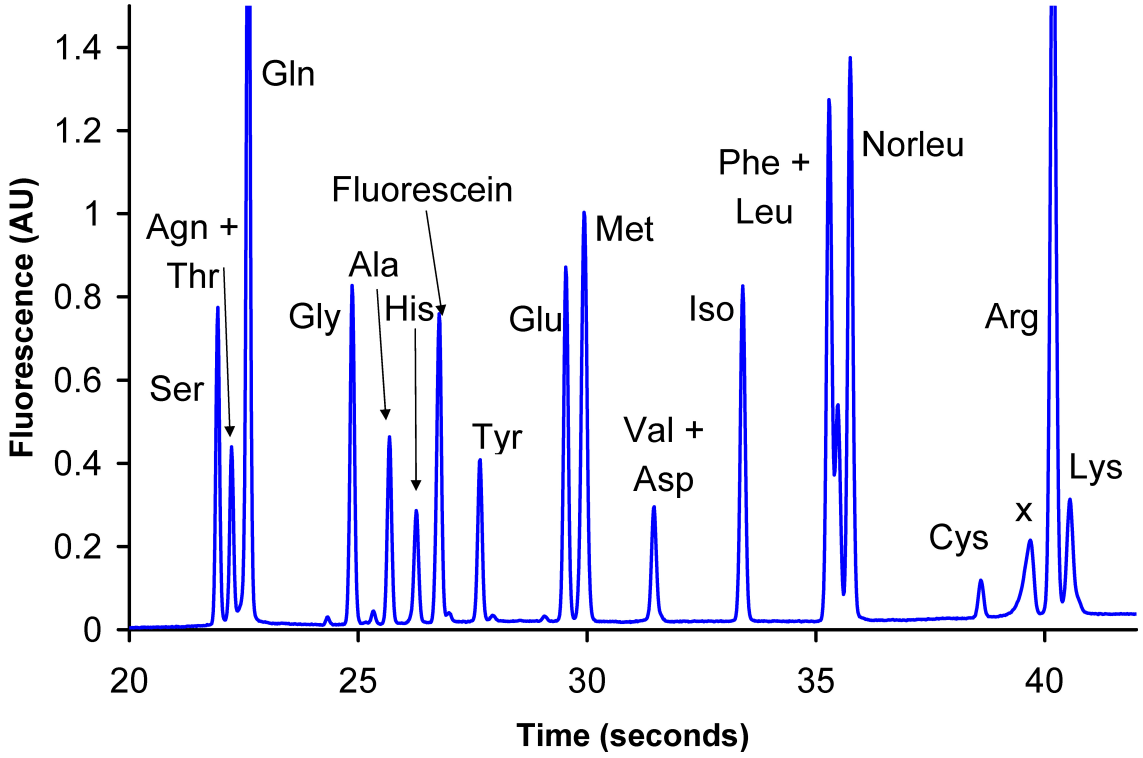

Figure 33. Example separation of primary amino acids in DMEM:F-12 base cell media and internal standards using the using Generation II AAFA. An unknown derivatization product is marked as X.

It has frequently been observed that the electropherograms decrease in resolution and increase retention time during extended experimental runs. The degree to which this occurs and the length of time it takes it to occur vary from experiment to experiment. During experiments with the Generation II AAFA, the severity and short time of onset of symptoms prevented further experimentation until a solution was found. After an

extensive trial and error process, it was discovered that the SDS brand was the source of the problem. The old brand of SDS, electrophoresis grade from Fisher Scientific, was replaced with SigmaUltra grade from Sigma-Aldrich. After making the change, the long-term reproducibility increased dramatically, and there was very little increase in retention time or decrease in resolution over a period of greater than 2 hours of continuous use.

The reproducibility of the Generation II AAFA was determined by collecting electropherograms every 1.0 min for over 2.5 hrs. The normalized % RSD of amino acid peak areas in DMEM:F-12 base media is shown in Table 11. The RSD is below 10% for 13 of the 15 amino acid peaks, and below 5% for 8. The two peaks which have an RSD of greater than 10%, aspartic acid and cystine, have peaks that are so small, they are barely above the baseline, making accurate quantitation problematic. During this test, no internal standards were added with the derivatization reagents, so normalization was done

Table 11. Long-term reproducibility of normalized peak areas for amino acid in DMEM:F-12 base media analyzed on the AAFA Generation II. Data are collected approximately every 60 s continuously for over 2.5 hours.

Amino Acid	%RSD
Serine	1.9
Asparagine + Threonine	5.1
Glutamine	1.9
Alanine	4.3
Glycine	3.4
Histidine	2.9
Tyrosine	3.1
Valine + Glutamic Acid	5.5
Aspartic Acid	25
Methionine	3.1
Isoleucine	3.3
Leucine + Phenylalanine + Tryptophan	2.4
Cystine	15
Arginine	7.2
Lysine	8.9

with glycine, with glycine being normalized with isoleucine. The reduction in % RSD in Generation II vs Generation I is largely attributable to the change in SDS brands.

The %RSD of peak area of the Generation II AAFA from Table 11 was compared to the expected change in amino acid concentration caused by insulin and glucagon found in Table 2. The N required for the standard error of the instrument reproducibility to be less than the change imparted by insulin or glucagon is shown in Table 12.

Table 12. Percent change in the amino acid concentration of DMEM:F-12 media caused by flux change upon exposure to insulin or glucagon[20] from table 2. The %RSD of peak areas from table 10, and the calculated N required for the standard error of RSD to be less than the change expected by insulin or glucagon

Amino Acid	% Change Caused by Insulin	% Change Caused by Glucagon	%RSD	N Required for Standard Error < Insulin Change	N Required for Standard Error < Glucagon Change
alanine	-4.6	-6.2	4.3	1	1
aginine	-0.75	-3.5	7.2	93	5
asparagine	-0.27	-0.45			
aspartate	-6.4	-3.2	25	16	61
cysteine	-8.9	-4.5	15	3	12
glutamate	17	0.0			
glutamine	-100	-100	1.9	1	1
glycine	-6.5	-19	3.4	1	1
histidine	-11	5.5	2.9	1	1
isoleucine	-2.3	1.0	3.3	3	11
leucine	-3.4	1.7			
lysine	-15	1.2	8.9	1	53
methionine	0.0	0.0	3.1		
phenylalanine	-5.6	-14			
proline	0.0	0.9			
serine	10.6	0.0	1.9	1	
threonine	-9.9	-3.3			
tyrosine	-6.4	-2.7	3.1	1	2
valine	-10	0.7			

Since the desired time resolution of the AAFA is 2 min as shown in table 1, an N of 3 would be only 2.25 minutes, very close to the desired 2 minutes. Nine out of 11 amino acids demonstrate detectability in less than two minutes for insulin. Five out of 11

amino acids demonstrate detectability in less than two minutes for glucagon. This demonstrates that the AAFA should be able to detect changes in amino acid concentration due to cellular perturbations for several amino acids.

Some of the variability in amino acid elution order and peak resolution between Figure 32 and Figure 33 are due to differences between the setup of the Generation I and II AAFAs. However, some differences are day-to-day and capillary-to-capillary variation. Before an experiment is begun, several test electropherograms with differing voltages are collected. The voltage which produces the best separation of amino acids of interest is the voltage used that day. For Generation I this was typically 20-24kV; for Generation II this was typically 14-20kV. The reason for the difference between generations is not known since both have the same electrophoresis buffer and had very similar capillary lengths. If the applied voltage was too low, the peaks were very broad and started to overlap, and separation time was significantly longer. If the applied voltage was too high, the separation time was so short that the peaks started overlapping.

A calibration curve of selected amino acids is shown in Figure 34. The calibration curves were generated from a single solution consisting of diluted amino acid standards (Thermo Scientific) or amino acids dissolved from solids (Sigma-Aldrich). The amino acids were chosen due to intermediate (isoleucine), or low (aspartic acid), peak areas in electropherogram of cell media. The variability in slope indicates that there is variability in the intrinsic fluorescence sensitivity or derivatization efficiency of the various NDA/CN^- derivatized amino acids.

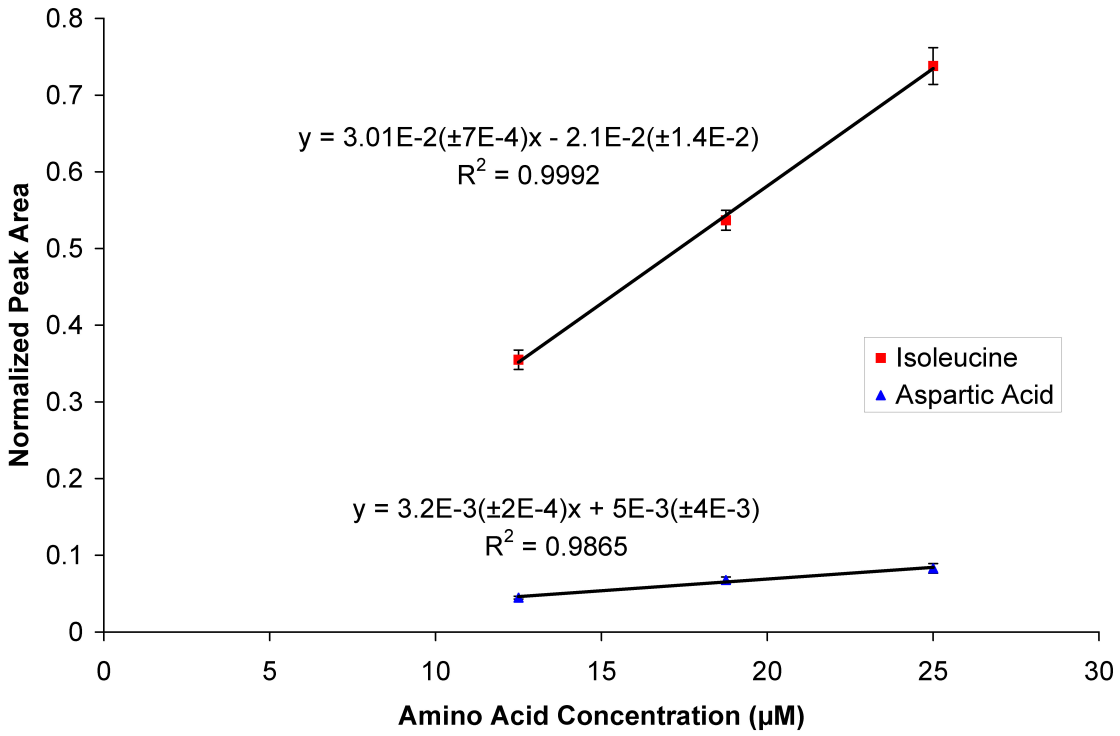

Figure 34. Calibration curves of isoleucine and aspartic acids using Generation II AAFA.

A table of sensitivities, intercepts, and correlation coefficients for all peaks is shown in Table 13, sorted by increasing sensitivity. There was variability in the sensitivities of the various amino acids. Lysine, aspartic acid, glutamic acid, and cystine have very low sensitivities. Arginine and phenylalanine + leucine have very high sensitivities. All other amino acids have similar sensitivities. Due to the low sensitivity, lysine and aspartic acid also have much lower correlation coefficients. These amino acids will most likely not be able to discern concentration changes caused by cellular flux form the MBR

Table 13. Calibration curve parameters for Generation II AAFA. The slope is the sensitivity, and R^2 is the Pearson's correlation coefficient. Error is the ± 95% confidence interval.

Amino Acid(s)	Slope (RFU·s/μM)	Intercept (RFU·s)	R^2
Lysine	3.0E-03 ± 8.E-04	7.E-04 ± 2.E-02	0.69
Aspartic Acid	3.0E-03 ± 5.E-04	8.E-03 ± 9.E-03	0.86
Glutamic Acid	6.5E-03 ± 3.E-04	-3.E-03 ± 6.E-03	0.99
Cystine	8.3E-03 ± 8.E-04	-1.E-02 ± 8.E-03	0.94
Asparagine + Threonine	2.0E-02 ± 1.E-03	5.E-03 ± 3.E-02	0.97
Serine	2.2E-02 ± 2.E-03	1.E-01 ± 4.E-02	0.94
Glutamine	2.2E-02 ± 2.E-03	1.E-02 ± 2.E-01	0.97
Methionine	2.3E-02 ± 1.E-03	9.E-03 ± 3.E-02	0.98
Glycine	2.4E-02 ± 1.E-03	5.E-02 ± 3.E-02	0.98
Alanine	2.5E-02 ± 1.E-03	6.E-02 ± 2.E-02	0.98
Histidine	2.7E-02 ± 1.E-03	-3.E-02 ± 3.E-02	0.99
Tyrosine	2.9E-02 ± 2.E-03	-3.E-02 ± 3.E-02	0.98
Isoleucine	3.1E-02 ± 2.E-03	-3.E-02 ± 4.E-02	0.98
Tryptophan	3.8E-02 ± 2.E-03	-2.E-01 ± 4.E-02	0.98
Valine	3.9E-02 ± 2.E-03	-7.E-02 ± 4.E-02	0.99
Arginine	7.9E-02 ± 4.E-03	-7.E-02 ± 7.E-02	0.99
Phenylalanine + Leucine	9.0E-02 ± 4.E-03	-3.E-01 ± 8.E-02	0.99

Conclusion

The design of a micellar electrokinetic chromatography instrument for fast separation of amino acids in cell media was presented. While the instrument began as a slight modification of a published instrument design, the instrument required significant changes due to difficulties with the flow-gate valve, and not being able to implement a separation capillary extension. This led to the development of a completely new design for the instrument.

The instrument is designed to take cell effluent and monitor changes to amino acid consumption on-line in sub-minute time scales. Generation II can separate 19 primary amino acids into 15 distinguishable peaks. This represents 12 amino acids with

baseline separation and 3 peaks that contain 2 or 3 amino acids which co-elute. Cell media, which is continually run for 2.5 hrs, collecting an electropherogram every 1.0 minutes, demonstrate RSD of peak areas of less than 10% for all but two peaks.

The high resolution of separation and high reproducibility of electropherograms indicate that analysis of cell effluent from the MBR could be undertaken. Amino acids with a high reproducibility and high sensitivity such as glutamine, and arginine will be very sensitive to small changes in concentration and changes in concentration from basal metabolism or application of a toxin should be discernable. Amino acids with a low reproducibility and sensitivity such as aspartic acid and lysine will not be able do discern the small concentrations changes expected.

CHAPTER V

MEASURING ONLINE CELLULAR AMINO ACID FLUX FROM A MICROBIOREACTOR USING THE AMINO ACID FLUX ANALYZER

Introduction

To demonstrate the feasibility of using amino acid flux to observe changes in metabolism, compounds that cause a known change in cellular metabolism were selected in order to observe the changes in amino acid flux. To that end, aminooxyacetate (AOA) and sodium arsenite (AsO_2^-) were selected. AML12 hepatocytes were seeded into the MBR and then perifused with the compounds. The changes in amino acid flux were determined online using the AAFA.

AOA is a well-studied general transaminase inhibitor which effects enzymes in both the cytoplasm and mitochondria.[95] In general, the inhibition is accomplished in enzymes requiring vitamin B6 by covalently binding to pyridoxal 5'-phosphate (PLP).[96,97] As a result, PLP is no longer able to bind amino acids and transamination is halted.

AOA has many effects on hepatocytes that encompass a variety of different processes in which amino acids play a role. AOA completely inhibits the urea cycle by stopping mitochondrial transaminases.[95] AOA significantly inhibits protein synthesis and eliminates any stimulatory effect by lactate, pyruvate, and amino acids on protein synthesis.[98] AOA also significantly reduces gluconeogensis.[95,99,100] However, it does not significantly effect overall energy production in the cell.[95,98] AOA was chosen as it

affects many processes which employ amino acids and thus it should also effect cellular amino acid fluxes.

AsO_2^-, which is arsenic in the +3 oxidation state, has long been recognized as a toxic agent. It was even used during WWI in chemical weapons.[101] The major effect of AsO_2^- is inhibition of 2-oxo-acid dehydrogenase complexes such as pyruvate dehydrogenase, and alpha-ketoglutarate dehydrogenase by binding to the two sulfhydryl groups of lipoamide.[101-103] This stops the TCA cycle and prevents cellular respiration. Since many amino acids are metabolized to TCA cycle intermediates and pyruvate, AsO_2^- should affect cellular flux of amino acids.

In this chapter, we measured amino acid concentration online from the effluent of AML12 hepatocytes in the MBR. The cells were then exposed to either AOA or AsO_2^- and the change in the concentration caused by the toxin was then observed. Finally, the change in concentration caused by AOA was compared to that due to AsO_2^-, and discrimination between the effects was made.

Methods

Combining the MBR and AAFA

The MBR is used as described in Chapter 3 from the standpoint of the design, procedure for seeding of cells, and the setup of the perifusion. However, the input and output have been modified. The input is from a valve that can switch between five different solutions entering into the MBR. Only two solutions were employed in the

study. The output from the MBR is directed into a second valve so the effluent can be analyzed online by the AAFA, rather than offline by HPLC.

In chapter 4, the AAFA was only used to analyze base cell media containing a known composition of small molecules. Cell effluent, on the other hand, contains protein, which adsorb to the walls of fused silica, leading to band broadening and complete loss of resolution of separated amino acids. To circumvent this problem, the effluent was dialyzed using a microdialysis probe. This technique eliminates small molecules from the media while still providing capability for online analysis. A CMA 11 microdialysis probe, along with tubing and adapters, all from CMA Microdialysis, was used. The probe was inserted into a 22-gauge needle, which was connected to a rotary valve, see Figure 35. The sample flows into the needle and around the dialysis probe and flows out of the needle to waste. The dialysate out contains small molecules from the effluent, but does not contain any proteins. Since the flow rate of the dialysate through the probe and the sample around the probe remains constant, the percent recovery, which is the percent concentration of the sample in the dialysate, will remain constant. Therefore, any change in concentration of amino acids in the dialysate should be indicative of a concentration change in the sample.

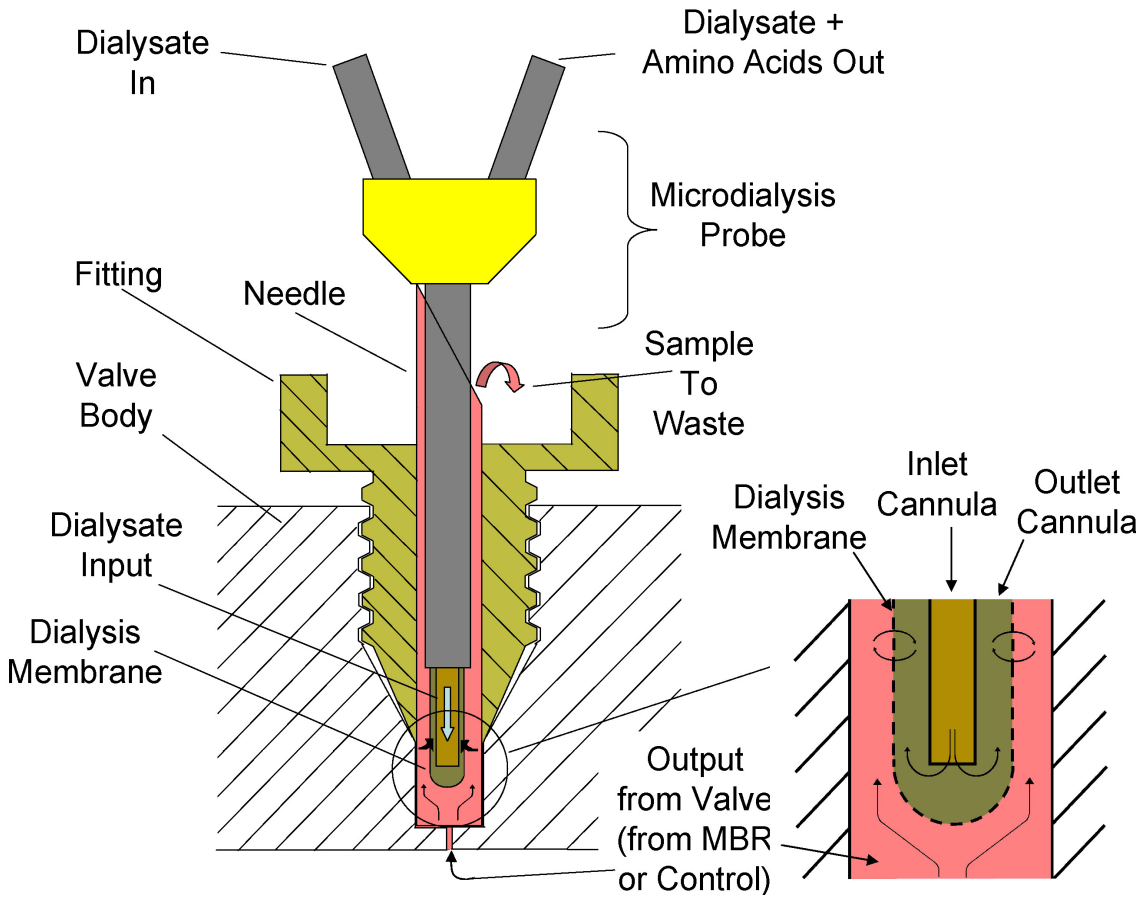

Figure 35. Diagram of online microdialysis of amino acid solutions. The sample flows out of the valve chamber into a hole in the valve body, and then into the needle into which a microdialysis probe is inserted. The sample then flows around the microdialysis probe and out the needle to waste. The dialysate flows down the inner cannula which is in the shaft of the probe. The dialysate flows back concentrically in contact with the dialysis membrane where small molecules diffuse in from the sample. The dialysate returns outside the inner canula, back though the shaft of the probe, and to the outlet.

The AAFA was used as described in Chapter 4 with modification to the flow rate. The amino acid solution entering the AAFA is dialyzed at 1.0 µL/min with the dialysate output containing a single-digit percentage of amino acids from cell media. The lower concentration of amino acids in the dialysate in comparison to cell media required

lowering the flow rate of the derivatization reagents in order to increase the concentration of derivatized amino acids. The new flow rates were 1.3 μL/min for the KCN and 0.7 μL/min for the NDA solution. The reaction capillary was shortened to 20 cm of 250 μm ID fused silica, to provide an internal volume of 10 μL which maintains the same derivatization reaction time of 200 s.

Experimental setup

Each AAFA experiment provides quantization of amino acids in three different solutions. A control media was used to provide a reference value for the starting concentration of each amino acid. The basal metabolism of the cells was determined by perifusing the MBR with regular media and analyzing the effluent. A test compound, either 0.5 mM AOA or 0.2 mM AsO_2^- added to the cell media was then perifused through the MBR and the change in the metabolism is observed by analyzing the effluent. The fluidics which brings these four solutions to the AAFA is shown in Figure 36. The details of the AAFA instrument are presented in Chapter 4.

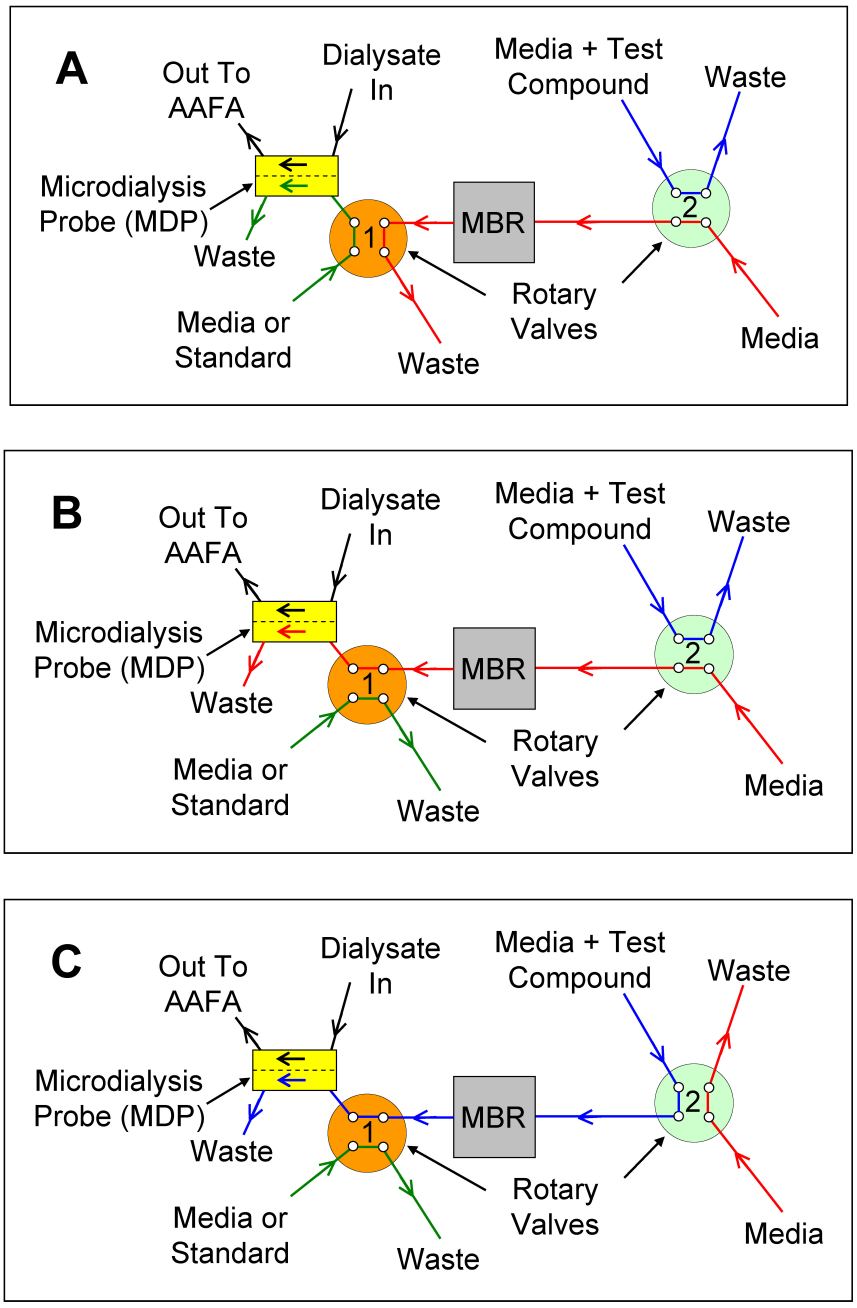

Figure 36. Experimental setup for AAFA experiments. Two rotary valves 1 and 2 are used to control flow to the microdialysis probe (MDP) and finally to the AAFA for analysis. All media is continuously flowing at 0.5 µL/min. Starting conditions are shown in panel A, where control media (green) flows to the MDP at valve 1 and cell effluent (red) flows to waste. The AAFA analyzes the control dialysate output. Valve 1 is then switched to place the system in mode B, where cell effluent is diverted to the MDP for AAFA analysis. Valve 2 is then switched to achieve mode C. The test compound (blue) then perifuses the MBR and the effluent flows to the MDP and the AAFA records the effect of the test compound.

Results and Discussion

Delay and Response Times of Solution Switching

Before experiments were run with live cells, the instrument was tested with an MBR without cells to determine the delay and response time of switching between solutions as shown in Figure 37. To observe the appearance and disappearance of each solution, cell media spiked with an amino acid was loaded into the experimental setup shown in Figure 36. A different amino acid was spiked into each solution. The delay time is defined as the time from when the valve is switched to the time when the signal changes by >10%. The response time is defined as the time from when the new solution starts being analyzed to the time when the signal has reached 90% of the final response. Electropherograms were analyzed as described in Chapter 4. The delay time for the first valve switch, represented by proceeding from Figure 1A to Figure 1B, was found to be 9 minutes and the response time was found to be 8 minutes. The delay time for the second valve switch, represented by Figure 1B to Figure 1C, was found to be 37 minutes and the response time was found to be 10 minutes. The delay times strongly agree with the predicted times which were calculated from the volume of the MBR, ports, and tubing, at the given flow rates. The predicted delay time for the first valve switch is 8.4 minutes determined from the flow rate and volume of the flow-through volumes of the port before the dialysis probe, the output of the dialysis probe, tubing from the dialysis probe to the derivatization cross, and time in the derivatization capillary. The predicted delay time for the second valve switch is 38.7 minutes which is calculated from the flow rate and volume of the tubing from valve 2 in Figure 36 to the MBR, the volume of the MBR, and

inlet and outlets, the tubing from the MBR to valve 1, and the time for the first valve switch.

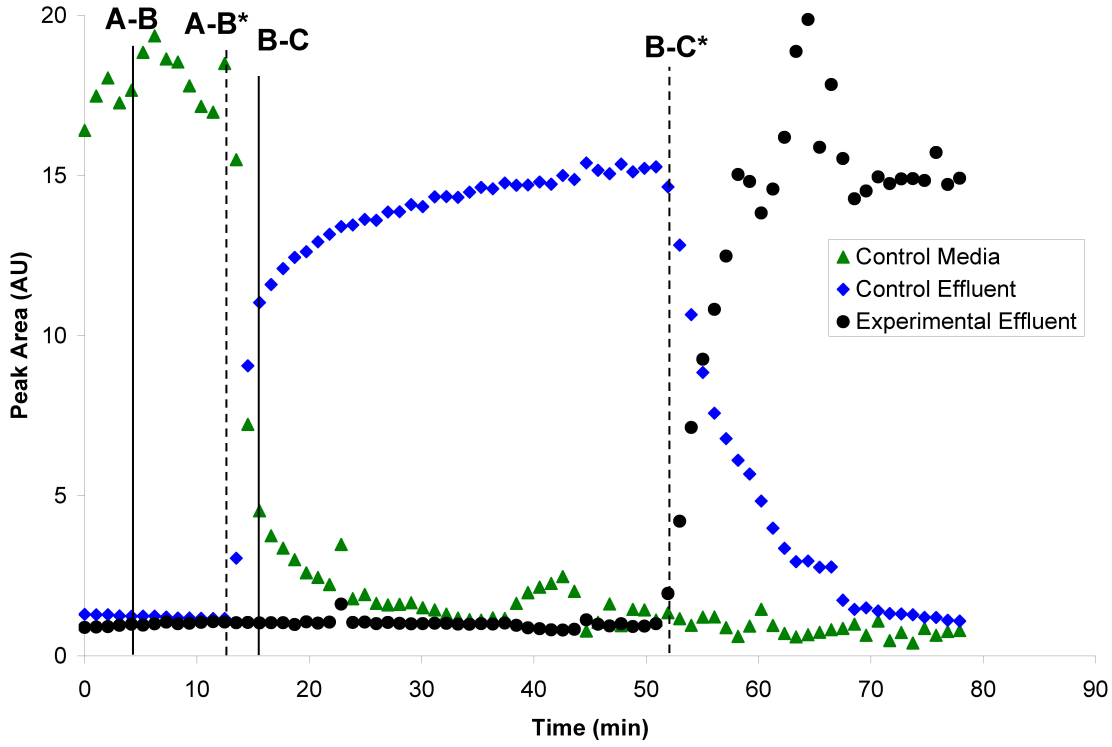

Figure 37. The response and delay times of each of the valve switches were visualized by using media spiked with an amino acid. At A-B, referring to **Figure 36**, valve 1 was switched from control to effluent. The effect of the switch was observed at A-B*. At B-C, valve 2 was switched from effluent to test compound. The effect of the switch was observed at B-C*. The time from A-B to A-B*, and B-C to B-C* represents the delay time of the valve switches.

Instrumental Achievements

In Chapter I, several instrumental specification goals were stated. These goals are compared to actual measured specifications as stated in Table 14.

Table 14. MBR and AAFA specification goals and measured parameters.

Characteristic	Goal	Actual
MBR Cell Number	~ 1×10^5	~ 2×10^5
MBR Volume	< 5 µL	4 µL
MBR Media Transit Time	< 5 min	8 min
Delay Time From MBR to AAFA	< 5 min	37 min
Response Time	< 2 min	10 min
AAFA Inject-to-Inject Time	< 2 min	30-45 s
Electropherogram Reproducibility (RSD)	< 15%	9 - < 5% 4- 5-15% 2 - ≥ 15%

MBR parameters are met or nearly so with cell number, MBR volume, and media transit time close to the specified values. The original goal of 1×10^5 cells was only designed to be an approximate guideline, so having doubled the number of cells is not of concern. The AAFA goals were met or exceeded for most values. The inject-to-inject time was less than half the the goal, and all but two amino acids were within the reproducibility goals. Those two amino acids had particularly small peaks, so accurate quantitation proved difficult.

Instrument specifications regarding attachment of the MBR to the AAFA were not met. The delay time of 37 minutes was more than seven times higher than the goal and the response time was five times higher. The low flow rate of 0.5 µL/min proved difficult to transport quickly in spite of using very small ID tubing of 100 µm. Smaller tubing resulted in too much backpressure and resulted in leaks at the MBR. Possible solutions are creating a larger MBR or integrating stop-flow perifusion. A larger MBR will require larger flow rates. Larger flow rates will be able to be transported faster and

with smaller pressure since volume contained withing tubing increased with the radius squared, but the pressure increases with the radius to the fourth power according to Poiseuille's Law. Stop-flow perifusion will allow accumulation of changes in the medium during the stop period that will be quickly swept to the instrument during the flow period.

Normalized Raw Peak Areas

Using this experimental setup, three MBR experiments with AML12 hepatocytes seeded in the MBR with AOA were completed. The results for glutamine are shown in Figure 38, alanine in Figure 39, and arginine in Figure 40 are shown as examples. Graphs were made for all resolvable amino acids.

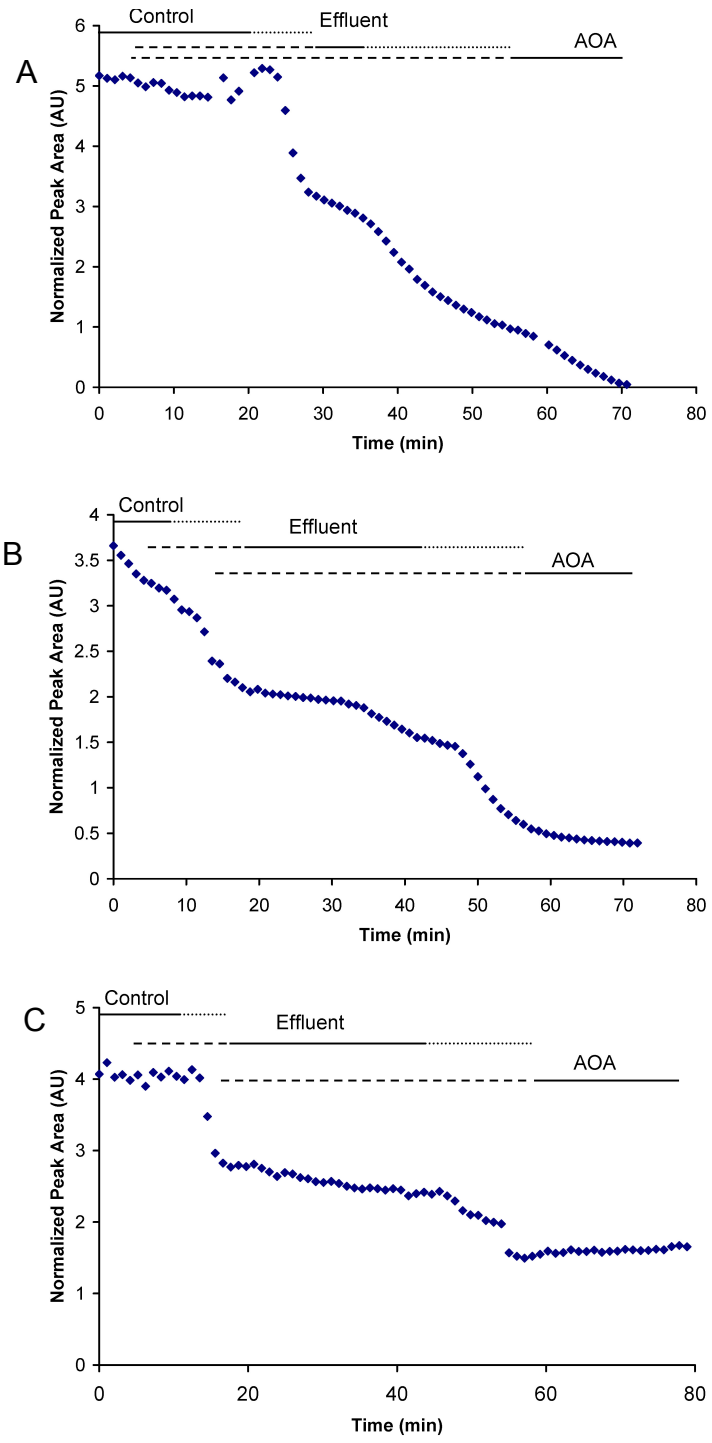

Figure 38. Effects of AOA on normalized glutamine peak areas for three independent experiments (A-C). Starting condition is control media. A rotary valve is switched at the beginning of each dashed line. The dashed line represents the delay time from when the valve is switched to when the solution starts being analyzed by the AAFA. AAFA analysis occurs during the solid line. The dotted line represents the response time of the AAFA, when solutions are transitioning from one to another.

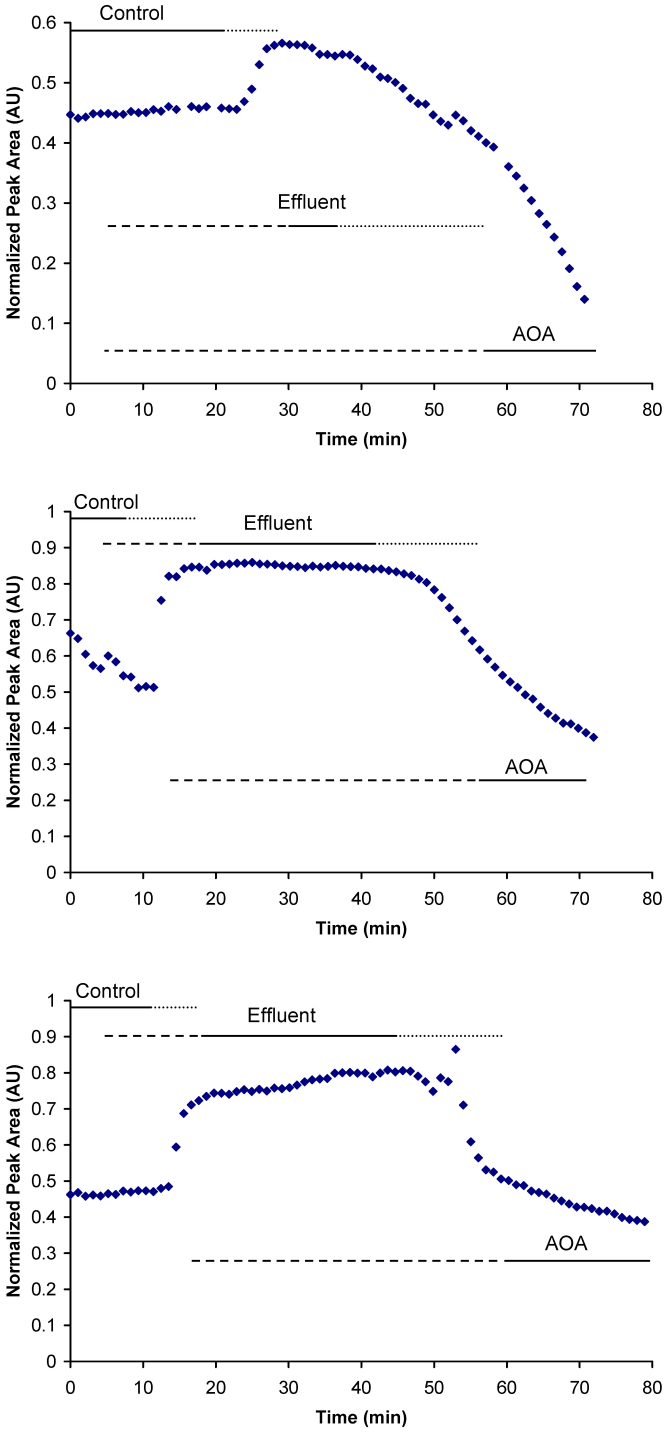

Figure 39. Effects of AOA on normalized alanine peak areas for three independent experiments (A-C). Starting condition is control media. A rotary valve is switched at the beginning of the dashed line. The dashed line represents the delay time from when the valve is switched to when the solution starts being analyzed by the AAFA. AAFA analysis occurs during the solid line. The dotted line represents the response time of the AAFA, when solutions are transitioning from one to another.

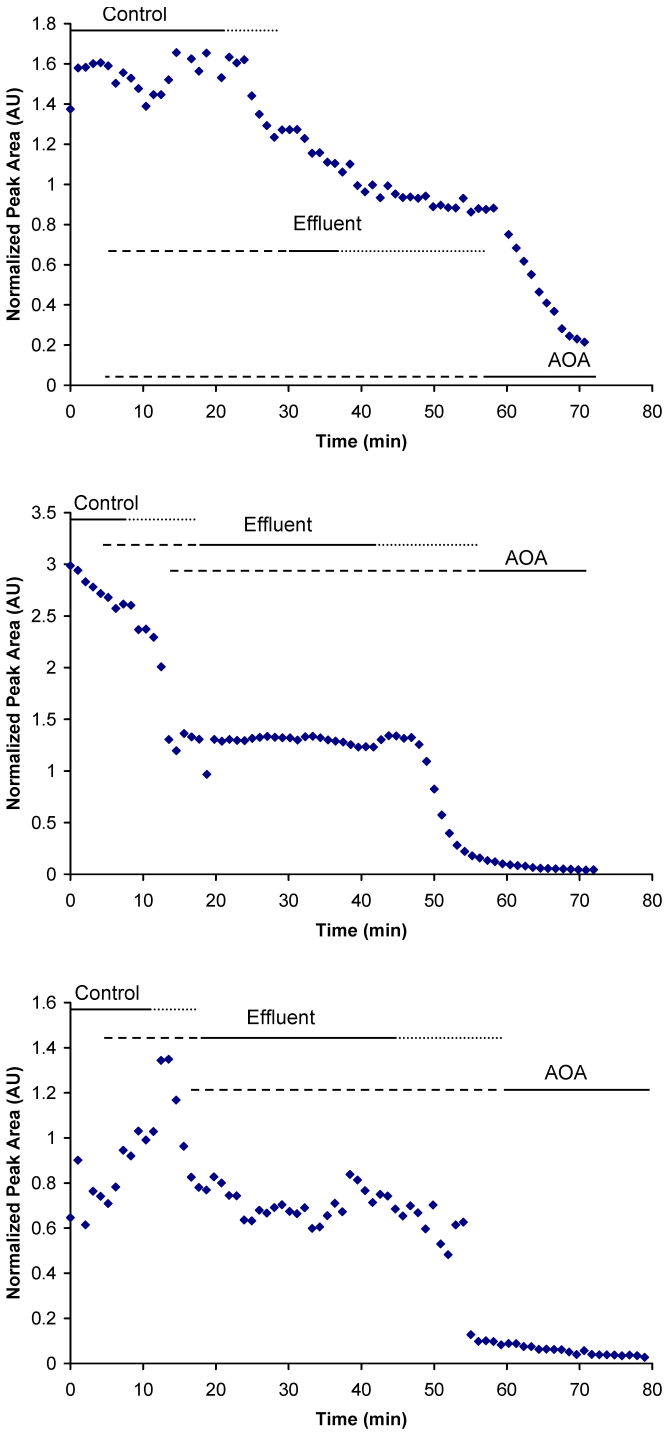

Figure 40. Effects of AOA on normalized arginine peak areas for three independent experiments (A-C). Starting condition is control media. A rotary valve is switched at the beginning of the dashed line. The dashed line represents the delay time from when the valve is switched to when the solution starts being analyzed by the AAFA. AAFA analysis occurs during the solid line. The dotted line represents the response time of the AAFA, when solutions are transitioning from one to another.

The data show that all three experiments demonstrate a similar trend. The glutamine experiments all showed a decrease in peak area for the cell effluent as compared to the control media, then a further decrease when AOA was applied, indicating that the flux rate increased upon application of AOA. The alanine concentration in the cell effluent was higher than in the control media, but, then decreased back to close to basal levels during application of AOA. The arginine concentration decreased relative to control during cell effluent measurement, but decreased even more strongly during AOA application.

A second inhibitor, AsO_2^-, was also utilized. AsO_2^- is an inhibitor of oxo-acid dehydrogenases. This includes pyruvate dehydrogenase, oxoglutarate dehydrogenase, and the branched chain oxo-acid dehydrogenases. Results are shown Figure 41, for glutamine, Figure 42, for alanine, and Figure 43 for arginine.

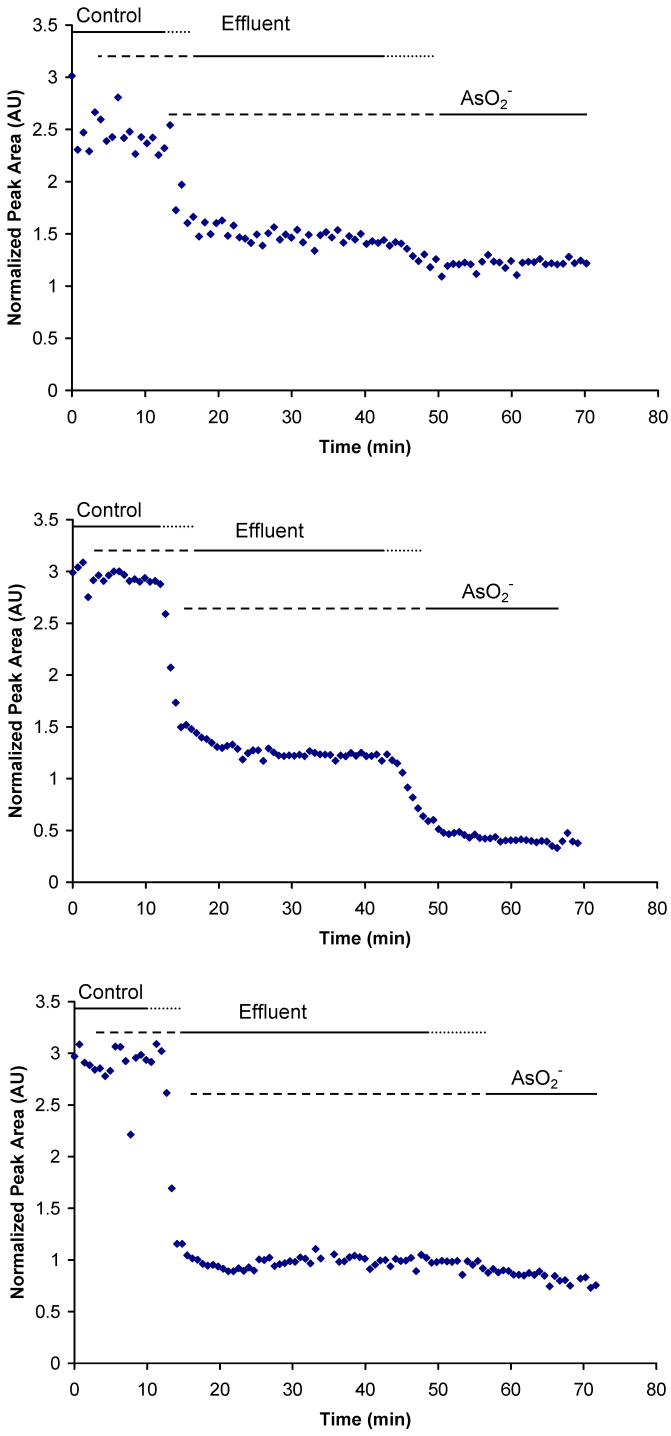

Figure 41. Effects of AsO_2^- on normalized glutamine peak areas for three independent experiments (A-C). Starting condition is control media. A rotary valve is switched at the beginning of the dashed line. The dashed line represents the delay time from when the valve is switched to when the solution starts being analyzed by the AAFA. AAFA analysis occurs during the solid line. The dotted line represents the response time of the AAFA, when solutions are transitioning from one to another.

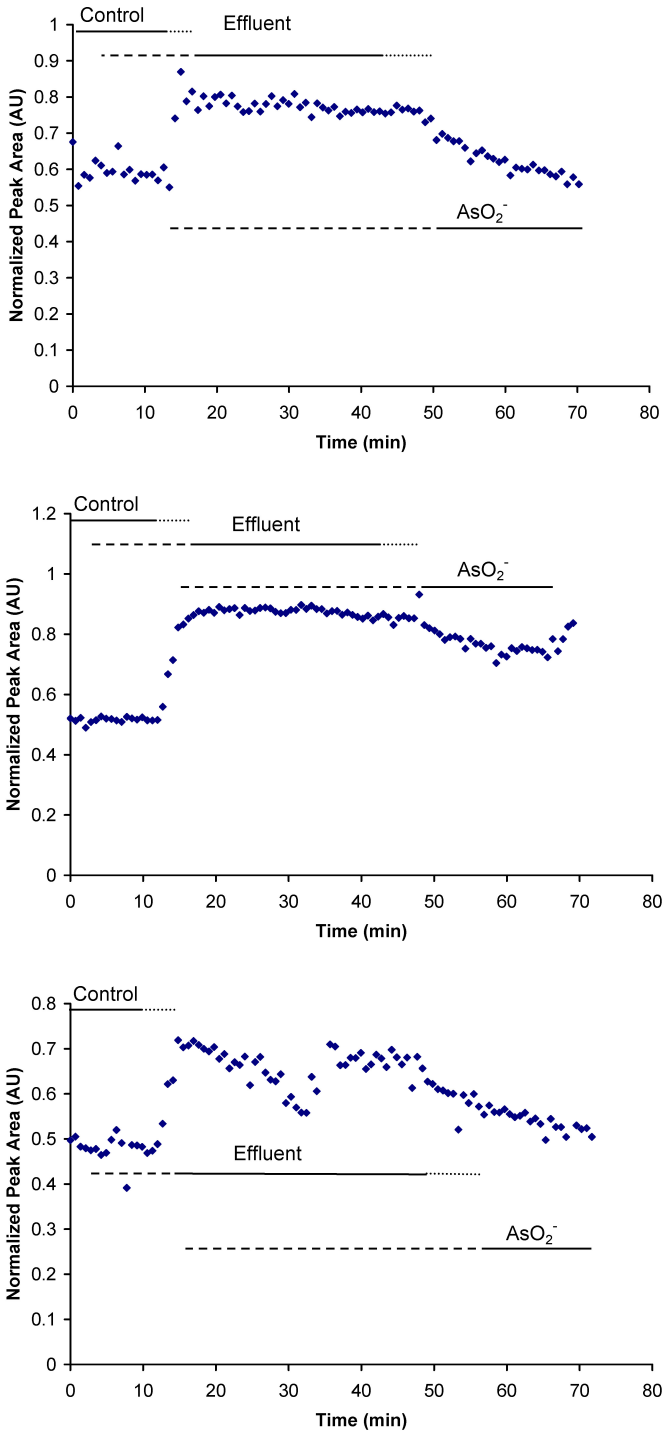

Figure 42. Effects of AsO_2^- on normalized alanine peak areas for three independent experiments (A-C). Starting condition is control media. A rotary valve is switched at the beginning of the dashed line. The dashed line represents the delay time from when the valve is switched to when the solution starts being analyzed by the AAFA. AAFA analysis occurs during the solid line. The dotted line represents the response time of the AAFA, when solutions are transitioning from one to another.

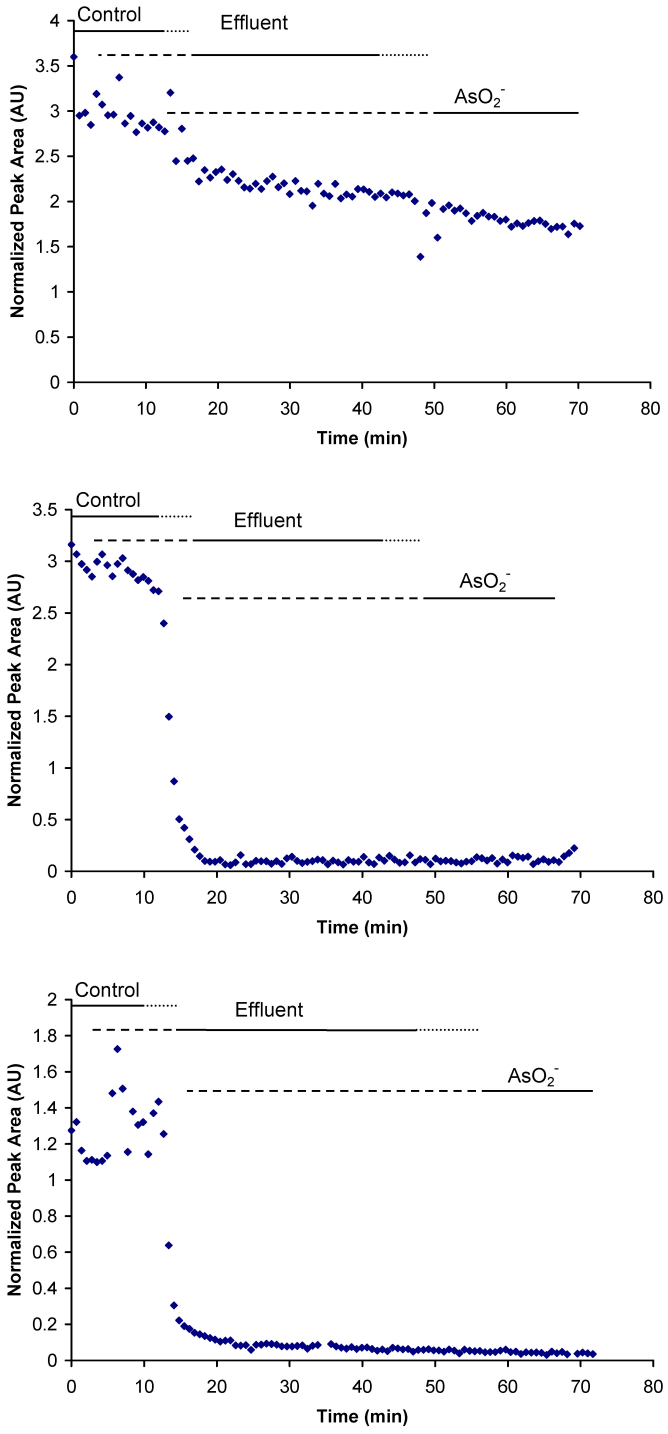

Figure 43. Effects of AsO_2^- on normalized arginine peak areas for three independent experiments (A-C). Starting condition is control media. A rotary valve is switched at the beginning of the dashed line. The dashed line represents the delay time from when the valve is switched to when the solution starts being analyzed by the AAFA. AAFA analysis occurs during the solid line. The dotted line represents the response time of the AAFA, when solutions are transitioning from one to another.

Most of the amino acids again behaved similarly in all three experiments. The glutamine concentration in the effluent was lower than in the control media, and further still with application of AsO_2^-. The alanine concentration increased with the effluent and decreased upon application of AsO_2^-, but the concentration only decreased to the basal metabolic level at the end of run in 2 out of 3 experiments. The arginine concentration decreased almost to 0 for the effluent for 2 of the 3 experiments, the remaining experiment showed a moderate decrease that continued to moderately decrease with AsO_2^- exposure.

After inhibitor exposure, an amino acid standard was analyzed by the AAFA where the solution contained a known concentration of amino acids for the purposes of calibration. This solution was not used during the data analysis for a variety of reasons. The standard frequently did not give steady responses for many of the amino acids and the observed concentration in the control media strongly disagreed with the nominal concentration in the base media; sometimes by more than a factor of two. Since absolute quantitation of amino acids was not needed for this study, the standards were not used.

Data Summary

A summary of responses for select amino acids, normalized to control media, illustrating the effect of AOA and ASO_2^- is shown in Figure 44. The values were calculated by pooling points from each of the solution types measured, and dividing them by the cell media control. Error is expressed as ± the 95% confidence interval of the data.

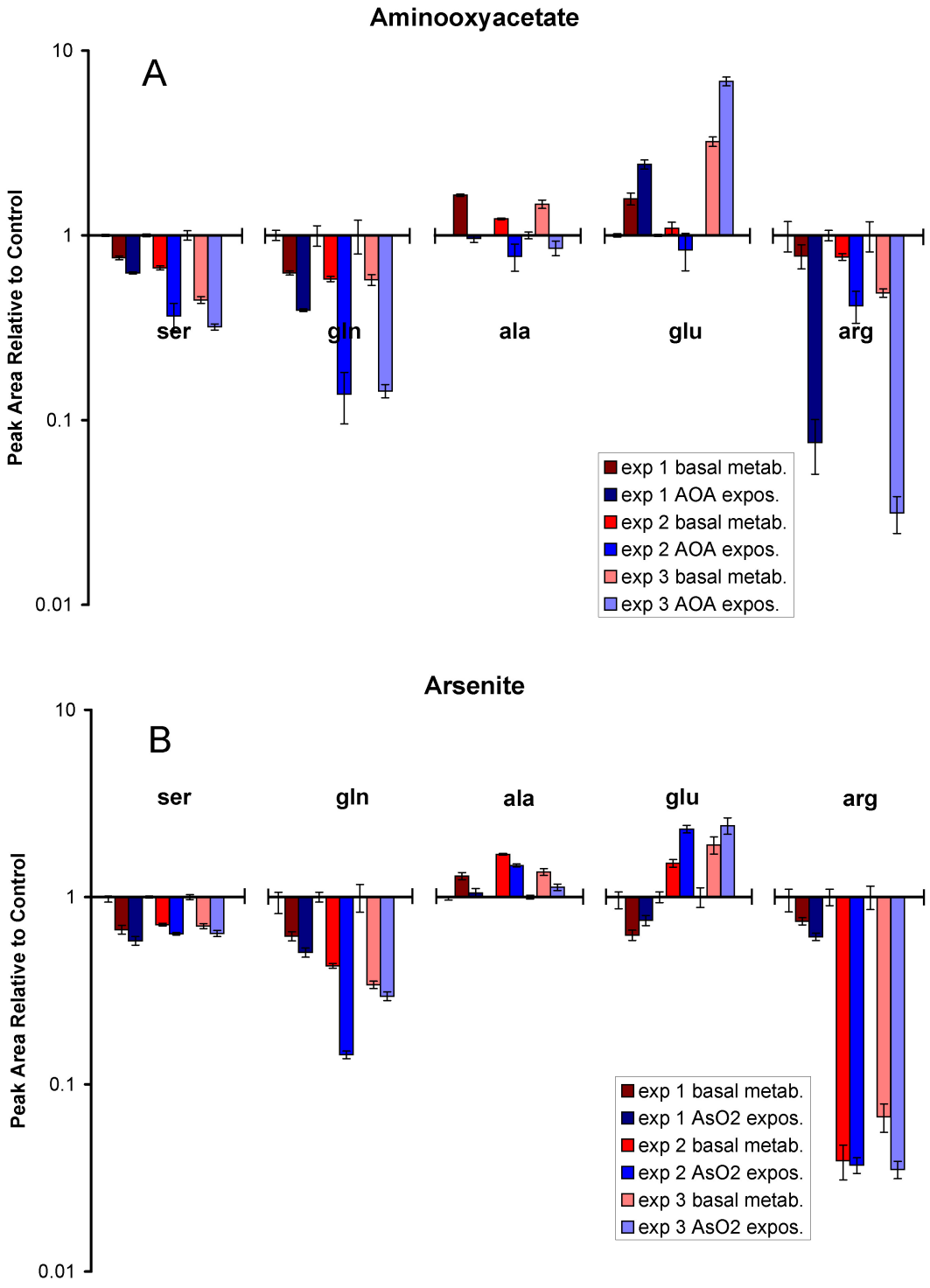

Figure 44. Effect of 0.5 mM aminooxyacetae (A) and 0.2 mM AsO_2^- (B) on peak areas relative to control media for three separate experiments. The error bars before the basal metabolism is the error in the control media. Basal cellular metabolism is shown in shades of red and AOA or AsO_2^- are shown in shades of blue. Error bars are the ±95% confidence interval.

The remainder of the amino acids are shown Table 15 for AOA and Table 16 for AsO_2^-.

Table 15. Effect of 0.5 mM AOA on peak areas relative to cell media control for three separate experiments. Control is normalized to unity after averaging. Basal and AOA are listed as fractional change relative to control.

Experiment 1			
	Control	Basal	AOA
Serine	1.00 ± 0.01	0.76 ± 0.02	0.63 ± 0.01
Asparagine+Threonine	1.00 ± 0.01	0.97 ± 0.03	0.77 ± 0.01
Glutamine	1.00 ± 0.06	0.63 ± 0.02	0.39 ± 0.01
Alanine	1.00 ± 0.01	1.65 ± 0.03	0.96 ± 0.05
Tyrosine	1.00 ± 0.01	1.01 ± 0.03	1.02 ± 0.04
Glutamate	1.00 ± 0.02	1.58 ± 0.12	2.42 ± 0.14
Valine	1.00 ± 0.04	1.05 ± 0.04	1.00 ± 0.03
Aspartate	1.00 ± 0.00	0.76 ± 0.09	0.74 ± 0.05
Methionine	1.00 ± 0.01	0.87 ± 0.03	0.88 ± 0.03
Isolelucine	1.00 ± 0.04	1.14 ± 0.06	1.15 ± 0.06
Tryptophan	1.00 ± 0.01	1.09 ± 0.10	1.17 ± 0.11
Leucine+Phenylalanine	1.00 ± 0.12	1.09 ± 0.08	1.11 ± 0.08
Cystine	1.00 ± 0.00	1.25 ± 0.17	1.33 ± 0.19
Arginine	1.00 ± 0.19	0.77 ± 0.12	0.08 ± 0.02
Lysine	1.00 ± 0.02	2.99 ± 0.67	6.77 ± 1.49

Experiment 2			
	Control	Basal	AOA
Serine	1.00 ± 0.02	0.67 ± 0.02	0.37 ± 0.06
Asparagine+Threonine	1.00 ± 0.01	0.71 ± 0.03	0.71 ± 0.13
Glutamine	1.00 ± 0.13	0.58 ± 0.02	0.14 ± 0.04
Alanine	1.00 ± 0.00	1.23 ± 0.01	0.77 ± 0.13
Tyrosine	1.00 ± 0.01	0.90 ± 0.02	0.85 ± 0.06
Glutamate	1.00 ± 0.01	1.09 ± 0.08	0.83 ± 0.19
Valine	1.00 ± 0.02	0.84 ± 0.01	0.69 ± 0.01
Aspartate	1.00 ± 0.00	0.26 ± 0.06	0.99 ± 0.79
Methionine	1.00 ± 0.00	0.75 ± 0.01	0.60 ± 0.17
Isolelucine	1.00 ± 0.02	0.87 ± 0.01	0.73 ± 0.02
Tryptophan	1.00 ± 0.01	0.87 ± 0.08	1.06 ± 0.63
Leucine+Phenylalanine	1.00 ± 0.03	0.78 ± 0.03	0.62 ± 0.04
Cystine	1.00 ± 0.00	0.86 ± 0.07	0.60 ± 0.10
Arginine	1.00 ± 0.06	0.76 ± 0.03	0.42 ± 0.08
Lysine	1.00 ± 0.01	1.30 ± 0.13	1.52 ± 0.17

Experiment 3			
	Control	Basal	AOA
Serine	1.00 ± 0.06	0.45 ± 0.02	0.32 ± 0.01
Asparagine+Threonine	1.00 ± 0.02	0.81 ± 0.02	0.71 ± 0.02
Glutamine	1.00 ± 0.21	0.57 ± 0.04	0.14 ± 0.01
Alanine	1.00 ± 0.04	1.48 ± 0.08	0.85 ± 0.08
Tyrosine	1.00 ± 0.03	0.88 ± 0.04	0.95 ± 0.04
Glutamate	1.00 ± 0.01	3.22 ± 0.19	6.83 ± 0.37
Valine	1.00 ± 0.06	0.85 ± 0.03	0.85 ± 0.03
Aspartate	1.00 ± 0.01	0.56 ± 0.11	0.93 ± 0.17
Methionine	1.00 ± 0.02	0.84 ± 0.04	0.85 ± 0.05
Isolelucine	1.00 ± 0.06	0.84 ± 0.03	0.89 ± 0.04
Tryptophan	1.00 ± 0.00	0.90 ± 0.05	0.89 ± 0.05
Leucine+Phenylalanine	1.00 ± 0.08	0.82 ± 0.03	0.90 ± 0.03
Cystine	1.00 ± 0.00	1.79 ± 0.33	1.71 ± 0.35
Arginine	1.00 ± 0.19	0.49 ± 0.03	0.03 ± 0.01
Lysine	1.00 ± 0.16	0.48 ± 0.11	0.69 ± 0.16

Table 16. Effect of 0.2 mM AsO_2^- on peak areas relative to cell media control for three separate experiments. Control is normalized to unity after averaging. Basal and AOA are listed as fractional change relative to control.

	Experiment 1		
	Control	Basal	AOA
Serine	1.00 ± 0.06	0.67 ± 0.04	0.58 ± 0.03
Asparagine+Threonine	1.00 ± 0.04	0.80 ± 0.05	0.71 ± 0.05
Glutamine	1.00 ± 0.18	0.62 ± 0.04	0.51 ± 0.03
Alanine	1.00 ± 0.04	1.30 ± 0.06	1.05 ± 0.06
Histidine	1.00 ± 0.02	0.83 ± 0.03	0.77 ± 0.03
Tyrosine	1.00 ± 0.05	0.82 ± 0.06	0.62 ± 0.05
Valine	1.00 ± 0.09	0.83 ± 0.05	0.76 ± 0.05
Glutamate	1.00 ± 0.13	0.63 ± 0.04	0.75 ± 0.05
Methionine	1.00 ± 0.03	0.74 ± 0.04	0.71 ± 0.04
Isolelucine	1.00 ± 0.09	0.80 ± 0.04	0.73 ± 0.04
Leucine+Phenylalanine	1.00 ± 0.06	0.88 ± 0.04	0.88 ± 0.04
Cystine	1.00 ± 0.01	0.74 ± 0.04	0.55 ± 0.03
Arginine	1.00 ± 0.17	0.74 ± 0.03	0.61 ± 0.03
Lysine	1.00 ± 0.02	0.98 ± 0.04	0.97 ± 0.06
	Experiment 2		
	Control	Basal	AOA
Serine	1.00 ± 0.01	0.71 ± 0.01	0.64 ± 0.01
Asparagine+Threonine	1.00 ± 0.01	0.83 ± 0.02	0.82 ± 0.02
Glutamine	1.00 ± 0.06	0.43 ± 0.01	0.14 ± 0.01
Alanine	1.00 ± 0.01	1.69 ± 0.02	1.47 ± 0.03
Histidine	1.00 ± 0.01	0.84 ± 0.01	0.81 ± 0.02
Tyrosine	1.00 ± 0.01	0.86 ± 0.02	0.88 ± 0.02
Valine	1.00 ± 0.04	0.86 ± 0.02	0.89 ± 0.02
Glutamate	1.00 ± 0.07	1.52 ± 0.07	2.31 ± 0.11
Methionine	1.00 ± 0.02	0.76 ± 0.02	0.79 ± 0.02
Isolelucine	1.00 ± 0.04	0.86 ± 0.02	0.87 ± 0.02
Leucine+Phenylalanine	1.00 ± 0.08	0.87 ± 0.03	0.94 ± 0.03
Cystine	1.00 ± 0.00	0.82 ± 0.03	0.82 ± 0.04
Arginine	1.00 ± 0.10	0.04 ± 0.01	0.04 ± 0.00
Lysine	1.00 ± 0.02	2.34 ± 0.12	2.25 ± 0.10
	Experiment 3		
	Control	Basal	AOA
Serine	1.00 ± 0.03	0.70 ± 0.02	0.64 ± 0.02
Asparagine+Threonine	1.00 ± 0.03	0.87 ± 0.05	0.83 ± 0.05
Glutamine	1.00 ± 0.17	0.34 ± 0.02	0.30 ± 0.02
Alanine	1.00 ± 0.02	1.36 ± 0.06	1.13 ± 0.05
Histidine	1.00 ± 0.02	0.90 ± 0.06	0.93 ± 0.05
Tyrosine	1.00 ± 0.04	0.93 ± 0.06	0.91 ± 0.06
Valine	1.00 ± 0.10	0.78 ± 0.06	0.82 ± 0.07
Glutamate	1.00 ± 0.12	1.89 ± 0.20	2.41 ± 0.24
Methionine	1.00 ± 0.03	0.83 ± 0.04	0.71 ± 0.03
Isolelucine	1.00 ± 0.10	0.91 ± 0.06	0.88 ± 0.06
Leucine+Phenylalanine	1.00 ± 0.17	0.93 ± 0.05	0.93 ± 0.05
Cystine	1.00 ± 0.01	0.95 ± 0.07	0.91 ± 0.07
Arginine	1.00 ± 0.14	0.07 ± 0.01	0.04 ± 0.00
Lysine	1.00 ± 0.09	1.31 ± 0.09	1.23 ± 0.09

There were large changes in four amino acid peak areas between the basal metabolism and the test compound in which the change was in the same direction for each of the three experiments. This indicates that the AAFA was able to reproducibly detect in less than one hour, a change in amino acid flux in AML12 hepatocytes caused by two different compounds. The amino acid flux change caused by both AOA and AsO_2^- are similar in direction. The peak areas for serine, glutamine, alanine, and arginine increase, thus indicating an overall increase in the influx of those amino acids. The area of glutamate decreases indicating and overall increase in the out flow of glutamate. The magnitude of the change generally appears to be smaller for AsO_2^- than for AOA. Calculating the magnitude of the change in amino acid flux upon exposure of AOA and AsO_2^- then comparing the magnitudes will allow for statistically significant differences to be observed.

Data Normalized to Basal Metabolism

The data summary shown in the previous section was used to determine if there was a differential response between AOA and AsO_2^-. The three replicates were tested with ANOVA and found to have larger variation between each replicate than with, therefore the data could not be combined as one large data set. Instead, the only the average values for each replicate was used. Figure 45 and Figure 46 demonstrate the magnitude of the change in peak areas caused by AOA and AsO_2^-, respectively, by combining the three experiments and normalizing to the basal metabolism. This was

done using three different mathematical methods. The first, was the ratio of the test compound peak area to that for the basal metabolism for each experiment was averaged for the three experiments to quantify the effect of the test compound relative to basal metabolism. The second, subtraction of the test compound from the basal metabolism for each experiment followed by averaging the differences, represents the absolute change in concentration of the amino acid when applying the test compound, as compared to basal metabolism. The third, the difference between the peak areas for the test compound and that for basal metabolism, then divide by the basal metabolism, represents change in concentration when applying the test compound, relative to basal metabolism.

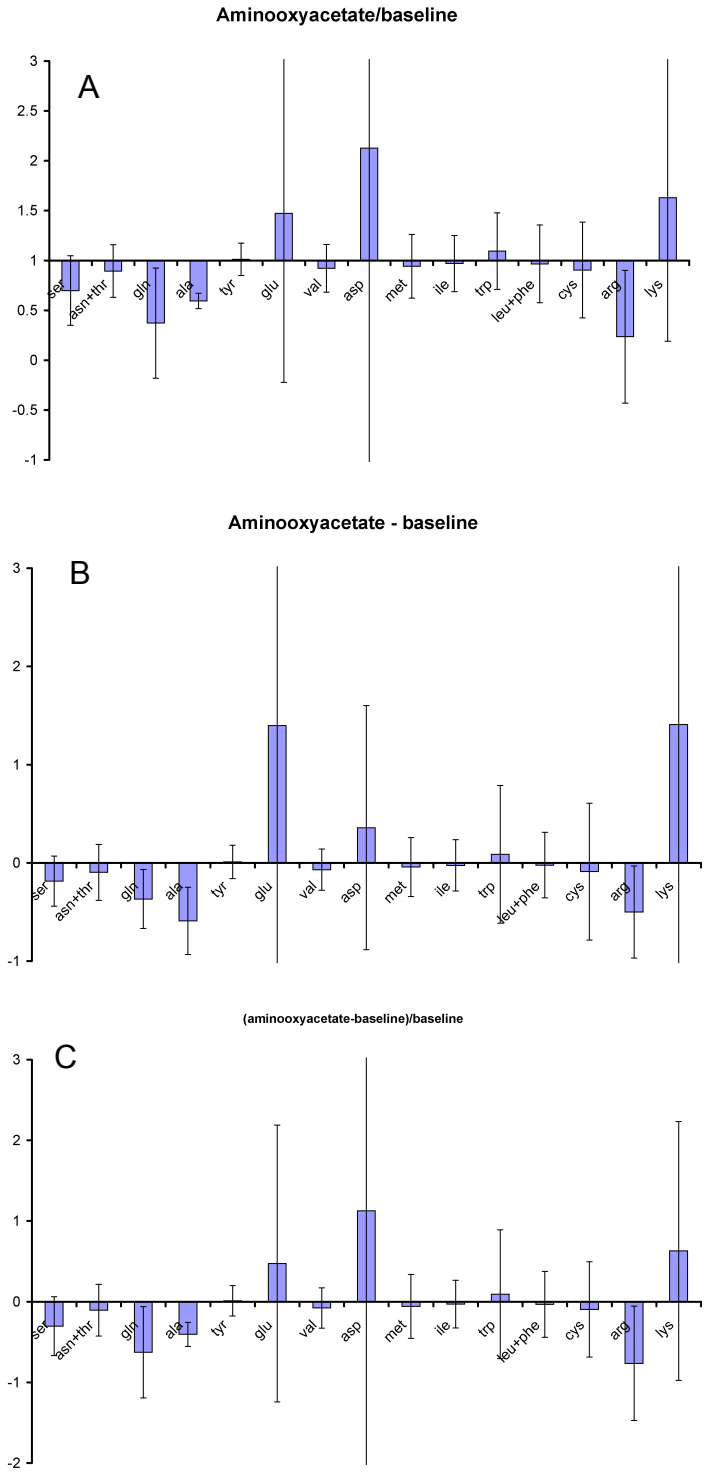

Figure 45. Effect of comparing amino acid peak areas of effluent of AOA exposure to basal cell metabolism using three different mathematical analyses. A) AOA peak area divided by basal cell metabolism peak area, B) AOA minus basal cell metabolism, C) (AOA minus basal cell metabolism) divided by basal cell metabolism. Error bars show ± the 95% confidence interval.

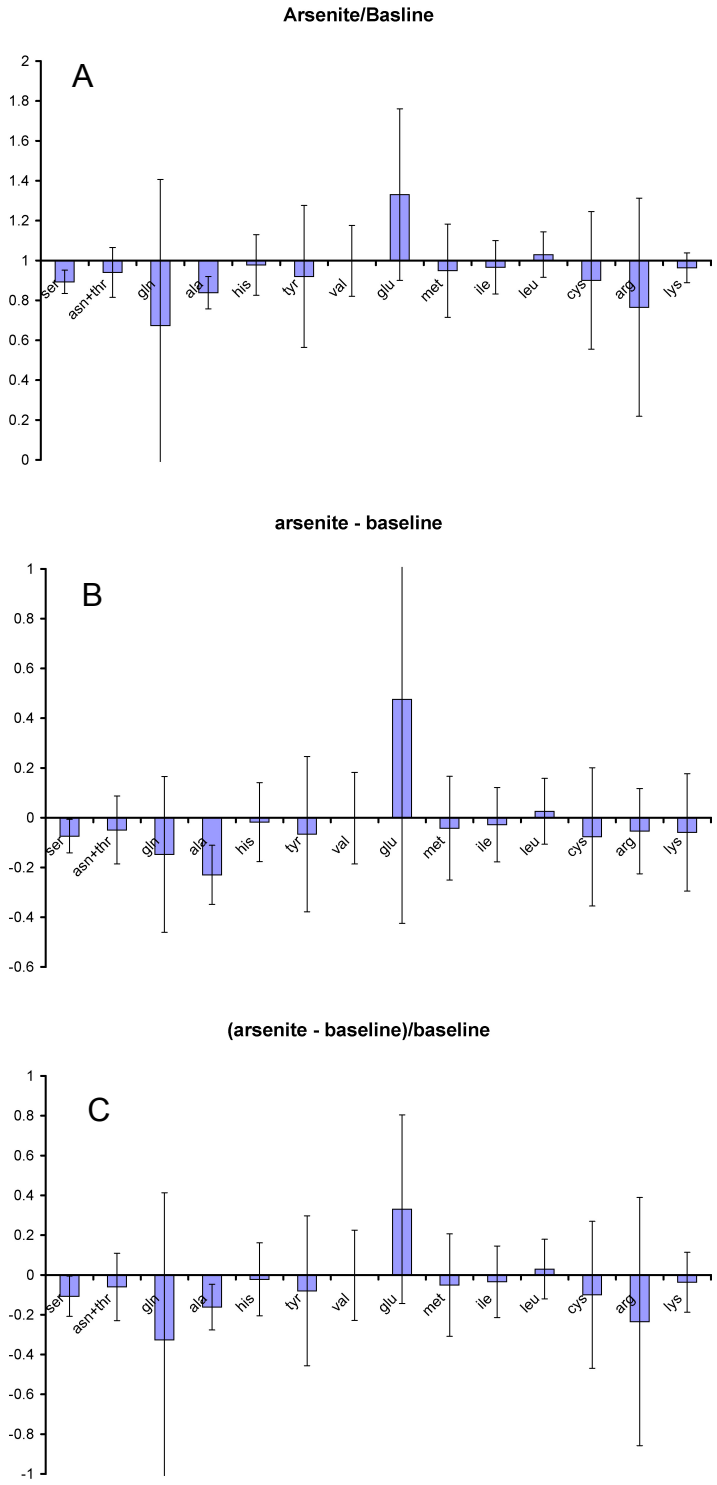

Figure 46. Effect of comparing amino acid peak areas of effluent of AsO_2^- exposure to basal cell metabolism using three different mathematical analyses. A) AsO_2^- peak area divided by basal cell metabolism, B) AsO_2^- minus basal cell metabolism, C) (AsO_2^- minus basal cell metabolism) divided by basal cell metabolism. Error bars show ± the 95% confidence interval.

Statistically significant differences, i.e. $p < 0.05$, between the peak areas of the basal metabolism and during AOA or AsO_2^- exposure are true whenever the confidence interval does not cross the baseline. Thus, glutamine, alanine, and arginine show significant changes upon exposure to AOA, and alanine upon exposure to AsO_2^-. For each case in Figure 45 and Figure 46, the confidence intervals were calculated by combining the confidence intervals that were already present for each of the three experiments with the confidence interval calculated by averaging the three experiments. This was done by propagating the errors of each of the data points, already present through the mathematical averaging used to generate the data. In addition, confidence intervals were calculated from the deviation between the three experiments. The propagated confidence intervals were combined with the calculated confidence intervals to get the total confidence interval for each amino acid.

In order to demonstrate which amino acids exhibited a significant difference in response to AOA versus AsO_2^-, p-values for a student's t test for each amino acid for each of the three analysis methods are shown Table 17. A p-value of <0.05 indicates a significant difference. The p-values were calculated using the averaged data for each of the three experiments for AsO_2^- and AOA.

Table 17. P-Values calculated between AOA and AsO_2^- for the various methods shown in figures 39-40. * indicates significant difference.

	Analysis method		
Amino Acid	test/baseline	test-baseline	test-baseline / baseline
ser	0.134	0.188	0.134
asn+thr	0.538	0.506	0.538
gln	0.236	0.090	0.236
ala	0.001 *	0.032 *	0.001 *
tyr	0.390	0.386	0.390
glu	0.755	0.508	0.755
val	0.330	0.305	0.330
met	0.938	0.991	0.938
ile	0.958	0.975	0.958
cys	0.979	0.925	0.979
arg	0.059	0.037 *	0.059
lys	0.179	0.342	0.179

The flux changes observed upon exposure to AOA is difficult to interpret metabolically. Since AOA is a general transaminase inhibitor, and transaminases are the first step in metabolism of most amino acids, AOA would be expected to inhibit the uptake and release of amino acids. As shown in Figure 44, with the exception of alanine, this was not the case, as indicated by the peak areas going farther from the control. The cause of this is not fully understood, but might involve cellular feedback, perhaps from amino acid transporters. Additionally, the concentration of AOA might not be optimized for this system. The concentration used, 0.5 mM was taken from literature values using primary hepatyctes in totally different experimental setup.[95] In future experiments, a dose-response experimets could be performed to optimize the concentration of AOA.

Exposure to AsO_2^- also affects amino acid flux in ways that are difficult to interpret. AsO_2^- effectively shuts down the TCA cycle by inhibiting entry by acetyl-coA as well as inhibiting α-ketoglutarate. This would be predicted to increase anaerobic metabolism. Thus amino acid that metabolize to pyruvate, such as alanine, glycine,

serine, tryptophan, cystine, and threonine, would be predicted to increase efflux from cells and thus have a higher concentration in effluent from the MBR. Other amino acids would be inhibited and would be predicted to have less flux and thus the amino acid concentration in MBR effluent would be closer to control media. This was not what was observed. From Figure 46, the only amino acid demonstrating significant change in concentration was alanine, which decreased in efflux. Like AOA, the cause for this inconsistency is not understood at this time, but could be due to dose discrepancies due to different experimental conditions than literature values where the concentration was derived.[104]. The cause of the variations were not due to AOA or AsO_2^- affecting the AAFA. There was no change in the peak area of any amino acid upon analysis of control media with either AOA or AsO_2- when compared to control media without addition of AOA or AsO_2^- (data not shown).

There was larger variation between each of the experimental three replicates than within each replicate for all amino acids in both the AOA and AsO_2^- data, and hence showed a significant difference with ANOVA. A one-way analysis of variance (ANOVA aka F test) computes the ratio of the variance between the means of several samples and the sum of the variance within each sample. This value is compared to a table and if the ratio is larger than the value on the table, there is a significant difference between the different groups. This was the case for each of my samples and as such all the values used in each of the replicates could not be combined into one data set. Instead, only the means were used to calculate the confidence intervals.

The experimental results indicate several areas of improvement which could be addressed to obtain better results for future experiments. The delay time between

changing the media that cells in the MBR are exposed and the time the effluent reaches the AAFA needs to be reduced. This could be addressed several ways such as increasing the size of the MBR chamber which allows for faster flow rates and thus faster transit time in tubing, or converting to stop-flow rather than continual perifusion. Reducing the delay time should also cause a reduction in the response time, thus allowing more rapid changes in metabolism to be observed. The choice of cell line needs to be reconsidered. AML12 cells were chosen because they are a hepatocytes cell line which have a high rate of amino acid metabolism for gluconeogenesis and the urea cycle. However, the metabolism of immortalized cell lines are typically vastly different from primary cells. Therefore, use of primary hepatocytes would allow more predicable metabolism to be used as well as non-pharmacolical interventions to be used. Insulin and glucagon cause known changes amino acid flux in long-term experiments and would therefore be ideal candidates to demonstrate the feasibility of the AAFA.[20,105]

Conclusions

The AAFA was able to reproducibly observe online changes in amino acid concentration caused by basal cell metabolism from cells in the MBR. The basal metabolism was altered by exposure to 0.5 mM AOA or 0.2 mM AsO_2^- and the change in the concentration in amino acids resulting from exposure to these compounds was able to be observed. Furthermore, the results from Table 17 indicate that a difference in cellular amino acid flux from the application of AOA and AsO_2^- can be observed online with the effluent of the MBR going to the AAFA. The change was able to be discerned with

alanine and arginine in spite of the flux changing in the same direction for both compounds.

Once changes to the MBR and AAFA are implemented, the results obtained from flux measurements from cellular perturbations should improve significantly. Results could then be implemented to observe dynamic metabolic changes in the cell. The results could be applied to metabolic flux analysis or similar techniques to quantitate dynamic intracellular fluxes. Application of toxins with unknown metabolic effect could be applied to cells and combined with data from the MMP in order to obtain a larger view of the dynamic of metabolism within cells.

APPENDIX A

LABVIEW PROGRAM FOR CONTROL AND AAFA AND DATA COLLECTION

The program was written in LabVIEW by Jonathan Shackman at the University of Michigan, a graduate student of Dr. Robert Kennedy. The program controls the high voltage power supply and the flow-gate valve while collecting the signal from the light detection module of the AAFA. The front panel is shown in Figure 47. The user inputs the post-injection delay, delay, injection time, ramp time, collection rate, separation time, separation voltage, and run delay and the electropherogram is displayed along with meters showing the voltage and current of the high voltage power supply. The laser power meter was never utilized.

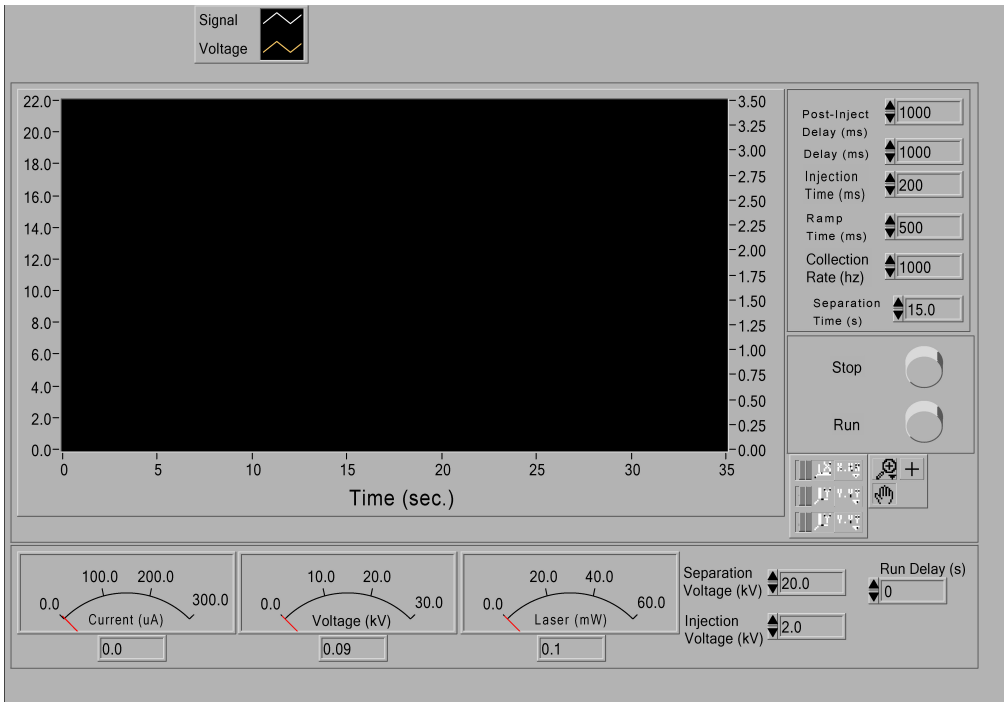

Figure 47. Front panel of the LabVIEW program which controls

A flow diagram showing in general how the program works is shown in Figure 48.

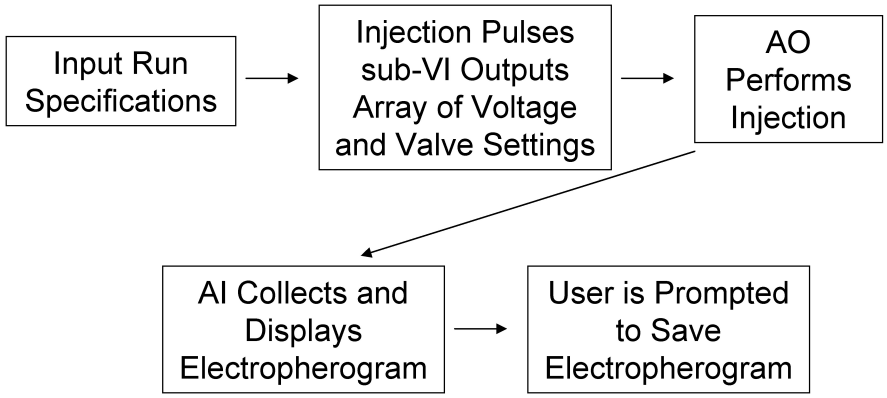

Figure 48. Flow diagram of LabVIEW program.

A portion of the block diagram of the LabVIEW program is shown in Figure 49. This portion inputs the user settings and sends them to the sub-VI Injection Pulses. The output of Injection Pulses is a 2-D array which contains information to control the high voltage power supply and the flow-gate valve for injection. The output is similar to that displayed in Figure 17. The array is sent to the AO loop which actually outputs the settings to the valve and power supply. The Time Delay function I added which allows the user to delay the start of the program after the start button is selected.

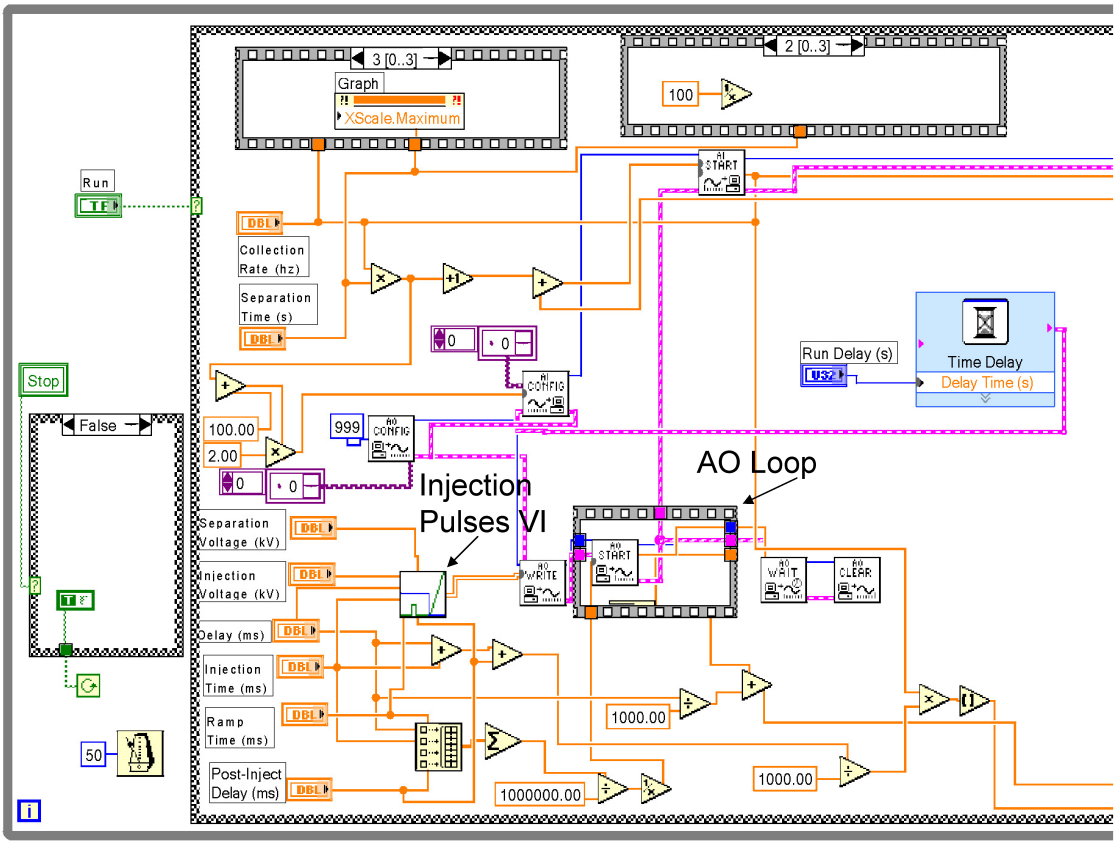

Figure 49. Block Diagram of LabVIEW program showing input, Injectin Pulses VI, and the AO loop.

The block diagram of the Injection Pulses sub-VI is shown in Figure 50. The top portion builds the array which controls the flow-gate valve while the bottom portion builds the voltage array. I rewrote the flow-gate valve control. Dr. Kennedy uses a solenoid valve which requires a constant voltage to be applied during the duration of the injection. I use a rotary valve which is controlled by contact closure by a pair of opto-isolators. When a positive voltage is pulsed, one of the opto-isolators is closed which switches the valve. When a negative voltage is pulsed, the second opto-isolator is closed

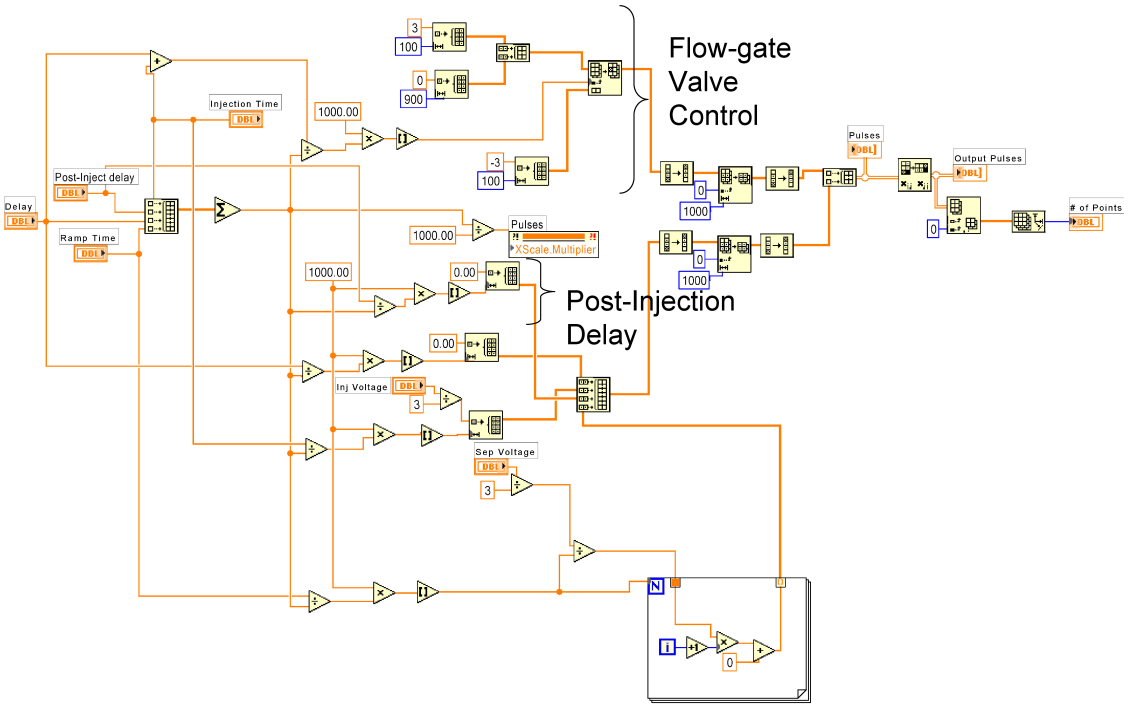

Figure 50. Block diagram of Injection Pulses sub-VI.

which switches the valve back. I also added the portion of the code which adds the post-injection delay. The power supply and valve control arrays are combined into a 2-D array which is the output of the VI.

The block diagram of the rest of the main LabView program is shown in Figure 51. The bulk of figure contains the loop which displays the electropherogram and stores data as well as updates the voltage and current meters. I had to change the conversion from input voltage to units of kV and µA. After the electropherogram is completed (or the stop button is pushed or there is an error) the user is prompted to save the file. Previously the high voltage would remain at the level of the separation voltage during the file saving process. I added code which zeroed the high voltage immediately after the data collection completed.

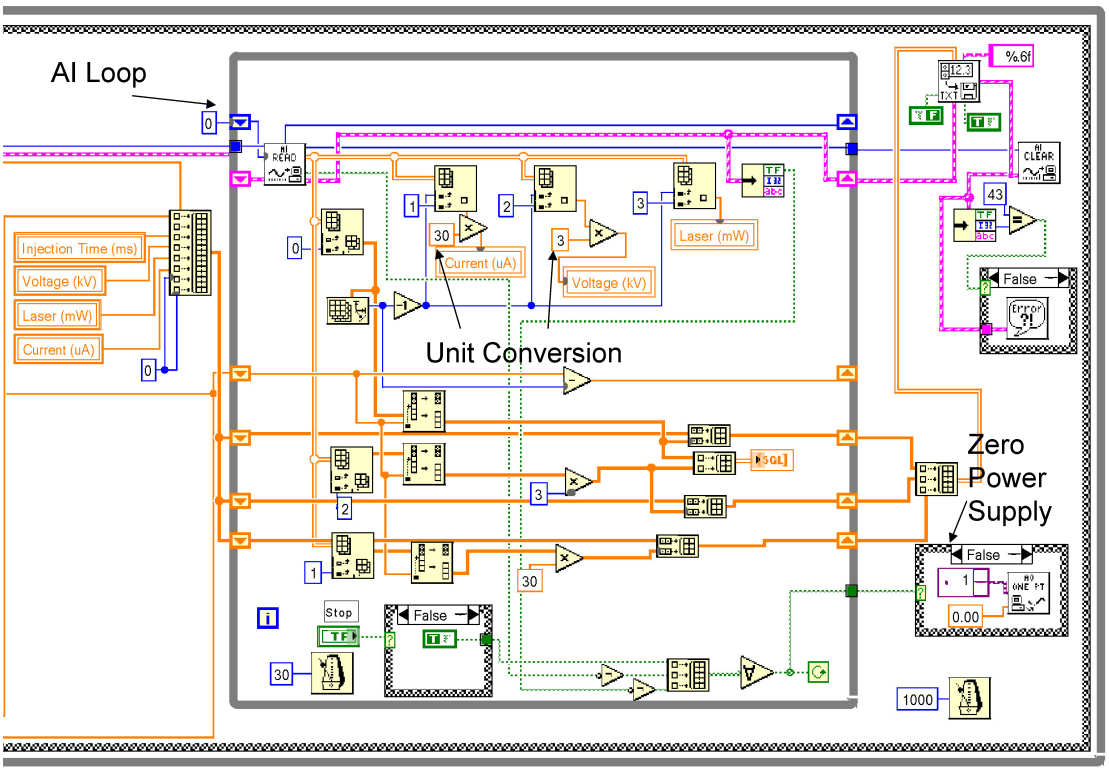

Figure 51. Block diagram of LabView program showing AI loop and file saving.

A second program which automates execution and collecting of multiple electropherograms was utilized during experimental runs. The front panel is shown in Figure 52. The program is identical to the one already presented accept that the program inputs the number of runs and time between runs and automatically saves each electropherogram.

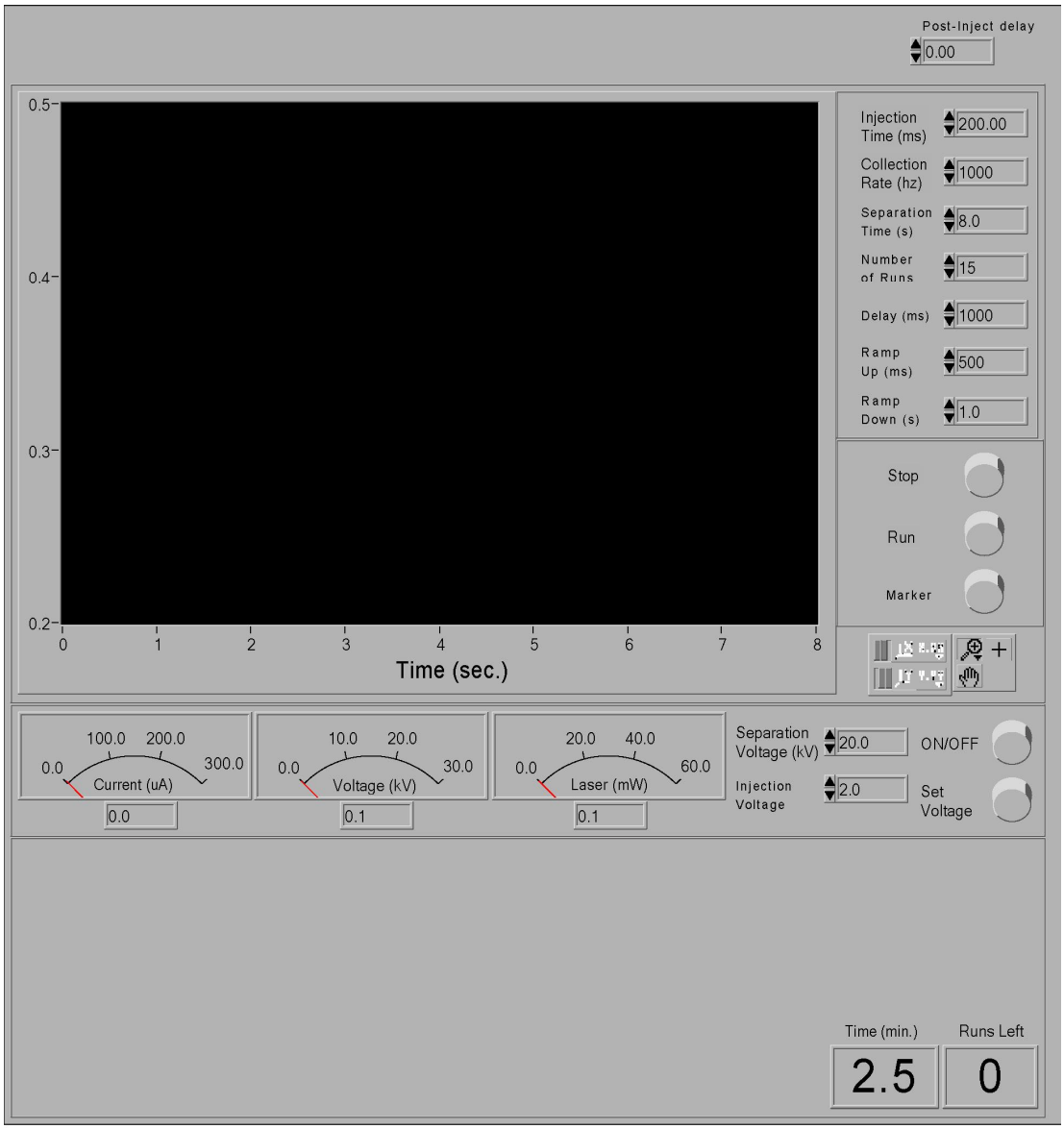

Figure 52. Front panel of extended run LabView program

REFERENCES

1. Chan, C., Berthiaume, F., Lee, K. & Yarmush, M. L. Metabolic flux analysis of cultured hepatocytes exposed to plasma. *Biotechnol. Bioeng.* **81**, 33-49 (2003).

2. Guidance for industry: bioanalytical method validation. 5-21-2001. U.S. Dept. of Health and Human Services. FDA. CDER. CVM.
   Ref Type: Report

3. Yang, Y. & Balcarcel, R. R. Method for Characterizing Changes in Metabolic State of Mammalian Cells. *Metab. Eng.* **In Preparation for submissiong in August**, (2005).

4. Owicki, J. C. *et al.* Continuous Monitoring of Receptor-Mediated Changes in the Metabolic Rates of Living Cells. *PNAS* **87**, 4007-4011 (1990).

5. Owicki, J. C. *et al.* The Light-Addressable Potentiometric Sensor - Principles and Biological Applications. *Annu. Rev. Biophys. Biomol. Struct.* **23**, 87-113 (1994).

6. Cao, C. J. *et al.* Toxicity of sea nettle toxin to human hepatocytes and the protective effects of phosphorylating and alkylating agents. *Toxicon* **36**, 269-281 (1998).

7. Cao, C. J. *et al.* Cytotoxicity of organophosphate anticholinesterases. *In Vitro Cellular & Developmental Biology-Animal* **35**, 493-500 (1999).

8. Chan, S. D. H. *et al.* Heregulin Activation of Extracellular Acidification in Mammary Carcinoma Cells Is Associated with Expression of HER2 and HER3. *J. Biol. Chem.* **270**, 22608-22613 (1995).

9. Cooke, D. & O'Kennedy, R. Comparison of the Tetrazolium Salt Assay for Succinate Dehydrogenase with the Cytosensor Microphysiometer in the Assessment of Compound Toxicities. *Anal. Biochem.* **274**, 188-194 (1999).

10. Ekelund, S., Larsson, R. & Nygren, P. Metabolic effects of the cytotoxic guanidino-containing drug CHS 828 in human U-937 lymphoma cells. *Anticancer Res.* **22**, 2269-2274 (2002).

11. Hafner, F. Cytosensor(R) Microphysiometer: technology and recent applications. *Biosens. Bioelectron.* **15**, 149-158 (2000).

12. Mioduszewski, R. J. *et al. Toxicity Assessment Alternatives: Methods, Issues, Opportunities*. Salem, H. & Katz, S. A. (eds.), pp. 143-154 (Humana Press, Inc., Totowa, NJ,1999).

13. Pitchford, S. *et al.* Characterization of functional activity of chemokine receptors using the cytosensor microphysiometer. *Met. Enzymol.* **288**, 84-108 (1997).

14. Wiley, C. & Beeson, C. Continuous measurement of glucose utilization in heart myoblasts. *Anal. Biochem.* **304**, 139-146 (2002).

15. McConnell, H. M. *et al.* The Cytosensor Microphysiometer: Biological Applications of Silicon Technology. *Science* **257**, 1906-1912 (1992).

16. Eklund, S. E., Taylor, D., Kozlov, E., Prokop, A. & Cliffel, D. E. A microphysiometer for simultaneous measurement of changes in extracellular glucose, lactate, oxygen, and acidification rate. *Anal. Chem.* **76**, 519-527 (2004).

17. Eklund, S. E., Kozlov, E., Taylor, D. E., Baudenbacher, F. & Cliffel, D. E. *NanoBiotechnology Protocols*. Rosenthal, S. & Wright, D. (eds.), pp. 209-223 (Humana Press, Totawa, NJ,2005).

18. Eklund, S. E. *et al.* Modification of the Cytosensor ™ Microphysiometer to Simultaneously Measure Extracellular Acidification and Oxygen Consumption Rates. *Anal. Chim. Acta* **496**, 93-101 (2003).

19. Eklund, S. E. *et al.* Metabolic discrimination of select list agents by monitoring cellular responses in a multianalyte microphysiometer. *Sensors* **9**, 2117-2133 (2009).

20. Takenaka, A., Ohishi, Y., Noguchi, T. & Naito, H. Effect of Some Essential Amino-Acid Deficiency in the Medium on the Action of Insulin on Primary Cultured-Hepatocytes of Rats - Hepatocytes do Not Respond to Insulin in Some Essential Amino Acid-Deficient Medium. *Int. J. Biochem.* **21**, 1255-1263 (1989).

21. Xia, Y. N. & Whitesides, G. M. Soft lithography. *Angew. Chem. Int. Ed.* **37**, 551-575 (1998).

22. Xia, Y. N. & Whitesides, G. M. Soft lithography. *Annual Review of Materials Science* **28**, 153-184 (1998).

23. Whitesides, G. M. The origins and the future of microfluidics. *Nature* **442**, 368-373 (2006).

24. Whitesides, G. M., Ostuni, E., Takayama, S., Jiang, X. & Ingber, D. E. Soft Lithography in Biology and Biochemistry. *Annu. Rev. Biomed. Engr.* **3**, 335-373 (2001).

25. Unger, M. A., Chou, H. P., Thorsen, T., Scherer, A. & Quake, S. R. Monolithic microfabricated valves and pumps by multilayer soft lithography. *Science* **288**, 113-116 (2000).

26. Kostov, Y., Harms, P., Randers-Eichhorn, L. & Rao, G. Low-cost microbioreactor for high-throughput bioprocessing. *Biotechnol. Bioeng.* **72**, 346-352 (2001).

27. Rahman, P. K. S. M., Pasirayi, G., Auger, V. & Ali, Z. Development of a simple and low cost microbioreactor for high-throughput bioprocessing. *Biotechnology Letters* **31**, 209-214 (2009).

28. Villain, L., Meyer, L., Kroll, S., Beutel, S. & Scheper, T. Development of a novel membrane aerated hollow-fiber microbioreactor. *Biotechnol. Progr.* **24**, 367-371 (2008).

29. Sud, D. *et al.* Optical imaging in microfluidic bioreactors enables oxygen monitoring for continuous cell culture. *J. Biomed. Opt.* **11**, 050504 (2006).

30. Vervliet-Scheebaurn, M., Ritzenthaler, R., Normann, J. & Wagner, E. Short-term effects of benzalkonium chloride and atrazine on Elodea canadensis using a miniaturised microbioreactor system for an online monitoring of physiologic parameters. *Ecotoxicology and Environmental Safety* **69**, 254-262 (2008).

31. Hung, P. J. *et al.* A novel high aspect ratio microfluidic design to provide a stable and uniform microenvironment for cell growth in a high throughput mammalian cell culture array. *Lab Chip* **5**, 44-48 (2005).

32. Borenstein, J. T. *et al.* Microfabrication technology for vascularized tissue engineering. *Biomed. Microdevices* **4**, 167-175 (2002).

33. Prokop, A. *et al.* NanoLiterBioReactor: Long-Term Mammalian Cell Culture at Nanofabricated Scale. *Biomed. Microdevices* **6**, 325-339 (2004).

34. Korin, N., Bransky, A., Dinnar, U. & Levenberg, S. Periodic "flow-stop" perfusion microchannel bioreactors for mammalian and human embryonic stem cell long-term culture. *Biomed. Microdevices* **11**, 87-94 (2009).

35. Korin, N., Bransky, A., Dinnar, U. & Levenberg, S. A parametric study of human fibroblasts culture in a microchannel bioreactor. *Lab Chip* **7**, 611-617 (2007).

36. Zhang, Z. Y. *et al.* Microchemostat - microbial continuous culture in a polymer-based, instrumented microbioreactor. *Lab Chip* **6**, 906-913 (2006).

37. Lee, H. L. T., Boccazzi, P., Ram, R. J. & Sinskey, A. J. Microbioreactor arrays with integrated mixers and fluid injectors for high-throughput experimentation with pH and dissolved oxygen control. *Lab Chip* **6**, 1229-1235 (2006).

38. Wu, M. H., Huang, S. B., Cui, Z. F., Cui, Z. & Lee, G. B. A high throughput perfusion-based microbioreactor platform integrated with pneumatic micropumps for three-dimensional cell culture. *Biomed. Microdevices* **10**, 309-319 (2008).

39. Gu, W., Zhu, X., Futai, N., Cho, B. S. & Takayama, S. Computerized microfluidic cell culture using elastomeric channels and Braille displays. *PNAS* **101**, 15861-15866 (2004).

40. Song, J. W. *et al.* Computer-controlled microcirculatory support system for endothelial cell culture and shearing. *Anal. Chem.* **77**, 3993-3999 (2005).

41. Sauer, I. M. *et al.* The SlideReactor - A simple hollow fiber based bioreactor suitable for light microscopy. *Artificial Organs* **29**, 264-267 (2005).

42. Gebhardt, R. Perifusion culture of hepatocytes. *Methods Mol. Biol.* **107**, 329-339 (1998).

43. Yu, C. B., Pan, X. P. & Li, L. J. Progress in bioreactors of bioartificial livers. *Hepatobiliary & Pancreatic Diseases International* **8**, 134-140 (2009).

44. Ostrovidov, S., Jiang, J. L., Sakai, Y. & Fujii, T. Membrane-based PDMS microbioreactor for perfused 3D primary rat hepatocyte cultures. *Biomed. Microdevices* **6**, 279-287 (2004).

45. Harris, D. C. *Quantitative chemical analysis*. W.H. Freeman, New York (1995).

46. Kennedy, R. T., German, I., Thompson, J. E. & Witowski, S. R. Fast Analytical-Scale Separations by Capillary Electrophoresis and Liquid Chromatography. *Chem. Rev.* **99**, 3081-3132 (1999).

47. Chen, D. Y. & Dovichi, N. J. Yoctomole detection limit by laser-induced fluorescence in capillary electrophoresis. *Journal of Chromatography B: Biomedical Sciences and Applications* **657**, 265-269 (1994).

48. Fister, J. C., Jacobson, S. C., Davis, L. M. & Ramsey, J. M. Counting Single Chromophore Molecules for Ultrasensitive Analysis and Separations on Microchip Devices. *Anal. Chem.* **70**, 431-437 (1998).

49. Moore, A. W., Jacobson, S. C. & Ramsey, J. M. Microchip Separations of Neutral Species via Micellar Electrokinetic Capillary Chromatography. *Anal. Chem.* **67**, 4184-4189 (1995).

50. Wind, H. Processing Magnetic Field data. *J. Comput. Phys.* **2**, 274-278 (1968).

51. Moore, A. W. & Jorgenson, J. W. Study of zone broadening in optically gated high-speed capillary electrophoresis. *Anal. Chem.* **65**, 3550-3560 (1993).

52. Hooker, T. F. & Jorgenson, J. W. A Transparent Flow Gating Interface for the Coupling of Microcolumn LC with CZE in a Comprehensive Two-Dimensional System. *Anal. Chem.* **69**, 4134-4142 (1997).

53. Lada, M. W. & Kennedy, R. T. Quantitative in Vivo Monitoring of Primary Amines in Rat Caudate Nucleus Using Microdialysis Coupled by a Flow-Gated Interface to Capillary Electrophoresis with Laser-Induced Fluorescence Detection. *Anal. Chem.* **68**, 2790-2797 (1996).

54. Lada, M. W. & Kennedy, R. T. Quantitative in Vivo Monitoring of Primary Amines in Rat Caudate Nucleus Using Microdialysis Coupled by a Flow-Gated

Interface to Capillary Electrophoresis with Laser-Induced Fluorescence Detection. *Anal. Chem.* **68**, 2790-2797 (1996).

55. Lemmo, A. V. & Jorgenson, J. W. Transverse Flow Gating Interface for the Coupling of Microcolumn-Lc with Cze in A Comprehensive 2-Dimensional System. *Anal. Chem.* **65**, 1576-1581 (1993).

56. Lada, M. W., Schaller, G., Carriger, M. H., Vickroy, T. W. & Kennedy, R. T. On-line interface between microdialysis and capillary zone electrophoresis. *Anal. Chim. Acta* **307**, 217-225 (1995).

57. Bowser, M. T. & Kennedy, R. T. In vivo monitoring of amine neurotransmitters using microdialysis with on-line capillary electrophoresis. *Electrophoresis* **22**, 3668-3676 (2001).

58. Shou, M., Smith, A. D., Shackman, J. G., Peris, J. & Kennedy, R. T. In vivo monitoring of amino acids by microdialysis sampling with on-line derivatization by naphthalene-2,3-dicarboxyaldehyde and rapid micellar electrokinetic capillary chromatography. *J. Neurosci. Methods* **138**, 189-197 (2004).

59. Huynh, B. H., Fogarty, B. A., Martin, R. S. & Lunte, S. M. On-Line Coupling of Microdialysis Sampling with Microchip-Based Capillary Electrophoresis. *Anal. Chem.* **76**, 6440-6447 (2004).

60. Sandlin, Z. D., Shou, M., Shackman, J. G. & Kennedy, R. T. Microfluidic Electrophoresis Chip Coupled to Microdialysis for in Vivo Monitoring of Amino Acid Neurotransmitters. *Anal. Chem.* **77**, 7702-7708 (2005).

61. vonHeeren, F., Verpoorte, E., Manz, A. & Thormann, W. Micellar electrokinetic chromatography separations and analyses of biological samples on a cyclic planar microstructure. *Anal. Chem.* **68**, 2044-2053 (1996).

62. Xu, B. *et al.* Two-dimensional electrophoresis on a microfluidic chip for quantitative amino acid analysis. *Analytical and Bioanalytical Chemistry* **394**, 1911-1917 (2009).

63. Culbertson, C. T., Jacobson, S. C. & Ramsey, J. M. Microchip devices for high-efficiency separations. *Anal. Chem.* **72**, 5814-5819 (2000).

64. Rodriguez, I., Jin, L. J. & Li, S. F. Y. High-speed chiral separations on microchip electrophoresis devices. *Electrophoresis* **21**, 211-219 (2000).

65. Ro, K. W. & Hahn, J. H. Precolumn diastereomerization and micellar electrokinetic chromatography on a plastic microchip: Rapid chiral analysis of amino acids. *Electrophoresis* **26**, 4767-4773 (2005).

66. Hutt, L. D., Glavin, D. P., Bada, J. L. & Mathies, R. A. Microfabricated Capillary Electrophoresis Amino Acid Chirality Analyzer for Extraterrestrial Exploration. *Anal. Chem.* **71**, 4000-4006 (1999).

67. Skelley, A. M. & Mathies, R. A. Chiral separation of fluorescamine-labeled amino acids using microfabricated capillary electrophoresis devices for extraterrestrial exploration. *J. Chromatogr. A* **1021**, 191-199 (2003).

68. Skelley, A. M. *et al.* Development and evaluation of a microdevice for amino acid biomarker detection and analysis on Mars. *PNAS* **102**, 1041-1046 (2005).

69. Chiesl, T. N. *et al.* Enhanced Amine and Amino Acid Analysis Using Pacific Blue and the Mars Organic Analyzer Microchip Capillary Electrophoresis System. *Anal. Chem.* **81**, 2537-2544 (2009).

70. Underberg, W. J. M. & Waterval, J. C. M. Derivatization trends in capillary electrophoresis: An update. *Electrophoresis* **23**, 3922-3933 (2002).

71. De Montigny, P. *et al.* Naphthalene-2,3-dicarboxyaldehyde/cyanide ion: a rationally designed fluorogenic reagent for primary amines. *Anal. Chem.* **59**, 1096-1101 (2002).

72. Matuszewski, B. K., Givens, R. S., Srinivasachar, K., Carlson, R. G. & Higuchi, T. N-substituted 1-cyanobenz[f]isoindole: evaluation of fluorescence efficiencies of a new fluorogenic label for primary amines and amino acids. *Anal. Chem.* **59**, 1102-1105 (2002).

73. Henderson, J. W., Ricker, R. D., Bidlingmeyer, B. A. & Woodward, C. Rapid, accurate, sensitive, and reproducible HPLC analysis of amino acids. Publication No. 5989-6297EN. 2007. Agilent Technologies.
Ref Type: Statute

74. Woodward, C. & Henderson, J. W. High-speed amino acid analysis (AAA) on 1.8 μm reversed-phase (RP) columns. 2007. Agilent Technologies.
Ref Type: Statute

75. Wu, J. C., Merlino, G. & Fausto, N. Establishment and Characterization of Differentiated, Nontransformed Hepatocyte Cell-Lines Derived from Mice Transgenic for Transforming Growth-Factor-Alpha. *PNAS (US)* **91**, 674-678 (1994).

76. Wikswo, J. P. *et al.* Engineering challenges of BioNEMS: the integration of microfluidics, and micro- and nanodevices, models, and external control for systems biology. *IEE Proc. -Nanobiotechnol.* **153**, 81-101 (2006).

77. Prokop, A. Systems-Analysis and Synthesis in Biology and Biotechnology. *International Journal of General Systems* **8**, 7-31 (1982).

78. Prokop, A. *Animal cell bioreactors*. Ho, C. S. & Wang, D. I. (eds.) (Butterworth-Heinemann, Boston,1991).

79. Scholtissek, C. & Rott, R. Metabolic Changes in Chick Fibroblasts after Infection with Newcastle Disease Virus. *Nature* **206**, 729-730 (1965).

80. Hanley, D. A., Takatsuki, K., Birnbaumer, M. E., Schneider, A. B. & Sherwood, L. M. Invitro Perifusion for the Study of Parathyroid-Hormone Secretion - Effects of Extracellular Calcium-Concentration and Beta-Adrenergic Regulation on Bovine Parathyroid-Hormone Secretion Invitro. *Calcif. Tissue Int.* **32**, 19-27 (1980).

81. Sweet, I. R. *et al.* Dynamic perifusion to maintain and assess isolated pancreatic islets. *Diabetes Technol. Ther.* **4**, 67-76 (2002).

82. Nolan, A. L. & O'Dowd, J. F. The measurement of insulin secretion from isolated rodent islets of langerhans. *Methods Mol. Biol.* **560**, 43-51 (2009).

83. Brenner, M. B. & Mest, H. J. A buffer temperature controlled perifusion system to study temperature dependence and kinetics of insulin secretion in MIN6 pseudoislets. *J. Pharmacol. Toxicol. Methods* **50**, 53-57 (2004).

84. Thompson, D. M. *et al.* Dynamic gene expression profiling using a microfabricated living cell array. *Anal. Chem.* **76**, 4098-4103 (2004).

85. Kane, B. J., Zinner, M. J., Yarmush, M. L. & Toner, M. Liver-specific functional studies in a microfluidic array of primary mammalian hepatocytes. *Anal. Chem.* **78**, 4291-4298 (2006).

86. Radisic, M. *et al.* Medium perfusion enables engineering of compact and contractile cardiac tissue. *Am. J. Physiol. Heart* **286**, H507-H516 (2004).

87. Leclerc, E., Sakai, Y. & Fujii, T. Microfluidic PDMS (polydimethylsiloxane) bioreactor for large-scale culture of hepatocytes. *Biotechnol. Progr.* **20**, 750-755 (2004).

88. Duffy, D. C., McDonald, J. C., Schueller, O. J. A. & Whitesides, G. M. Rapid prototyping of microfluidic systems in poly(dimethylsiloxane). *Anal. Chem.* **70**, 4974-4984 (1998).

89. Dumenco, L., Oguey, D., Wu, J., Messier, N. & Fausto, N. Introduction of a murine p53 mutation corresponding to human codon 249 into a murine hepatocyte cell line results in growth advantage, but not in transformation. *Hepatology* **22**, 1279-1288 (1995).

90. Greene, J., Henderson, J. W., Jr. & Wikswo, J. P. Rapid and precise determination of cellular amino acid flux rates using HPLC with automated derivatization with absorbance detection. Application Note. 5990-3283EN, http://dx.doi.org/10.1016/S0091-679X(08)00604-3. 2-11-2009. Agilent Technologies.
Ref Type: Report

91. Altria, K. D. Improved performance in capillary electrophoresis using internal standards. *Lc Gc Europe* **15**, 588-594 (2002).

92. Cellar, N. A. & Kennedy, R. T. A capillary-PDMS hybrid chip for separations-based sensing of neurotransmitters in vivo. *Lab Chip* **6**, 1205-1212 (2006).

93. *CRC handbook of chemistry and physics: a ready-reference book of chemical and physical data*. CRC Press, Boca Raton, FL (2008).

94. Shackman, J. G., Watson, C. J. & Kennedy, R. T. High-throughput automated post-processing of separation data. *J. Chromatogr. A* **1040**, 273-282 (2004).

95. Meijer, A. J., Gimpel, J. A., Deleeuw, G. A., Tager, J. M. & Williamson, J. R. Role of anion translocation across the mitochondrial membrane in the regulation of urea synthesis from ammonia by isolated rat hepatocytes. *J. Biol. Chem.* **250**, 7728-7738 (1975).

96. Davanzo, J. P., Matthews, R. J., Yoeng, G. A. & Winderson, F. Studies on the mechanism of action of aminooxyacetic acid. ii. possible pyridoxine deficiency as a mechanism of action of aminooxyacetic acid toxicity. *Toxicol. Appl Pharmacol.* **6**, 396-401 (1964).

97. Liu, W. S. *et al.* Crystal structures of unbound and aminooxyacetate-bound Escherichia coli gamma-aminobutyrate aminotransferase. *Biochem.* **43**, 10896-10905 (2004).

98. Seglen, P. O. & Solheim, A. E. Effects of aminooxyacetate, alanine and other amino acids on protein synthesis in isolated rat hepatocytes. *Biochim. Biophys. Acta* **520**, 630-641 (1978).

99. Zahlten, R. N., Kneer, N. M., Stratman, F. W. & Lardy, H. A. The influence of ammonium and calcium lons on gluconeogenesis in isolated rat hepatocytes and their response to glucagon and epinephrine. *Arch. Biochem. Biophys.* **161**, 528-535 (1974).

100. Rognstad, R. & Clark, D. G. Effects of aminooxyacetate on the metabolism of isolated liver cells. *Arch. Biochem. Biophys.* **161**, 638-646 (1974).

101. Petrick, J. S., Jagadish, B., Mash, E. A. & Aposhian, H. V. Monomethylarsonous acid (MMA(III)) and arsenite: LD(50) in hamsters and in vitro inhibition of pyruvate dehydrogenase. *Chem. Res. Toxicol.* **14**, 651-656 (2001).

102. Voet, D., Voet, J. G. & Pratt, C. W. *Fundamentals of biochemistry*. Wiley, New York (1999).

103. Kerscher, L. & Oesterhelt, D. The catalytic mechanism of 2-oxoacid:ferredoxin oxidoreductases from Halobacterium halobium. One-electron transfer at two distinct steps of the catalytic cycle. *Eur. J. Biochem.* **116**, 595-600 (1981).

104. Souza, K. *et al.* Arsenite activation of PI3K/AKT cell survival pathway is mediated by p38 in cultured human keratinocytes. *Molecular Medicine* **7**, 767-772 (2001).

105. Chan, C., Berthiaume, F., Lee, K. & Yarmush, M. L. Metabolic flux analysis of hepatocyte function in hormone- and amino acid-supplemented plasma. *Metab. Eng.* **5**, 1-15 (2003).